AD-A071 574 AEROSPACE MEDICAL RESEARCH LAB WRIGHT-PATTERSON AFB OH F/G 5/8
COMBINED DISCRETE NETWORK--CONTINUOUS CONTROL MODELING OF MAN-M--ETC(U)
MAR 79 D J SEIFERT

UNCLASSIFIED AMRL-TR-79-34 NL

1 OF 3
AD
A071574

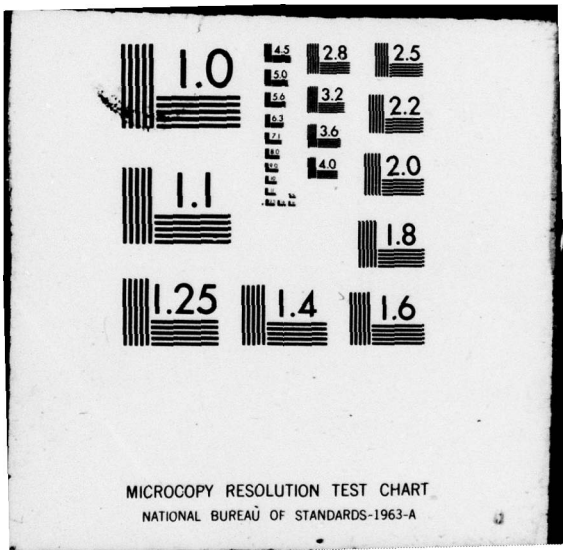
1.0
1.1
1.25
1.4
1.6
1.8
2.0
2.2
2.5
2.8
3.2
3.6
4.0
4.5
5.0
5.6
6.3
MICROCOPY RESOLUTION TEST CHART
NATIONAL BUREAU OF STANDARDS-1963-A

AD A071574

LEVEL II

AMRL-TR-79-34

COMBINED DISCRETE NETWORK — CONTINUOUS CONTROL MODELING OF MAN-MACHINE SYSTEMS

DEBORAH J. SEIFERT, PhD
AEROSPACE MEDICAL RESEARCH LABORATORY

DDC
RECEIVED
JUL 24 1979
B

March 1979

DDC FILE COPY

Approved for public release; distribution unlimited.

AEROSPACE MEDICAL RESEARCH LABORATORY
AEROSPACE MEDICAL DIVISION
AIR FORCE SYSTEMS COMMAND
WRIGHT-PATTERSON AIR FORCE BASE, OHIO 45433

79 07 20 026

NOTICES

When US Government drawings, specifications, or other data are used for any purpose other than a definitely related Government procurement operation, the Government thereby incurs no responsibility nor any obligation whatsoever, and the fact that the Government may have formulated, furnished, or in any way supplied the said drawings, specifications, or other data, is not to be regarded by implication or otherwise, as in any manner licensing the holder or any other person or corporation, or conveying any rights or permission to manufacture, use, or sell any patented invention that may in any way be related thereto.

Please do not request copies of this report from Aerospace Medical Research Laboratory. Additional copies may be purchased from:

National Technical Information Service
5285 Port Royal Road
Springfield, Virginia 22161

Federal Government agencies and their contractors registered with Defense Documentation Center should direct requests for copies of this report to:

Defense Documentation Center
Cameron Station
Alexandria, Virginia 22314

TECHNICAL REVIEW AND APPROVAL

AMRL-TR-79-84

This report has been reviewed by the Information Office (OI) and is releasable to the National Technical Information Service (NTIS). At NTIS, it will be available to the general public, including foreign nations.

This technical report has been reviewed and is approved for publication.

FOR THE COMMANDER

Charles Bates, Jr.

CHARLES BATES, JR.
Chief
Human Engineering Division
Aerospace Medical Research Laboratory

SECURITY CLASSIFICATION OF THIS PAGE *(When Data Entered)*

REPORT DOCUMENTATION PAGE

READ INSTRUCTIONS BEFORE COMPLETING FORM

1. REPORT NUMBER: AMRL-TR-79-34 ✓	2. GOVT ACCESSION NO.
3. RECIPIENT'S CATALOG NUMBER: Technical rept.	
4. TITLE *(and Subtitle)*: COMBINED DISCRETE NETWORK--CONTINUOUS CONTROL MODELING OF MAN-MACHINE SYSTEMS	5. TYPE OF REPORT & PERIOD COVERED: Ph.D. Dissertation
	6. PERFORMING ORG. REPORT NUMBER
7. AUTHOR(s): Deborah J. Seifert, PhD	8. CONTRACT OR GRANT NUMBER(s)
9. PERFORMING ORGANIZATION NAME AND ADDRESS: Aerospace Medical Research Laboratory, Aerospace Medical Division, Air Force Systems Command, Wright-Patterson Air Force Base, Ohio 45433	10. PROGRAM ELEMENT, PROJECT, TASK AREA & WORK UNIT NUMBERS: 61102F, 2313-V1-21
11. CONTROLLING OFFICE NAME AND ADDRESS: Same as Block 9	12. REPORT DATE: March 1979
	13. NUMBER OF PAGES: 204
14. MONITORING AGENCY NAME & ADDRESS *(if different from Controlling Office)*: 204p.	15. SECURITY CLASS. *(of this report)*: Unclassified
	15a. DECLASSIFICATION/DOWNGRADING SCHEDULE

16. DISTRIBUTION STATEMENT *(of this Report)*

Approved for public release; distribution unlimited

17. DISTRIBUTION STATEMENT *(of the abstract entered in Block 20, if different from Report)*

DDC RECEIVED JUL 24 1979 B

18. SUPPLEMENTARY NOTES

19. KEY WORDS *(Continue on reverse side if necessary and identify by block number)*

Man-Machine Systems
Network Models
Optimal Control
Combined Simulation
SAINT
Discrete Event Simulation
Continuous Process Simulation
Pilot Performance Modeling
Human Engineering Evaluation

20. ABSTRACT *(Continue on reverse side if necessary and identify by block number)*

→ The role of the human operator in control systems is evolving towards that of a supervisor who plans, sequences, and monitors and away from strictly tracking. New modeling approaches and techniques are required to realistically represent and examine these new system configurations and resulting performance issues. This dissertation study proposed an alternate modeling approach comprised of discrete network models in combination with elements of an open-loop optimal control model formulation.

DD FORM 1 JAN 73 1473 EDITION OF 1 NOV 65 IS OBSOLETE

SECURITY CLASSIFICATION OF THIS PAGE *(When Data Entered)*

009 850

20. ABSTRACT (Cont'd)

The feasibility of employing this combined modeling approach was demonstrated through its application to the DAIS (Digital Avionics Information System) system in which pilot duties involve information retrieval and cognitive processing tasks in addition to flight control. This model differs from conventional models in that system status sampling is not necessarily continuous or periodic, due to the secondary keyboard entry tasks imposed upon the pilot. The pilot reads system status displays only as time permits and operates in a so-called "open-loop" preprogrammed fashion between sampling.

The study illustrates how this combined modeling technique can facilitate the examination of alternate state variable sampling algorithms and their effects on flight control performance. Flight control interruptions for the performance of monitoring activities and discrete tasks were modeled. The approach's utility as an analysis tool in the design of man-in-the-loop experiments was also demonstrated. It can be used to evaluate and establish operator and experimental procedures prior to actually running the experiment. Models which attempt to capture the parallel or simultaneous performance activities of the human controller were also examined.

These results indicate that this approach is both feasible and appropriate for examining man-machine design issues. This modeling technique greatly reduces the weaknesses of employing either network or continuous optimal control techniques independently in modeling monitoring and supervisory control systems. The discrete task activities and cognitive decision-making processes of the human operator can now be explicitly represented along with his continuous tracking behaviors. A discussion of strengths and weaknesses of the modeling approach, along with directions for future research, is presented.

PREFACE

This research was conducted by the Systems Research Branch, Human Engineering Division, Aerospace Medical Research Laboratory. The research was performed under Project 2313, "Fundamentals for Man-Machine Integration," Task 2313V121 "Simulation Methods for Manned Systems Analysis and Design."

I wish to thank Dr. R. A. Miller, whose inspiration, guidance, and timely suggestions have been invaluable throughout the preparation of this thesis. I would also like to express my appreciation to Constance Hoyland for her programming support and insightful comments during our many discussions.

Without the extensive cooperation of the Aerospace Medical Research Laboratory (AMRL) this research would have been impossible, and I am extremely grateful. I wish to extend my thanks to my many colleagues at AMRL, in particular the constant support of Dr. Donald A. Topmiller. I also wish to acknowledge the masterful jobs of typing performed by Cynthia Budde and Marya Choice.

Finally, I owe a special debt of gratitude to my husband, Tom, for his encouragement and understanding throughout a long graduate program.

Accession For
NTIS GRA&I ☑
DDC TAB ☐
Unannounced ☐
Justification
By
Distribution/
Availability Codes
Dist | Avail and/or special
A

TABLE OF CONTENTS

LIST OF TABLES

LIST OF FIGURES

INTRODUCTION

MAN-MACHINE SYSTEM TRENDS

With the advent of computer automation and graphical and alpha-numeric multipurpose displays, the role of the human operator in control systems is evolving towards that of a supervisor who plans, sequences, and coordinates, and away from strictly tracking (Sheridan, 1976). The human is valued in these systems precisely for his information processing abilities and his ability to provide an adaptive decision-making capability in an otherwise automated system. The human operator is on board as a manager or supervisor of the overall system. He monitors the input and output variables of the automatic vehicle control loop via displays. He can change the modes of the automatic controller via push buttons or continuous control devices as a function of mission phases, environmental conditions, or as a consequence of failures.

Johannsen (1976) states that the tasks of the human operator have changed very much compared with those in manual control. He is now forced to operate in a multi-task environment which requires that he perform tracking tasks and discrete tasks along with information management and planning activities. Johannsen also suggests that in many automated systems the sensomotor activities are much less frequent and, consequently, that vigilance and decision-making behavior has taken on a more important role.

While automation can greatly enhance system performance, it does not generally reduce the demands on the operator. Although systems

exist in which the monotony of the task may increase in such a way that additional tasks have to be invented, Edwards (1976) points out that "typically the operational effectiveness of the man-machine system is enhanced, involving changes rather than reductions in the human contribution."

Edwards also states that the requirement for ergonomics input into the design and operation of systems is in no way diminished by automation. He suggests that the nature of the human factors problems has changed, without reducing their significance. There are now new issues in the man-machine, man-computer interface. The operator's cognitive and perceptual activities are becoming more important than his skill at motor tasks. This indicates that in order to evaluate possible advantages of automation to the human operator, it is necessary to measure not only system performance, but also human operator workload.

It is apparent that the structure of man as a supervisor, planner, and information processor is hierarchical. To coordinate and manage the system he must function at many different levels concurrently. The following excerpt from Singleton (1976) provides an excellent description of the different levels of operator performance.

> . . . At the lowest level he is an information processing device using eyes to scan instruments and hands to select data streams but he does this in the context of rules, procedures, flight plans, aircraft performance characteristics and so on -- his general situation knowledge. He is also monitoring his own performance in relation to long term and short term objectives, changing his and the computers strategy, adjusting his arousal level and even switching objectives. The computer will presumably aid him at different levels and participate in monitoring computer performance and human performance as well as hardware performance.

Johannsen (1976) also addresses the hierarchical multilevel structure of automated man-machine systems. He defines this structure in terms of "loops" along with the relationships and decision rules for moving back and forth between loops. He also provides some insight as to the nature of these loops:

> While the controller activity in the inner loops is mainly continuous tracking, i.e., sensomotor activity, the activity of the controller in the outer loops becomes more and more discrete involving decision-making and problem-solving, i.e., mental activity.

Manned systems such as these involve complex, highly interactive types of tasks. Many of these systems entail continuous tracking and flight control tasks performed in parallel with discrete operational tasks, such as setting radio frequency dials, retrieving information displays via keyboard entries, performing communications with ground control, etc. These flight operations involve the encoding and processing of vast amounts of information in the form of visual displays, system status updates, and operator perception of parallel and interactive task performance. Highly involved cognitive and psychomotor processes are apparently employed in the operation of these systems. The intent of man-in-the-loop system studies is to examine these psychological and behavioral processes to gain adequate insights into the cognitive operational mechanisms in order to effect good system design. Optimal system design includes not only the obvious considerations of human engineering, such as equipment placement and display layouts, but also less apparent factors such as operational procedures, control strategies, priority structures, and task loading. It is the combined interactive effect of these components that make the study of these complex systems both important and challenging.

Real-time man-in-the-loop laboratory experimentation typically utilizes a computer and associated apparatus to simulate all hardware and environmental components of interest, while employing trained subjects to execute all tasks assigned to the system operator. Performance data are collected via computer in real-time.

A more recent approach has been to use a digital computer to simulate not only the hardware and environmental configurations, but to model and simulate the human element as well. There are obvious advantages to this approach in terms of time savings (often several hours of system performance can be simulated in a few minutes), types of systems that can be simulated (one can impose conditions on simulated operators that could never be imposed on live operators, e.g., nuclear radiation effects), and the minimization of problems in operator-in-the-loop experimentation such as hardware failure, subjects not appearing at the appointed time, etc. Digital computer simulation of the entire system, including the human operator has the potential of becoming a tremendous tool for the system engineer in assessing system performance.

The major disadvantage of such an approach is our lack of knowledge of human performance in the systems context and, in particular, the lack of adequate techniques for modeling human performance in a highly complex interactive environment. Despite these two drawbacks, simulation can be a powerful device in examining human performance, particularly cognitive and decision-making behavior processes. Simulation can provide the engineer a cost and time efficient way of determining the combinations of variables and environmental conditions to be included in

real-time manned experiments. The intent is not to replace real-time man-in-the-loop experimentation, but rather to use it when warranted, to empirically reduce the uncertainties that remain, to test hypotheses suggested to be critical design issues, and to enhance and refine the data from which future models can be derived.

The following section details the description and characteristics of a system which exemplifies the trends in man-machine systems and which provided the motivational impetus and data source for this study. A glossary of terms pertinent to this discussion is contained in Appendix A.

DAIS SYSTEM DESCRIPTION

Background

Before the advent of the CRT and the wide use of digital computers, display systems were almost entirely configured with display and control elements, each of which represented a single data output or input. Numerous examples of systems with relatively pure usage of dedicated displays and controls are still found throughout the spectrum of current man-machine system designs. The modern submarine control station is almost entirely composed of single-function display and control elements. Similarly, the engineering station of most commercial aircraft is also an arrangement of displays and controls largely dedicated to single functions. Although a relatively large body of research literature has been accumulated which suggests techniques for improved display/control integration, Bauerschmidt and La Porte (1976) contend that systems employing single function display and control elements will generally result in less than optimal operator performance.

With the advent of CRT and associated computer processing capabilities, the option of relatively low-cost multi-function displays has become a reality. Individual display elements may be depicted, arranged, and combined with great flexibility. Similarly, a multi-function keyboard provides for centralized data input and some flexibility in the presentation of input options.

The Air Force has a research program termed DAIS (Digital Avionics Information System) exploring the man-machine design/performance issues which arrise when such concepts are employed in advanced avionics subsystems. DAIS involves a broad plan of engineering developments and experimental tests designed to exhaustively investigate the feasibility, advantages, and applicability of several new avionics concepts. The engineering developments which have led to the feasibility of these systems have opened up possibilities for aircraft cockpits which are radically different in terms of configuration, information presentation, and control mechanics. The extent of these changes is so great as to call into question the degree to which design principles used in the past can be applied to human engineering questions in new systems. For example, the proposed use of multipurpose displays and multifunction switches as primary flight instruments may drastically revise not only the skill requirements for a pilot, but his workload, his information input requirements, and the very style with which he approaches the task of flying. Without dedicated displays, the pilot is forced to rely much more on memory, and to take a much more active role in acquiring the information he needs in functioning as a controller. No longer will a simple eye movement be sufficient to bring

a required piece of information into his field-of-view. With the new systems, he may be required to (1) decide which information he needs; (2) recall the particular cognitive and motor behaviors, such as codes and switching sequences, which will bring up the appropriate information; (3) perform the actual movements to acquire the information; and (4) move his eyes to the point of information presentation. In traditional systems only the first and last of these tasks are required.

The human engineering questions raised by the proposed DAIS and DAIS-like systems extend farther than the simple questions of deciding which mode of information presentation is best and where particular instruments should be located. Since information may now be presented on a sample basis rather than being continuously present, a great number of questions arise concerning the kinds of information required by the pilot during certain kinds of missions. It will be necessary to specify the ease with which certain types of information should be made available. For instance, some data will be so critical that it may be desirable to cycle it routinely and to display it on a regular basis whether the pilot requests it or not. On the other hand, some less critical information perhaps should be made easily accessible but not routinely presented. Other information may be used infrequently and at noncritical intervals, so that its acquisition could be made relatively complex. The need for information and the most efficient way to present it therefore represents a significant effort in human engineering, and one without a great deal of precedent in systems such as those being considered for DAIS.

DAIS Simulator Study

The Aerospace Medical Research Laboratory (AMRL) has been supporting the analysis of DAIS advanced design concepts via man-in-the-loop experimentation studies. The DAIS simulator cockpit replaces many of the traditionally dedicated instruments, displays, and subsystems controls with interactive multipurpose displays (MPD) and multifunction keyboard switching (MFK). The mock-up cockpit has a forward station configured similar to a single-engine, single-place, transonic light attack aircraft (see Figure 1). The front panel of the cockpit is equipped with three CRT-type displays, two serve multipurpose functions and the center display is used to present information concerning basic flight parameters in a moving tape format (see Figure 2). The flight control display presents current readouts of the aircraft angle of attack, g-load, indicated airspeed, percent of total throttle, mach number, vertical velocity, and heading. Information storage and retrieval can be achieved through the use of the multi-function keyboard and the alphanumeric keyboard located on the left side of the cockpit. The cockpit also contains a throttle with afterburner switch (left side panel) and a center-mounted joystick control which are used, in combination with the displayed flight information, to "fly" various maneuvers. Analog outputs from the stick, throttle, and MFK are processed by an A/D converter for input to a digital computer where further processing is performed. The aircraft motion equations are simulated digitally and updated to respond to the most recent positions of the stick and the throttle. Similarly, switching instructions

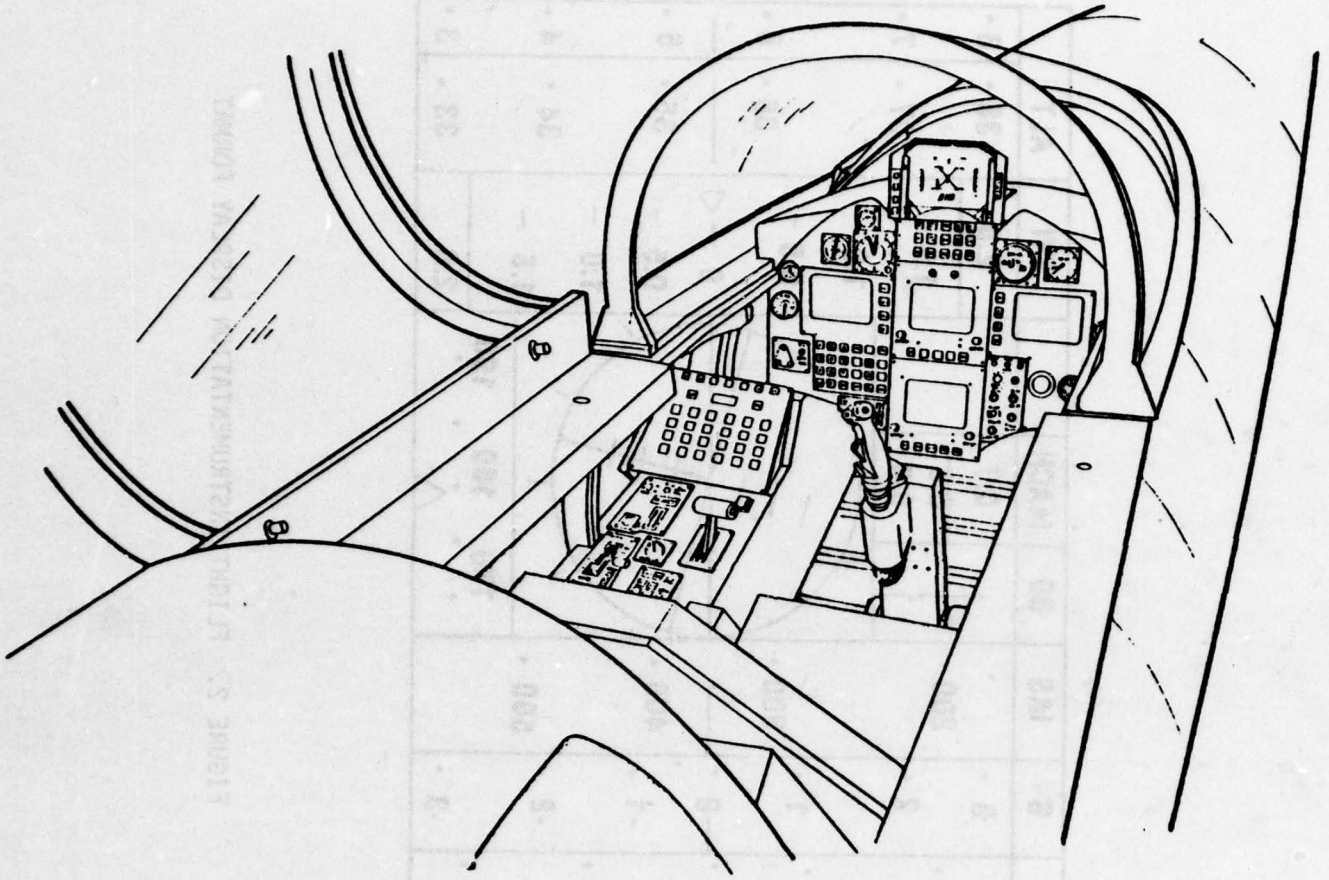

FIGURE 1. DAIS AIRCRAFT COCKPIT SIMULATOR

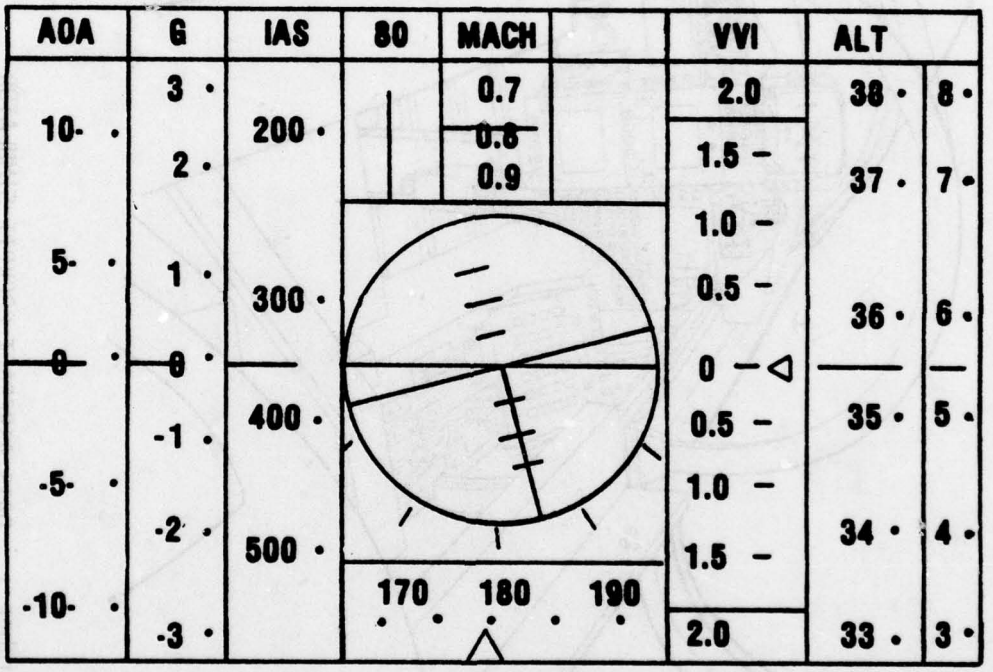

FIGURE 2. FLIGHT INSTRUMENTATION DISPLAY FORMAT

communicated to the pilot via audio headsets are entered through the MFK causing the MPDs to be updated (see Figure 3).

Due to the extensive information retrieval capabilities of the DAIS configuration, the pilot now has access to vast amounts of information for decision-making which previously must have been either committed to memory or based upon estimates or perceptions of system status. Information which is not required by the pilot can be stored and presented on demand either automatically, as related programmed mission events transpire, or in response to operator requests via manual control actions. An additional advantage exists in that, with a reduced number of instruments competing for limited cockpit panel space, the multi-purpose controls and displays can now be located in a prime reach and viewing area.

However, the pilot's total workload has now taken on a different form. He must not only perform flight control tasks, but must also simultaneously process discrete interrupts to perform the information display MFK tasks. There exists the prospect of possible added activity -- both mental and physical -- required to gain access to information which is normally present on dedicated instruments. Should the demand for such activities occur during times of peak operator workload, the impact on mission success might not be offset by the increased calculating power, speed, or accuracy afforded by the digitally-based systems. It is this information-workload tradeoff that is being investigated by AMRL in its man-in-the-loop experiments.

Flight control variables are recorded in terms of the error between the actual values and the command or desired levels. Performance

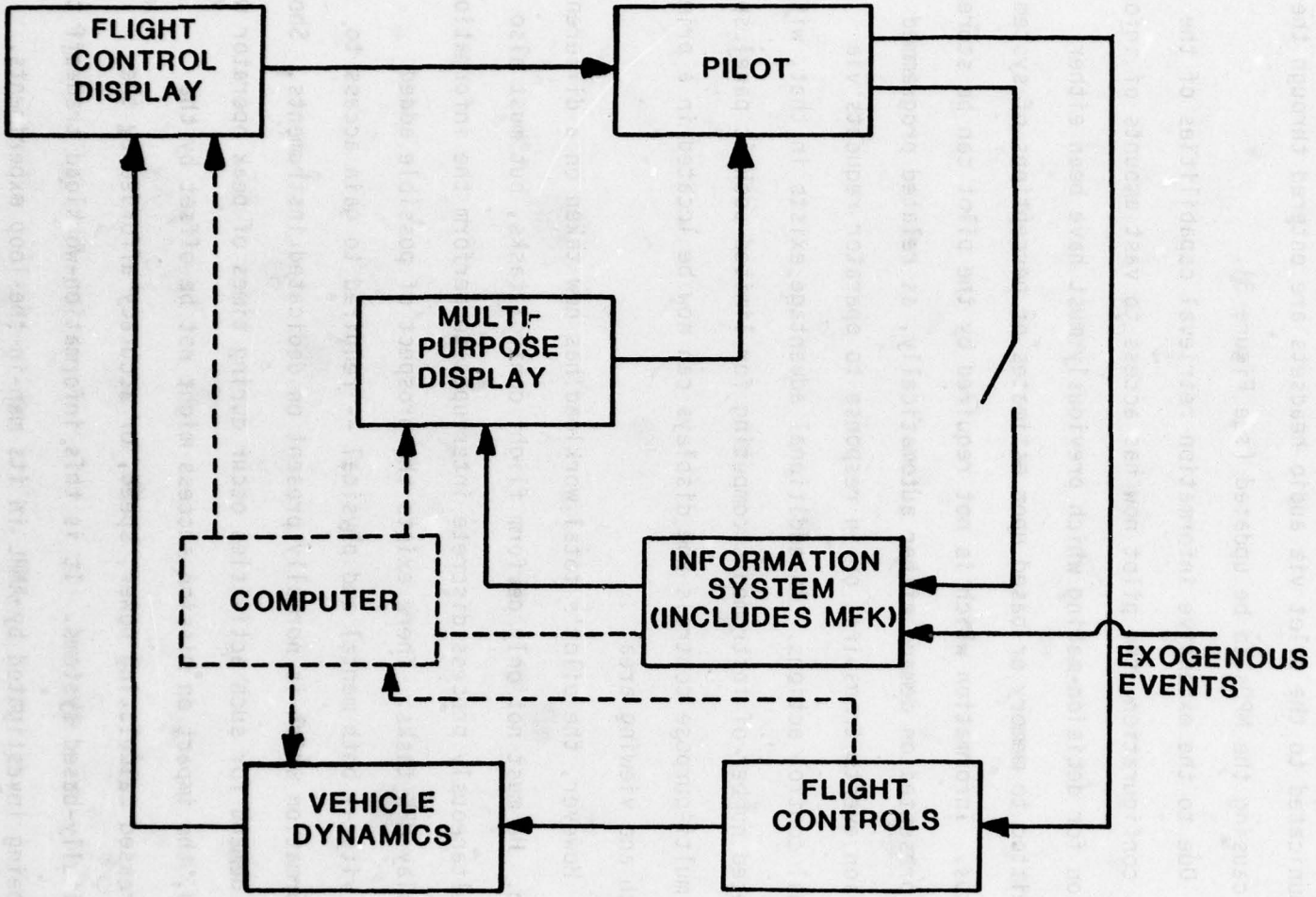

FIGURE 3. DAIS MOCK-UP SYSTEM CONFIGURATION

scores are computed for both the flight control alone and flight control performed in conjunction with MFK switching configurations of the mission. These scores along with data collected concerning discrete information retrieval task times are used to compare and evaluate the information workload tradeoff of the proposed DAIS system.

This system has been selected for study for several reasons: (1) it appears to be representative of many contemporary man-machine systems in that it requires monitoring and discrete information processing behaviors as well as motor control tasks, (2) preliminary performance estimates are available, and (3) results of this endeavor may have immediate implications upon ongoing research and experimental studies.

DISSERTATION OBJECTIVES AND ORGANIZATION

The research effort described herein defines and examines an alternate approach to simulating man-machine systems such as DAIS. This approach combines elements of an open-loop continuous optimal control model with a discrete event-oriented network model. Because many man-machine systems involve tasks with both discrete and continuous elements, it is deemed appropriate to explore the relevance and effectiveness of employing a combined simulation approach as a possible alternative to traditional methods. This research study is dedicated to that objective, which includes examining the strengths and weaknesses of such a combined application as well as determining its feasibility.

The following chapter provides a review and critique of existing modeling methodologies, and outlines the structure of the alternative

approach which combines elements of these traditional techniques. The next chapter relates more details of the DAIS real-time man-in-the-loop simulation and presents the empirical results of the experiment. These results form the data base for the baseline model development. The fourth chapter describes the continuous state space model formulation along with the rudiments of the open-loop closed-loop control model. The following chapter discusses the discrete task network model structure for the DAIS system, along with its interaction with the continuous control model. The results of the baseline construction of the combined model are presented in the sixth chapter. This includes a summary of the parameter estimation exercise, results of baseline model runs, and a discussion of problems, strengths, and possible implications for the real-time simulation. The results of employing several different sampling algorithms and schemes in this combined context are explored in the following chapter. These results indicate that this approach is both feasible and appropriate for examining man-machine design issues. A discussion of strengths and weaknesses of the modeling approach, along with suggested directions for future research, comprise the concluding chapter.

MAN-MACHINE MODELING APPROACHES

PHILOSOPHICAL APPROACHES

Two approaches to modeling human decision-making and behavior have traditionally been advocated -- rational man models and cognitive processing models. Rational man models are normative or prescriptive models and attempt to indicate how a person should decide (or should want to decide) in a given choice situation. Cognitive processing decision models, on the other hand, are descriptive models that attempt to describe and predict actual human choice behavior.

Rational man models are represented by the economic and utility theory models. The theory is not concerned with the problem of how an individual actually selects a course of action in a situation, but rather with the problem of determining what course of action should be taken. This theory of prescriptive behavior indicates how one ought to behave in complex situations to be consistent with some basic preferences, judgments, and principles of so-called rational behavior. The choice situation is characterized by the existence of two or more alternative courses of action, for each of which there are two or more possible outcomes. The theory requires that the individual making the choice must know the alternative courses of action. He must also know the possible outcomes for each of the courses of action, although he does not necessarily know which outcome will actually occur. In some cases it is assumed that the individual can assign a probability of

occurrence and a utility to each possible outcome. According to the theory, the individual chooses his course of action in such a way as to maximize the expected utility.

The engineering "black box" model description appears to be representative of rational man models (see Figure 4). The concern is for the inputs and outputs of the decision exercise and not the intervening process (black box). The inputs consist of the possible choice alternatives, possible decision outcomes, utility functions, and both objective and subjective probability estimates. The single output consists of the "optimal" alternative which should maximize the results or payoff in accordance with one's utility function. No attempt is made to model how the decision is made. Rather, the model prescribes "what" alternative to choose.

The descriptive cognitive processing models attempt to represent how people make decisions, how they rationalize their choices of behavior, how they learn, and so on. They are portrayed by models which have a structural or mechanistic correspondence to the decision-making environment (see Figure 5). They are conducive to flow diagram or network representations and attempt to capture the adaptive considerations of the decision process. Those variables which are thought to influence the decision process can be included in the model structure. Probabilities may be an important part of the model, but not in the same sense that they are employed in the rational man models. In those models they are used to designate the probabilities of the possible outcomes. In the cognitive models they represent the probabilities of branching between the different elements of the network structure. The

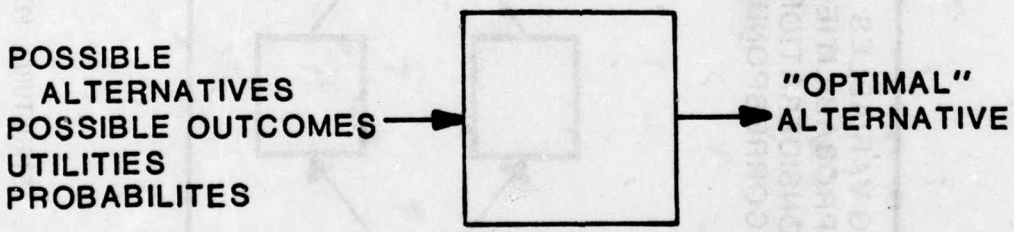

FIGURE 4. "BLACK-BOX" MODEL OF RATIONAL MAN THEORY

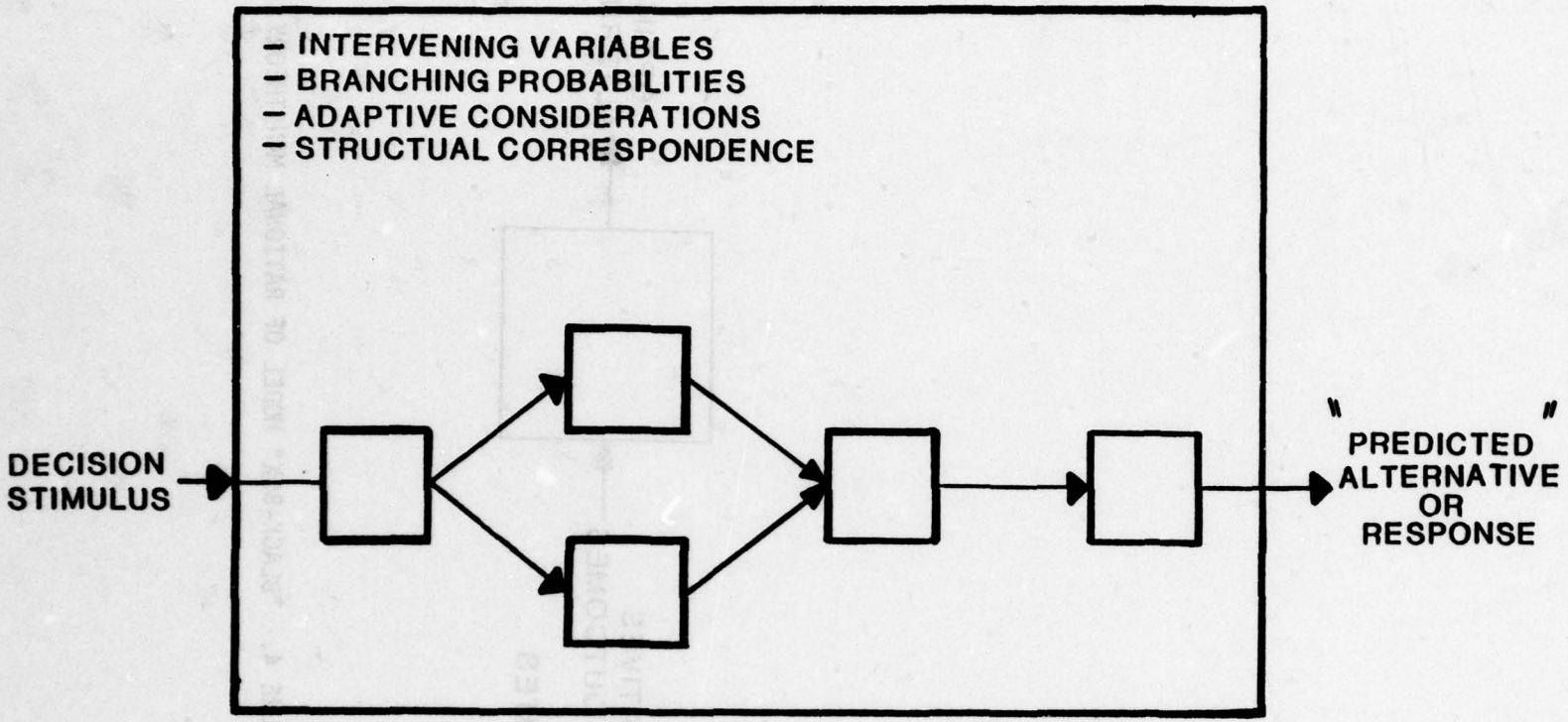

FIGURE 5. STRUCTURAL MODEL OF COGNITIVE DECISION-MAKING

output of the cognitive processing model is a prediction of the alternative or response selected. This is to be contrasted with the optimal alternative that is specified by the rational man models. The cognitive processing model prediction may in fact be optimal, but in general, it is an estimate of what he "does" and not of what he "should do."

While it could be argued that every system is a black box at some level, the key difference extends beyond the level of analysis. Network models involve certain primitive components (tasks or activities) which are organized to produce behaviors. These systems can be designed and hence can be embodiments of rational structures. The rational man notions, however, usually don't examine such questions of realizability.

Both of these philosophies have been employed in man-machine modeling exercises. The rational man approach has been primarily advocated through the use of continuous state analytic models as represented by optimal control theory. The cognitive processing approach, on the other hand, has been frequently applied in discrete event network simulations. As can be expected, both have advantages and disadvantages in their application, and like most techniques, each is more suited to particular phases of a system than to others. These issues will be discussed in more detail in the following sections.

OPTIMAL CONTROL MODEL

The underlying assumption of the optimal control model is that the well-trained, highly-motivated controller will adopt an optimal response strategy, subject to the constraints on the accuracy with which he may observe state variables and process information. That is, he acts to minimize some performance criterion or cost function in view of its own

constraints. The criterion is usually stated as a quadratic function of error e and control effort u.

The system model is illustrated in Figure 6. The model includes representations of system dynamics, environmental disturbances, commands, the display system, and the "optimal-control model" for the human operator. The system dynamics are comprised of the linearized dynamics of the controlled element and any dynamics associated with measurement, control and display systems (also linearized). The equations for these dynamics are expressed in the state-variable form:

$$\dot{\underline{x}}(t) = A\underline{x}(t) + B\underline{u}(t) + E\underline{w}(t), \tag{1}$$

where $\dot{\underline{x}}(t)$ is the n-vector which describes the state of the system, $\underline{u}(t)$ is the r-vector of human control inputs, and $\underline{w}(t)$ is a vector of white Gaussian noise processes.

The display variables are assumed to be linear combinations of the state and control variables and are given by the m-dimensional "display vector":

$$\underline{y}(t) = C\underline{x}(t) + D\underline{u}(t). \tag{2}$$

The matrices, A, B, C, D, and E may be constant corresponding to a given fixed condition, or they may vary with time to reflect changing dynamics or displays.

Both random and deterministic disturbances may be treated, although validation data are most extensive for random inputs. If the external forcing functions are rational noise spectra of first order or higher, as is the case, for example, for most air turbulence models, they are represented by white Gaussian noise ($\underline{w}$) passed through a linear filter. In such a case, "input states" are augmented to the systems state and

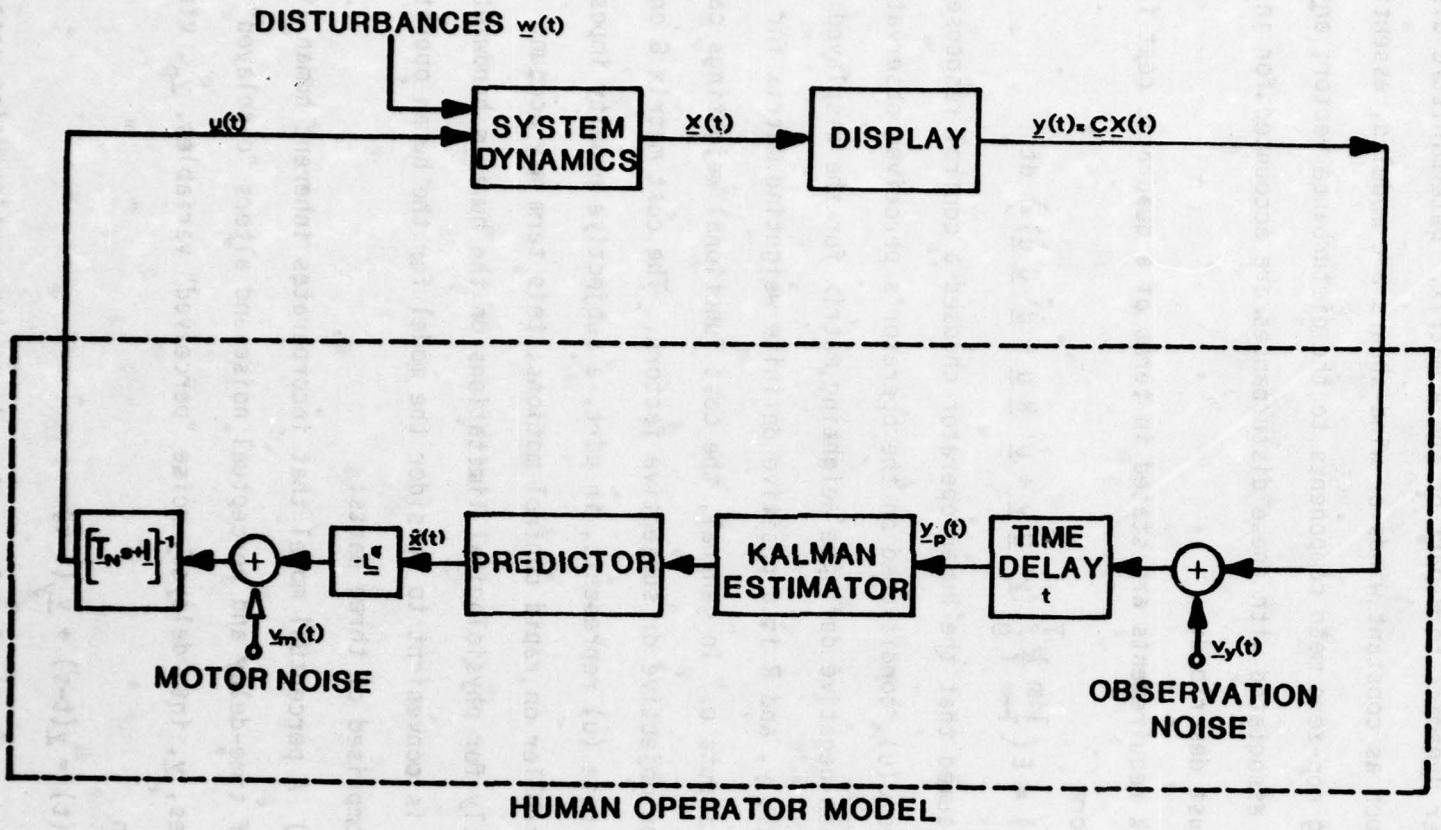

FIGURE 6. OPTIMAL CONTROL MODEL STRUCTURE

the filter dynamics form part of the A matrix. Deterministic disturbances such as constant winds or wind-shears are modeled, essentially, by adding non-zero mean components to the disturbance vector; any dynamics associated with these disturbances are accounted for in the manner just described.

Task requirements are stated in terms of a quadratic cost function of the form

$$J(u) = E\left\{ \lim_{T\to\infty} \frac{1}{T} \int_0^T (\underline{y}' \underline{Q} \underline{y} + \underline{u}' \underline{R} \underline{u} + \dot{\underline{u}}' \underline{G} \dot{\underline{u}}) \right\} dt \qquad (3)$$

It is assumed that the human operator chooses a control response that minimizes J(u), conditioned on the operator's perceived observations. Q is a non-negative definite weighting matrix for the displayed variables, y, and R is a positive definite weighting matrix for the control inputs u. In general, the cost functional weightings can depend on objective or subjective factors. The cost matrix G on control-rate ($\dot{u}$) represents, in part, a subjective penalty imposed by the controller on rapid control motions; this term may account indirectly for physiological limitations on the human's bandwidth.

It is convenient to consider the model for the human operator as being comprised of three parts:

(1) A perceptual model that incorporates inherent human limitations of time-delay and perceptual noise and alters "displayed" variables, $\underline{y}$, into delayed, noise "perceived" variables, $\underline{y}_p$, via the relation

$$\underline{y}_p(t) = \underline{y}(t-\tau) + \underline{v}_y(t-\tau) \qquad (4)$$

where τ is perceptual delay and $\underline{v}_y$ is an observation noise vector.

(2) A "motor" or output model that accounts for possible "bandwidth" limitations of the human and the inability to generate perfect control responses, by transforming "commanded" controls, $\underline{u}_c$, into "actual" control inputs, u, via the relation

$$\underline{T}_N \dot{\underline{u}} + \underline{u} = \underline{u}_c + \underline{v}_m \tag{5}$$

where $\underline{T}_N$ is a "neuro-motor" lag-matrix and $\underline{v}_m$ is a motor-noise vector.

(3) An estimation and control-command generation process, consisting of a Kalman filter, a least mean-squared predictor and a set of "optimal gains" L* (see Figure 6), that models human information processing and compensation behavior.

The time delay, observation noise, motor noise, and, to some extent, the "neuro-motor" lag parameters of the model represent inherent human limitations that cannot be optimized. Numerical values for these parameters (or rules for obtaining such numerical values) must be decided prior to the analysis on the basis of past data or adjusted in an iterative scheme to match human response characteristics in a particular situation.

The observation noise, $\underline{v}_y$, and the motor noise, $\underline{v}_m$, are lumped representations of human randomness that account for the combined effects of random perturbations in response characteristics and parameters as well as for errors in observation and execution. From the standpoint of classical describing function theory, the observation and motor noises may be thought of as a model for human controller remnant.

Sheridan (1974) expounds on why the idea of an optimal model is attractive. "It assumes that the human operator, when sufficiently

trained, is familiar with his own dynamics, with the controlled process dynamics, with the statistical nature of his own variability and that of the external disturbances, and with the criterion describing the best control, i.e., the tradeoff between error and control effort. Thus, if the human operator is intelligent, it is plausible that he will attempt to behave optimally to the best of his ability to perceive and remember signals and produce the best control responses."

One can readily see the correspondence of the optimal control model (OCM) with the rational man approach. The OCM is indeed a normative model in which "optimal" controller strategy is prescribed. The rational man utility function concept is represented by the quadratic cost function to be optimized. A review of the background and the current literature of the OCM follows.

The theory of the optimal controller is not a new one. Elkind (1956) made use of Wiener's optimization theory. Leonard (1960) and Roig (1962) found that the mean-square error from human tracking data approximated the mean-square error of various optimal controllers. The first large-scale attempt at using optimal control theory to model the human controller was initiated by Elkind, et al. (1968). Their study demonstrated the feasibility of predicting control characteristics and display requirements by systems analysis techniques based on optimal control. What is essentially the current structure of the OCM was first proposed by Baron and Kleinman (1969).

The OCM has been successfully applied and demonstrated for a number of different systems. Kleinman, Baron, and Levison (1970) showed that the model could be used to predict performance in three basic tracking

tasks involving a range of control strategies. Excellent agreement between experimental data and model predictions of describing functions, remnant spectra, and state and control variances was obtained. Baron and Kleinman (1971) applied the model to study the human's precision control of a hovering VTOL-type vehicle. The results were compared with experimental simulator data, and showed excellent correlation in most cases. Kleinman and Baron (1971) analyzed a piloted approach-to-landing task to evaluate pictorial display requirements. The model and data agreements were again excellent and demonstrated the model's ability to predict the time-varying adaptability of a pilot to updraft disturbances.

Several extensions of the model have also been made. Levison, et al. (1971) developed a mechanism for predicting task interference in multi-variable tasks (not involving scanning) and for estimating the relative attentional workload associated within a given task. This fractional attention model formulation of the OCM has also been applied more recently in performing display monitoring (Kleinman and Curry, 1976) and display analysis (Baron and Levison, 1977). Baron and Levison (1974) applied the OCM to data obtained from a simulated anti-aircraft tracking task. This application demonstrated the capability of incorporating a time-varying model. A number of additional applications and studies have been made employing the OCM. A more complete discussion of the background, applications, and concepts can be found in an article by Baron (1976).

The strengths of the optimal control approach for modeling man-machine systems are quite impressive. Its formal and robust

mathematical structure is a particularly important attribute and is especially amenable to engineers familiar with the state space differential equation modeling of dynamic systems. The goal-oriented assumption of controller behavior is attractive and tractable for the well-trained highly motivated operator. Probably most importantly, in numerous case studies the OCM has the distinction of being demonstrated as a highly useful tool for the design and analysis of man-machine tracking tasks and other closed-loop systems.

There are, however, some severe limitations to the optimal control approach, especially in light of the trend towards the more supervisory, planning, and information processing role of the human operator. Baron and Levison (1977) state that "more work is required to treat the operator in monitoring and managerial tasks (supervisory control)." Certainly the requirement of a continuous state environment is a severe restriction. Many man-machine tasks do not meet this structural condition.

Another limitation of the OCM that would apply in multi-task supervisory systems is the assumption of continuous (or periodic) sampling of state variables. Because the operator is now performing other discrete activities such as radio communications, information display storage and retrieval tasks, etc., he is no longer in the position of being able to afford continuous monitoring of his displays. Previous applications of the OCM have assumed continuous updates of all states variables simultaneously. (Levison, et al. (1971) assumed that

if a variable was not viewed directly it was minimally viewed peripherally and simply imposed a higher noise term on those state variables.)

Although it has not been applied in this manner, the OCM formulation is flexible enough to accommodate asynchronous interruptions for the performance of discrete tasks. However, its structure does not allow one to explicitly model cognitive processing and discrete event tasks. These tasks are much more amenable to representation by network model formulations as will be discussed later in more detail.

The optimal control approach does not purport to model in detail or explicitly (structural correspondence) operator behavior and variabilities. Rather, the OCM tends to lump those aspects of human behavior which are poorly understood or which cannot be explained by the basic model formulation into the remnant term. This philosophy is best described by an excerpt from Kleinman, et al. (1970):

> Controller remnant is taken to be the component of human response that is unpredictable in other than a statistical sense. It is assumed that the various sources of inherent human randomness are manifested as errors in observing system outputs and executing control inputs.

This assumption of operator behavior being modeled as "noise" terms is unacceptable in systems where these behaviors comprise a large percentage of the operator's activities and which play an active role in determining system performance. These behaviors quite often exhibit the critical system design parameters and we can no longer afford to simply represent them as noise.

The assumption of linearity is also of question in supervisory systems. Linearity is usually interpreted to mean superposition, that

is, linear combinations of inputs imply linear combinations of outputs. Because of the number of discrete asynchronous events, this is hard to conceptualize in the supervisory control situation.

Moray (1976) discusses another problem with Optimal Control models in that they are based on long-term averages and do not describe momentary fluctuations in performance. Most stable control systems are designed to rapidly damp the effects of transients, and long-term average statistics will not show much evidence of their existence. This is an especially severe limitation in applying the model to systems such as DAIS where it is expected that there may be drastic performance decrements over short periods of time which could be extremely significant but which may not show up in overall mission scores.

Another problem confronting this approach is the uncertainty as to what the operator's internal subjective criterion is. Also, what is optimal with respect to a particular cost functional and set of parameters is apt also to be optimal with respect to another criterion and parameter set. Sheridan (1974) suggests that more research is needed in this area and that in the meantime one should rely on "plausibility" arguments. This problem is symptomatic of all models in which there is little or no structural correspondence between the model and the system being represented. The task environment cannot have much say about criterion when this model is used. In this case math technicalities are directing the modeling, not problem substance.

DISCRETE NETWORK MODELS

A second approach to modeling manned systems is discrete or event-oriented simulation and is often represented by a network formulation. In this method operator actions and system status changes do not occur continuously, but rather are in discrete time and state increments. Discrete event simulation is highly suited for modeling those actions which occur on an occasional or an aperiodic basis, and includes such operations as performing communication tasks, selecting a given radio frequency, setting switches, etc. (Fishman, 1973; Zeigler, 1976). A discrete modeling approach is also ideal for representing the cognitive and decision-making processes employed by the human operator. Operations where a sequence or a hierarchy of activity occurs are particularly well suited to the discrete approach.

A sequential, task-analytic approach to modeling man-machine systems has been advocated in the Siegel-Wolf model (Siegel and Wolf, 1969). Task performance times and branching probabilities are the basic parameters of the model. The model has been applied with good results a number of times. In one study (Siegel, Wolf, and Ollman, 1962) the model was used to analyze Apollo vehicle operator actions and information exchanges. More recently, Bauerschmidt (1976) employed this approach to compare performance times using an integrated control/display design to times exhibited when employing conventional designs.

Network modeling and simulation techniques have been employed in a wide variety of man-machine system analysis efforts. Wortman, et al. (1976) employed network techniques for evaluating system alternatives for a Remotely Piloted Vehicle/Drone Control Facility (RPV/DCF) in

which operators monitor and control the flight of RPV's through the use of visual displays and keyboard entry systems. These techniques have also been used by Purdue University researchers to investigate the effects of higher degrees of automation, different capacities of process limiting operations, and alternative task allocations on the operator's idle times in a hot strip mill (Maltas and Buck, 1975). The Army Research Institute employed task network models to analyze human system performance in an AN/TSQ-73 guided missile air defense system operation (Wortman, Hixson, and Jorgensen, 1978). The Air Force Human Resources Laboratory utilized network simulation techniques for evaluating human performance effects on nuclear systems safety in a missile loading operation (Askren, et al., 1976). The Aerospace Medical Research Laboratory is developing network simulation models to analyze design proposals in a B-52 strategic navigation system involving complex crew activities and task management (Chubb and Berisford, 1977).

Simon (1957) makes a case for employing psychological theories of perception and cognition in describing behavior:

> . . . The analysis set forth here casts serious doubt on the usefulness of current economic and statistical theories of rational behavior as bases for explaining the characteristics of human and other organismic rationality. It suggests an alternate approach to the description of rational behavior that is more closely related to psychological theories of perception and cognition, and that is in closer agreement with the facts of behavior as observed in laboratory and field.

Network models have been employed in representing numerous psychological theories (Jacobs, et al., 1973). For example, Randolph and Ringeisen (1974) employed network techniques to analyze the teaching-learning process. Hann and Kuperman (1975) developed a network model

of the theoretical stages of a choice reaction time task. Teichner (1976) compared the theoretical human performance predictions of an information processing task with empirically derived performance data using network techniques. Excellent correspondence was achieved.

Network type models of human performance have been employed by disciplines other than psychology or human factors; for example, the artificial intelligence models developed in computer science. In the preface of his text, Kantowitz (1974) notes that traditional control theories are used in psychology primarily for skill tasks, while theories of cognition tend more toward the types of theories used in computer science, e.g., automata theory.

Perhaps one of the most important aspects of the network structure is its flexibility in representing dynamic decision processes as a result of changes in system status. Decision functions need not be specified a priori, but rather may be designated as a function of on going events. Thus, dynamically changing control strategies, sampling behaviors, and communication activities may all be represented in realistic fashion via network models. Rare events and emergency conditions can also be modeled, along with the corresponding operator response behavior. Peak loads and performance decrement statistics can now be established; whereas, in the OCM most of this behavior would have been "averaged out."

However, network models are not without problems. The major problem is the nonavailability of generic performance models and behavioral data. The model may be richer than data available or experimentally obtainable. Seldom are experimental results reported

in a fashion that allows one to generalize beyond the specific system under study. See Pew, et al. (1977) for a more detailed discussion of psychological performance models and issues.

Another problem in considering this approach for modeling the DAIS system is that, while it appears ideal for representing discrete activities, the effectiveness of network representations in modeling continuous tracking tasks has never been demonstrated. (While Kuperman, et al. (1975, 1977) successfully employed network techniques in modeling the DAIS system, the continuous control task was only superficially treated.)

DISCUSSION

Obviously, neither of the two modeling approaches is adequate within itself for modeling the type of complex, interactive systems represented by DAIS in which both types of behavior (continuous and discrete) are required. Nor can these techniques be used as they stand to study the design implications of different sampling rules, different operational strategies, and task priorities. In addition, these methods are not individually capable of representing the perceptual and decision-making aspects of the psychomotor tasks of concern, since these processes involve the simultaneous performance of both continuous and discrete operations.

Singleton (1976) sums up fairly well the dilemma in choosing a modeling approach:

> Theoretically we feel more secure when we are able to use a rigorous mathematical approach but, at present, the available mathematics are tiresomely complex and yet inept as descriptors and predictors of supervisory performance. On the other hand, to use the flexibility of verbal methods is to invite ambiguity and difficulties of communications.

It is proposed that an approach which combines components of discrete event network models with an open-loop optimal control model be explored in an attempt to take advantage of the strengths of both approaches, while eliminating or reducing many of their weaknesses. In this approach, the continuous state (flight control display) sampling interval would be a dynamic function of system status and other operator demands. Various sampling rules and priority configurations could be investigated. Also, the timing and sequencing of discrete events would be influenced by the control status of the system. Models which attempt to capture the parallel or simultaneous performance activities of the human controller can also be examined under this combined technique.

Combined discrete/continuous simulation approaches have been utilized in the past. However, while the vehicle dynamics have been represented in a continuous fashion, the operator is modeled in a strictly discrete state mode as compared to the combined discrete/continuous mode proposed here. An example of such a model is an air-to-air refueling simulation in which a receiver aircraft is being refueled from a tanker aircraft. The pilot's operational tasks of instrument panel scanning and aircraft velocity control are modeled as

discrete state events. The vehicle dynamics of both the tanker and receiver aircrafts are represented as differential equations (Wortman, et al., 1974).

A summary of the structure of the combined simulation model that was developed, the sampling rules and priority schemes to be exercised, and the expected results and possible implications of applying a combined approach such as this are discussed on the following pages.

COMBINED SIMULATION MODEL STRUCTURE

Two basic maneuver types out of the seven employed in the DAIS real-time simulation have been simulated: straight and level flying and a turning dive. These are considered to be the easiest and hardest flight maneuvers, respectively. An open-loop closed-loop control model for these maneuvers based on the flight equations employed in the DAIS simulation has been developed. Conventional optimal control models, in which the pilot is assumed to be sampling system status variables continuously (or periodically in the discrete time case), are termed "closed-loop" models. The proposed model differs from that above in that system status sampling is not necessarily continuous nor periodic, due to the secondary multifunction keyboard tasks imposed upon the pilot. Therefore, the pilot reads the system status displays only as time permits and operates in a so-called "open-loop" preprogrammed fashion between sampling.

Figure 7 depicts the structure of the open-loop closed-loop control system. The pilot must encode and process information from flight control displays, multipurpose displays, and exogenous events such as

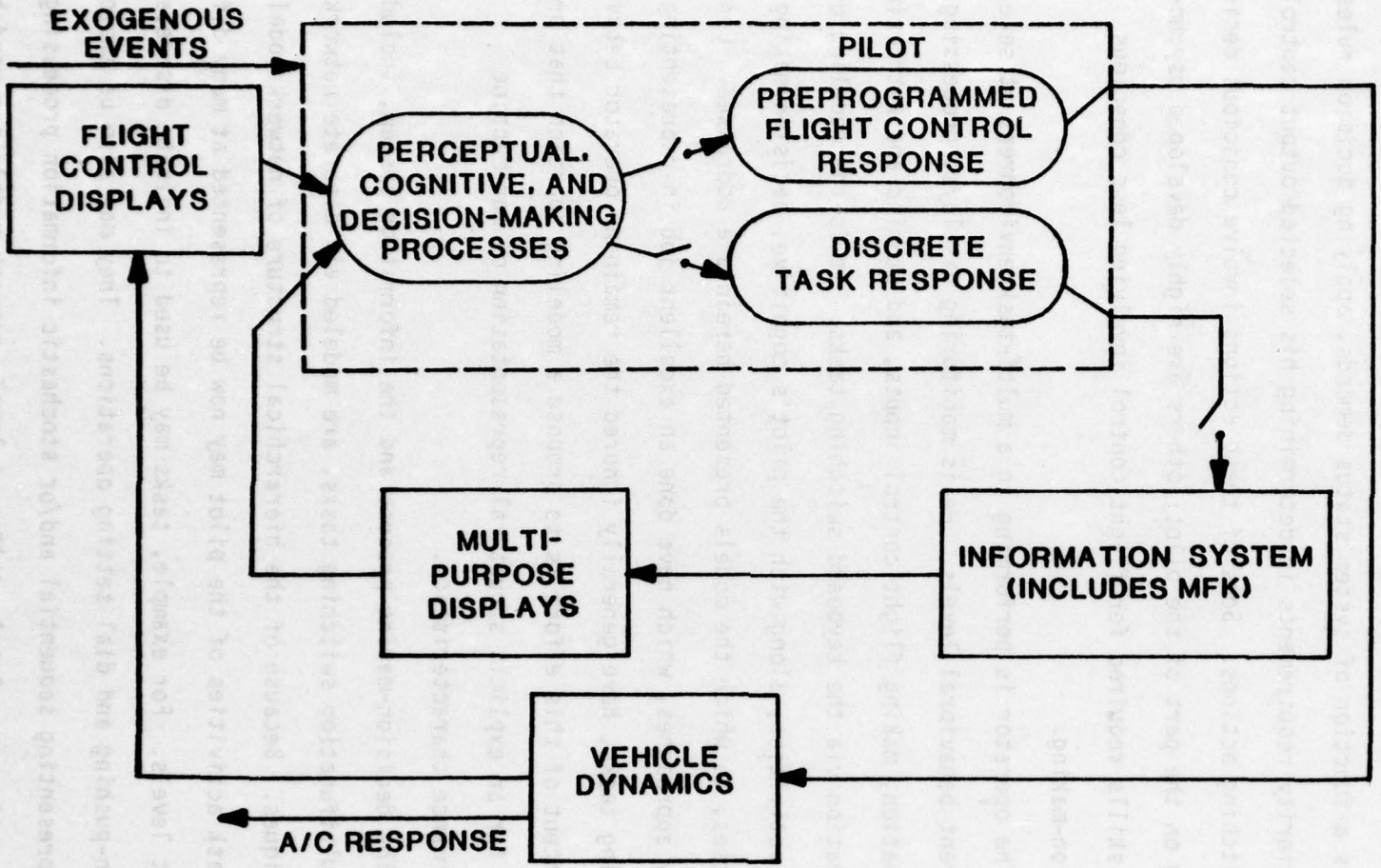

FIGURE 7. OPEN-LOOP CLOSED-LOOP CONTROL SYSTEM STRUCTURE

audio switching instructions. The pilot then evaluates this information as a function of system status demands, applying decision rules and priority requirements in determining his selected output control or switching actions. Some of these actions involve conscious decision-making on the part of the pilot; others are highly developed psychomotor skills required for flight control involving less conscious decision-making.

The operator is performing in a multi-task environment at several different behavioral levels. He is monitoring displays, processing information, making flight control inputs, and storing and retrieving information via the keyboard switching tasks. It is the modeling of these activities, along with the pilot's cognitive, decision-making processes, to which the models presented herein are addressed. Control theory approaches, which have done an excellent job in representing tracking tasks, have generally ignored the remaining operator behaviors. The intent of this effort is to propose a modeling approach that provides for an explicit structural representation of man-machine performance characteristics.

The decision-making process and the information system, including the multifunction switching tasks, are modeled via discrete network techniques. Because of the hierarchical structure of network models, the task activities of the pilot may now be represented at many different levels. For example, tasks may be used to indicate discrete button-pushing and dial setting operations. They may also be employed in representing sequential and/or stochastic information processing models. On a completely different level, network models are used here

to achieve desired state variable sampling intervals and priority schemes. The network structure is designed to operate at many different levels simultaneously and thus is capable of representing sophisticated man-machine system behaviors. In its application here, the network also serves a supervisory role in interfacing with the open-loop optimal control model representation of the pilot's tracking task. These two modeling approaches are meshed together to form a combined discrete network-continuous optimal control model of the human operator.

GOALS AND OBJECTIVES

The focus of this endeavor is the exploration of the feasibility of a combined simulation approach for man-machine modeling. In the context in which it is being investigated, this technique is expected to be valuable in describing total system performance, in evaluating different model formulations, and in exhibiting tradeoffs between strategies employed. One goal of this effort is the identification of strengths and weaknesses of the given approach that surface during the course of this examination.

Besides the obvious design implications, it is anticipated that this approach to simulation could have a great impact upon experimental procedure and protocol. The exploration of new and varied flight control strategies and operating procedures could yield fresh insights into performance. The system under consideration is especially amenable, since the particular combination of flight control and information retrieval tasks is a new one. Therefore, the operating

procedure and flight strategy taught in subject training are "best guesses" rather than tried and true performance standards.

To conclude, this endeavor in combined simulation is but an initial attempt to explore the feasibility and appropriateness of applying such an approach to man-machine systems. The results of this research will not allow one to accept or to reject this technique, but rather, will offer insight as to its possible utility and effectiveness.

The following chapter describes the DAIS real-time man-in-the-loop experiment which provides the data base and a baseline scenario for the construction of the combined simulation model.

DAIS MAN-IN-THE-LOOP STUDY: PROCEDURES AND RESULTS

This chapter describes the real-time man-in-the-loop DAIS experiment in sufficient detail for the reader to understand the basic task requirements and flight conditions. It also presents summary statistics of the results of the study. These results, coupled with the scenario and procedures of the experiment, provide the structure for the baseline simulation model development.

DESCRIPTION OF EXPERIMENT AND PROCEDURES

Seven different maneuvers were employed in the flight control task. They are identified in terms of command flight parameters as defined in Table 1.

TABLE 1
BASELINE FLIGHT CONTROL MANEUVERS

Maneuver	Altitude (ft)	Velocity (kt)	Vertical Velocity (ft/min)	G-Load
1 - straight and level	20,000	500	0	1.0
2 - left turn	30,000	500	0	1.5
3 - right turn	30,000	500	0	1.5
4 - turning dive	--	500	-2500	1.5
5 - stall	20,000	240	0	1.0
6 - turning ascent	--	500	2500	1.5
7 - high-g turn	30,000	600	0	3.0

The subjects were instructed to "maintain" these parameters for the duration of the mission (approximately 200 secs.). Flight control was scored as a function of the difference between the desired control parameters and the actual ones. These "delta" (Δ) values were computed

every 200 milliseconds. The flight parameters on which scoring was based were chosen through consultation with pilots and other researchers who were able to specify on an experiential basis the minimum number of significant parameters for each mission, and the importance of a given amount of error in each parameter. Working from this basis, a combinatorial formula was derived for each maneuver (Woodruff, 1972). The specific formulas chosen for the maneuvers used in this study are presented in Table 2.

TABLE 2
MANEUVER PERFORMANCE SCORES

Straight and Level Flying	(.01) Δ altitude + (.1) Δ speed
Dive/Climb	(.005) Δ vertical velocity + (.1) Δ speed
Diving/Climbing Turn	(.005) Δ vertical velocity + (.1) Δ speed + Δ g-load
Level Turn	(.01) Δ altitude + (.1) Δ speed + (1.1) g-load

NOTE: Δ represents the mean absolute error from the command value.

Four levels of task difficulty were utilized for the MFK switching tasks, which required approximately 4, 6, 8, or 12 push-button switch actions per task. The MFK task was scored on the basis of correct completion of the switching sequence, total time required for correct completion, and time per switch action.

Three different configurations were considered: flight control alone, MFK alone, and the combination of flight control with switching. Four college students served as subjects for the experiments. Each received approximately 40 hours of training on the primary flight control task and at least 20 hours of training on both the secondary MFK and combined tasks. In every case, training was to asymptotic performance.

In the flight control alone segment, there were 28 trials per subject -- four for each of the seven maneuvers. At the beginning of a trial the subject was told which maneuver he was to fly, including the flight parameter values to be maintained. Then he was allowed to "fly" the simulated aircraft until he was confident he was prepared to start the maneuver, which he indicated by pulling a trigger on the control stick, designated as the "hotswitch." At that point a 200-second trial began with automatic scoring and termination by the supporting computer program. There were 30-second intervals between trials.

In the MFK task alone, each subject was also given 28 200-second trials. There were seven trials for each of the four levels of MFK difficulty investigated. Thirty-second rest intervals separated trials. Four different MFK tasks of the given difficulty level were performed during each trial period. The subject received pre-recorded instructions via his earphones concerning the task he was to perform. The instructions were followed by a tone which was the signal to start the MFK task. The subject depressed a "stop" button on the left side panel to the right and ahead of the throttle, to indicate he had completed the MFK task. The experimenter monitored the duplicate displays at his station to ascertain the correctness of subject action on the MFK.

The combined flight control with MFK session was identical to the flight control single task condition except as follows. Thirty seconds after the subject's signal that he was ready for scoring of the flight maneuver to start, the recorded instructions for the first MFK task were presented. Thus the flight control and MFK single task scenarios were "overlayed" so that each subject had to divide his attention

between them throughout the standard 28 200-second trial periods. The subjects were instructed to give first priority to flight control. A more detailed description of the procedures can be found in Crawford, et al. (1978) and Brandt (1974).

A presentation and discussion of the analysis of the DAIS MFK experiment are provided by Berisford (1975). The appropriate portions of this effort will be summarized here.

ANALYSES AND RESULTS

Flight Control Performance

The simple flight control scores were subjected to a one-way analysis of variance using a within-subjects (or repeated measures) design. Significant differences between maneuvers were found and further analysis was performed to determine which means were significantly different. The results of the analysis suggest that flight control scores for maneuvers 1, 2, and 3 (straight and level, left and right turns) are significantly different from maneuvers 4 and 6 (turning dives and ascents). The flight control scores for maneuvers 5 and 7 (stall and high G turn) were not statistically significantly different from flight control scores obtained in any of the other maneuvers.

The maneuvers were grouped into two classes. The first group of maneuvers is composed of maneuvers 1, 2, and 3, and the second group is composed of maneuvers 4 and 6. Scheffe's S was computed to determine if flight control scores were significantly different for these two maneuver groups. The results provided the basis for dealing with the flight control data in subsequent analyses and comparisons in terms of

two levels of task difficulty, "easy" and "difficult." Means and standard deviations of performance scores for the two levels are shown in Table 3.

TABLE 3
FLIGHT CONTROL PERFORMANCE: SINGLE TASK CONDITION

	Weighted Error Score	
	Mean	SD
Easy Flight Control	1.09	.17
Difficult Flight Control	5.11	1.51

Multifunction Keyboard Task Performance

A one-way analysis of variance was performed on the time scores for the simple MFK switching task (see Table 4), and differences were found between the levels of task difficulty. A test for linear fit indicated that the relationship between the number of switch actions required for a task and the total time required for its correct execution accounted for 88 percent of the variability in the data.

TABLE 4
MFK PERFORMANCE: SINGLE TASK CONDITION

MFK	Task Time (Sec.)	
Difficulty	Mean	SD
I	3.97	.32
II	5.95	.53
III	7.43	.68
IV	9.87	.83

Combined Flight Control with MFK Performance

The dual task was submitted to a similar analysis. The same grouping of maneuvers, by difficulty, was observed. Although mean flight control error was greater when the flight control task was

combined with MFK tasks, the differences were not statistically significant. Crawford (1978) suggests that this is probably due to the small number of subjects (4). The data are summarized in Table 5.

TABLE 5
WEIGHTED ERROR SCORES FOR FLIGHT CONTROL ALONE AND WITH MFK

	Condition	
	Single Task	With MFK
Easy Flight Control	1.09	1.92
Difficult Flight Control	5.11	5.85

Similarly, MFK task times generally increased under dual task conditions, although the differences were not statistically significant. MFK task time mean and standard deviation statistics are presented in Table 6.

TABLE 6
MFK TASK TIMES (SECS.) FOR MFK ALONE AND WITH FLIGHT CONTROL

MFK	Single Task		With Flight Control	
Difficulty	Mean	SD	Mean	SD
I	3.97	.32	4.63	1.78
II	5.95	.53	7.36	2.67
III	7.43	.68	9.65	3.35
IV	9.87	.83	12.49	3.89

Table 7 contains a more detailed breakdown of the individual push-button times for each subject and MFK difficulty level.

TABLE 7

INDIVIDUAL MULTI-FUNCTION KEYBOARD SWITCHING
TASK TIME STATISTICS (SECONDS)

	MFK DIFFICULTY LEVEL				POOLED OVER MFK LEVELS
	1	2	3	4	
SUBJECT 1	$\bar{x}$= .98 σ= .33	$\bar{x}$=1.13 σ=1.13	$\bar{x}$=1.04 σ=1.16	$\bar{x}$=1.08 σ= .83	$\bar{x}$=1.06 σ= .96
SUBJECT 2	$\bar{x}$=1.20 σ= .88	$\bar{x}$=1.14 σ=1.09	$\bar{x}$=1.37 σ=1.35	$\bar{x}$=1.34 σ=1.23	$\bar{x}$=1.33 σ=1.19
SUBJECT 3	$\bar{x}$= .84 σ= .53	$\bar{x}$= .99 σ= .56	$\bar{x}$=1.03 σ= .65	$\bar{x}$= .86 σ= .73	$\bar{x}$= .94 σ= .65
SUBJECT 4	$\bar{x}$= .95 σ= .95	$\bar{x}$= .96 σ= .91	$\bar{x}$=1.01 σ= .77	$\bar{x}$= .94 σ= .60	$\bar{x}$= .97 σ= .77
					OVERALL STATISTICS
POOLED OVER SUBJECTS	$\bar{x}$=1.00 σ= .76	$\bar{x}$=1.33 σ=1.19	$\bar{x}$=1.11 σ=1.03	$\bar{x}$=1.06 σ= .91	$\bar{x}$=1.08 σ= .93

CONTROL MODEL FORMULATION

MATHEMATICAL MODEL OF AIRCRAFT DYNAMICS

General mathematical models of the dynamics of an aircraft moving through the atmosphere have been developed for use in simulations and design of aircraft control systems (e.g., Etkin, 1972, and Fogarty and Howe, 1969). For purposes of this analysis, the aircraft is modeled by the simplified equations for aircraft dynamics employed in the DAIS real-time man-in-the-loop studies. This aircraft model was derived as a first attempt to provide a fairly reasonable and realistic task to relatively naive subjects. For non-flyers it is a demanding task and believable. For flyers and knowledgeable engineers, the simulation is anything but real and represents an expedient compromise to obtain a workable set up for controlled, laboratory experiments. Despite these drawbacks, the components of this task reflect representative man-machine issues and the required operator workload is realistic.

Assumptions

The following assumptions apply to the aircraft model incorporated in the simulation:

- The aircraft is traveling at a speed less than MACH 3.
- The thrust vector is aligned with the fuselage reference line.
- The vehicle is a rigid body having a plane for symmetry, i.e., the right side of the aircraft is configured the same as the

left (i.e., same size, weight, and shape of components and attachments -- fuel pods, weapons, etc.).*

- The atmosphere is at rest relative to the earth, i.e., the wind is zero.
- The earth is considered a plane fixed in space, i.e., a flat earth.
- The reference axes are a north, east, and down system fixed to the earth.
- The side-slip angle is neglected, i.e., assumed to be zero.
- The aircraft is assumed to be a point mass, in that moments of inertia are ignored.
- The rate of change of roll angle is approximately proportional to stick position.
- The equations describing angular acceleration are neglected.
- The rate of change of the angle of attack is approximated as being proportional to stick position plus a term due to lift.
- The reference frame for the aircraft is a combined wind and body axes system.
- The rudder is automatically set to give coordinated turns.

Under the assumptions given above, the very complicated set of equations for aircraft dynamics given on pages 149-150 of Anderson and Moore (1971) reduce down to the simplified set of equations used in the simulation. Generally, these assumptions are valid for the mission

---

* While this is true in many cases, it may not be true for some segments where a weapon releases from one wing but none from the other.

segments considered since the aircraft flights are over short distances and at relatively low speeds. Figures 8 and 9 show the notation for the angles, forces, and associated reference frames for the aircraft.

The Aircraft Model

The resulting set of simplified equations for the aircraft dynamics are:

$$\dot{x} = v \cos\gamma \cos\psi \tag{1}$$

$$\dot{y} = v \cos\gamma \sin\psi \tag{2}$$

$$\dot{z} = v \sin\gamma \tag{3}$$

$$\dot{\phi} = u_2 \tag{4}$$

$$\dot{\psi} = \frac{L \sin\phi}{m\, v \cos\gamma} \tag{5}$$

$$\dot{\gamma} = \frac{L \cos\phi - W \cos\gamma}{m\, v} \tag{6}$$

$$\dot{\alpha} = u_1 + (L/W - 1)\ (AL1) \tag{7}$$

$$\dot{v} = \frac{u_3\ (MT) \cos\alpha - D - W \sin\gamma}{m} \tag{8}$$

where u_1 is functionally related to the pilot's pitch input (fore-aft stick movement),

u_2 is functionally related to the pilot's roll input (side-to-side stick movement),

and u_3 is functionally related to the pilot's throttle settings.

The variable AL1 takes on two values:

$$AL1 = \begin{cases} \frac{-K}{MAXG}, \text{ for } \frac{L}{W} \geq 1 \\ \\ \frac{+K}{MING}, \text{ for } \frac{L}{W} < 1 \end{cases} \tag{9}$$

L	=	Lift	α	=	Angle of attack	ψ	= Heading angle
D	=	Drag	γ	=	Flight path angle	ϕ	= Roll angle
V	=	Velocity	m	=	Mass of the aircraft	g	= Gravitational constant (32 ft./sec.^{2})
MT	=	Maximum thrust	w	=	Weight of the aircraft		

X
Y
-Z
} = Earth fixed coordinates

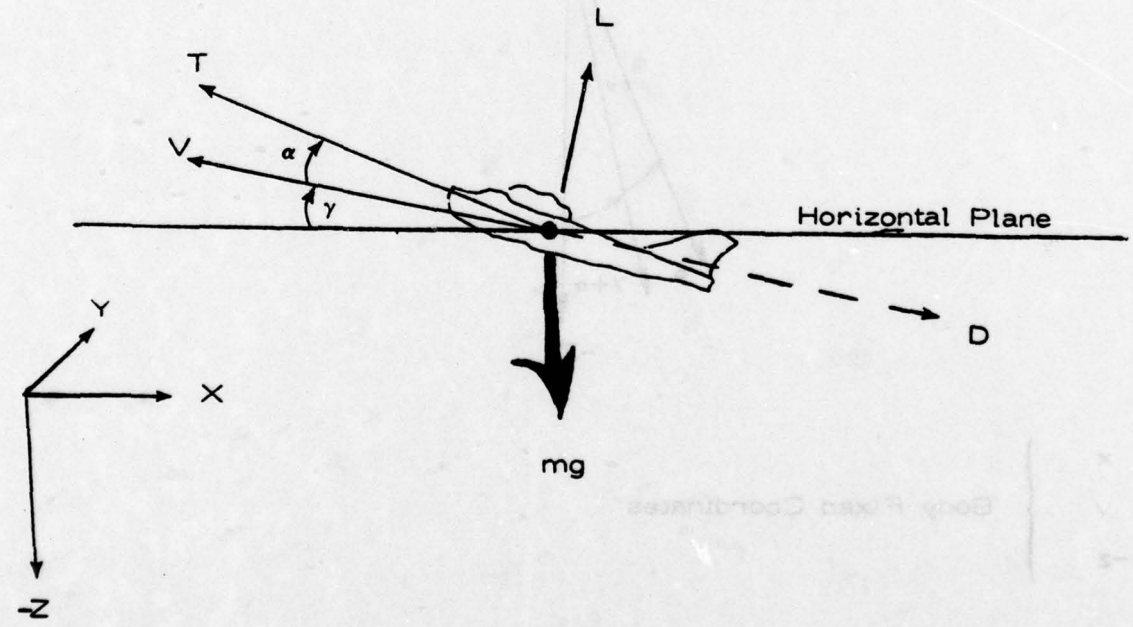

FIGURE 8. AIRCRAFT REFERENCE FRAMES

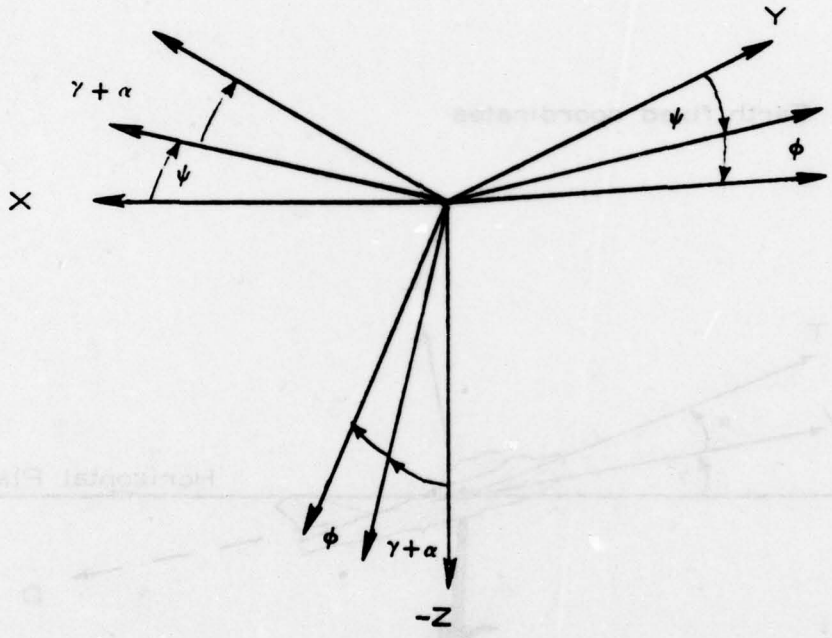

x
y
-z
} Body Fixed Coordinates

FIGURE 9. CONVENTIONAL AIRCRAFT EULER ANGLES

where K is a scaling parameter which is used to specify the aircraft pitching rates with respect to the lift to weight ratio. It has been assigned a value of 0.9. MAXG refers to the largest allowable positive acceleration; MING refers to the largest allowable negative acceleration. Chosen properly, MAXG (+15) and MING (-5) prevent the execution of "impossible" turns, dives, and climbs. The maximum thrust is given by:

$$MT = [A_{MT} (2327. + 0.172\ z - 0.0000031\ Z^2) \frac{v}{SS} + 11500. - 0.25\ z] \quad (10)$$

where

$$A_{MT} = \begin{cases} 2, \text{ if the afterburner is on} \\ \frac{1}{2}, \text{ if the afterburner is off} \end{cases}$$

and SS is the speed of sound which is a function of altitude.

The aircraft weight (W) is 17,000 lbs. or a mass (m) of 528 slugs. The drag force (D) is a function of the altitude, velocity, and angle of attack. The lift force (L) is a function of angle of attack, altitude, thrust, and velocity. Appendix B contains defining equations for the drag and lift forces.

The control variables (or inputs) for the model are u_1 (t) which controls the rate of change of the angle of attack and is proportional to longitudinal stick position, u_2 (t) which controls the rate of change of the roll angle and is proportional to lateral stick position, and u_3 (t) which is normalized percent throttle.

The state variables for the model are:

$z(t)$ = Altitude of aircraft (feet)

$\phi(t)$ = Roll angle (radians)

$\psi(t)$ = Heading angle (radians)

$\gamma(t)$ = Flight path angle (radians)

$\alpha(t)$ = Angle of attack (radians)

$v(t)$ = Velocity of aircraft (feet/second).

Appendix B contains a more detailed summary of these nonlinear state equations.

STATE SPACE FORMULATION OF AIRCRAFT EQUATIONS

This section contains the definition and derivation of the optimal control problem and its solution. The mathematics of this derivation involves a number of variable changes and transformations which the noninterested reader may wish to skim.

The Control Problem

The last section defined the nonlinear aircraft dynamics and pilot controls. Let $\underline{y}(t)$ be the vector of system state variables

$$\underline{y}(t) = \begin{bmatrix} z(t) \\ \phi(t) \\ \psi(t) \\ \gamma(t) \\ \alpha(t) \\ v(t) \end{bmatrix} = \begin{bmatrix} \text{altitude} \\ \text{roll angle} \\ \text{heading angle} \\ \text{flight path angle} \\ \text{angle of attack} \\ \text{velocity} \end{bmatrix} \tag{11}$$

and let $\underline{u}(t)$ be the vector of control inputs

$$\underline{u}(t) = \begin{bmatrix} u_1(t) \\ u_2(t) \\ u_3(t) \end{bmatrix} = \begin{bmatrix} \text{angle of attack} \\ \text{roll angle} \\ \text{throttle} \end{bmatrix} \tag{12}$$

Then the nonlinear system equation (1-8) can be summarized as

$$\dot{y}(t) = f(\underline{y}(t), \underline{u}(t)). \tag{13}$$

The solution to a nonlinear control problem is formidable and has been successfully employed in only a limited number of cases. Therefore, a linearized system representation will be utilized. The linearization process will be achieved by utilizing the nominal values for the state equation variables and parameters. Some values are set by the maneuver task definitions (see Table 1). Others are obtained by determining what is required for certain derivatives to be zero, i.e., steady state. The rationale for determining the nominal values for individual variables employed in the model follows. With the exception of altitude, the nominal and command values are identical.

1. Altitude (z_o)

The nominal values for altitude are based on the average initial values from the real-time man-in-the-loop DAIS experiment.

(SL) z_o = 18,130 ft.

(TD) z_o = 30,000 ft.

where SL indicates the straight and level maneuver and TD designates turning dive maneuver. The SL command value is also 18,130 ft. TD has a command value of 10,000 ft.

2. Velocity (v_o)

The nominal values are based on the task definitions and are defined for both maneuvers to be 500 knots/hour = 844.47 ft/sec.

3. Weight (W)

The weight of the aircraft is a constant 17,000 lbs.

4. G-load (g_o)

The g-load nominal values are defined by the maneuver command values.

(SL) $g_o = 1.0$

(TD) $g_o = 1.5$

5. Lift (L_o)

G-load (g) is a function of lift and weight

$$g = L/W. \tag{14}$$

Using the nominal value for g-load, a nominal value for lift can be expressed as

$$L_o = g_o W \tag{15}$$

(SL) $L_o = 17{,}000$ lbs.

(TD) $L_o = 25{,}500$ lbs.

6. Vertical velocity (vv_o)

Nominal values for vertical velocity are determined by the maneuver command values.

(SL) $vv_o = 0.0$ ft/sec.

(TD) $vv_o = -2500.$ ft/min $= -41.7$ ft/sec.

7. Density (ρ)

The equation for density is defined in Appendix B to be

$$\rho = .002378 \left(1. - \frac{.00357\ z}{518.4}\right)^{4.256} \tag{16}$$

Substituting z_o for z results in:

(SL) $\rho = .001348$

(TD) $\rho = .001738.$

8. Flight path angle (γ_o)

Substituting nominal values for z, v, and γ in equation (3) results in

$$\dot{z}_o = v_o \sin \gamma_o \tag{17}$$

Assuming $\sin \gamma_o \approx \gamma_o$,

$$\gamma_o = \dot{z}/v_o \tag{18}$$

$\dot{z}_o$ is equivalent to the nominal values for vertical velocity defined in 6. above. Substituting these into equation (18) produces:

(SL) $\gamma_o = 0.0$ radians

(TD) $\gamma_o = -.0494$ radians.

9. Throttle (u_{3_o})

Assuming that $\dot{v} = 0$ and $\cos \alpha = 1$, then from equation (8)

$$u_{3_o} MT - D_o - W \sin \gamma_o = 0. \tag{19}$$

Solving for u_{3_o} yields

$$u_{3_o} = \frac{D_o + W \sin \gamma_o}{MT} \tag{20}$$

(SL) u_{3_o} = .800 Afterburner off

u_{3_o} = .200 Afterburner on

(TD) u_{3_o} = .724 Afterburner off

u_{3_o} = .181 Afterburner on

10. Drag (D_o)

The drag equation is defined in Appendix B. Substituting nominal values for v and α yields

$$D_o = .5 \rho v_o^2 (.0327 + .135 \alpha_o + 1.6875 \alpha_o^2)A \quad (21)$$

where A = area of aircraft = 202 ft^2.

(SL) D_o = 3715.558

(TD) D_o = 5141.409

11. Angle of attack (γ_o)

From Appendix B,

$$L = .5 \rho v^2 (.1 + 2.5\alpha) A + u_3 MT \alpha \quad (22)$$

where A = area of aircraft = 202 ft^2.

Substituting in nominal values for L, v, and α, and equation (20) for u_{3_o} yields

$$L_o = .5 \rho v_o^2 (.1 + 2.5 \alpha_o) A + (D_o + W \sin \gamma_o)\alpha_o. \quad (23)$$

Substituting equation (21) for D_o and re-arranging terms, results in the following:

$$(.05 \rho v_o^2 A - L_o) + [\rho v_o^2 A(1.26635) + W \sin \gamma_o]\alpha_o$$

$$+ (.0675 \rho v_o^2 A) \alpha_o^2 + (.84375 \rho v_o^2 A)\alpha_o^3 = 0. \quad (24)$$

Solving this cubic equation determines the nominal values for α.

(SL) α_o = .030 radians

(TD) α_o = .041 radians

12. Roll Angle (ϕ_o)

Assuming that $\dot{\gamma}$ = 0, the following relationship can be derived from equation (6):

$$L_o \cos \phi_o - W \cos \gamma_o = 0$$

Solving for ϕ_o yields

$$\phi_o = \cos^{-1} \left[\frac{W \cos \gamma_o}{L_o} \right] \tag{25}$$

(SL) ϕ_o = 0.0 radians

(TD) ϕ_o = -.842159 radians

A summary of the nominal values for the state equation variables can be found in Table 8.

The linearized error states $\underline{x}$ are derived based on the following rationale: $\dot{\underline{x}}(t)$ is a function of both $\underline{x}(t)$ and $\underline{u}(t)$ and can be written as

$$\dot{\underline{x}}(t) = f(\underline{x}(t), \underline{u}(t)). \tag{26}$$

Both $\underline{x}$ and $\underline{u}$ can be expressed in terms of their nominal values plus the deviation in those values from the nominal. Thus,

$$\underline{x}(t) = \underline{x}_o(t) + \delta\underline{x}(t) \tag{27}$$

$$\underline{u}(t) = \underline{u}_o(t) + \delta\underline{u}(t). \tag{28}$$

However, $\underline{x}_o$ at any time t is constant. Therefore,

$$\frac{d}{dt} (\underline{x}_o(t) + \delta\underline{x}(t)) = \frac{d}{dt} (\underline{x}(t)) = \frac{d}{dt} (\delta\underline{x}(t)). \tag{29}$$

TABLE 8

NOMINAL VALUES FOR STATE EQUATIONS VARIABLES

VARIABLE	STRAIGHT AND LEVEL	TURNING DIVE
altitude	18,130 ft.	30,000 ft.
velocity	844.47 ft/sec.	844.47 ft/sec.
weight	17,000 lbs.	17,000 lbs.
g-load	1.0	1.5
lift	17,000 lbs.	25,500 lbs.
vertical velocity	0.0 ft/sec.	-41.7 ft/sec.
density (ρ)	.001348	.001738
flight path angle (γ)	0.0 radians	-.0494 radians
throttle (u_{3_o})	.800 (off) .200 (on)	.724 (off) .181 (on)
drag	3715.558	5141.409
angle of attack (α)	.030 radians	.041 radians
roll angle (ϕ)	0.0 radians	-.842159 radians

Then, employing equations (26) to (29)

$$\dot{\underline{x}}(t) = \delta\dot{\underline{x}}(t) = f(\underline{x}_o(t) + \delta\underline{x}(t), \underline{u}_o(t) + \delta\underline{u}(t)). \tag{30}$$

The Taylor's Series expansion of equation (30) about the nominal values can be expressed as:

$$\delta\dot{\underline{x}}(t) = f(\underline{x}_o, \underline{u}_o) + [\frac{\partial f}{\partial x}\delta\underline{x} + \frac{\partial f}{\partial u}\delta\underline{u}]$$

$$+ [\frac{\partial^2 f}{\partial_x^2}\delta\underline{x} + \frac{\partial^2 f}{\partial_u^2}\delta\underline{u}]/2! + \ldots \tag{31}$$

However, since the state variables are close to their nominal values, all but the first order terms can be eliminated. Thus equation (31) reduces to

$$\delta\dot{\underline{x}}(t) = f(\underline{x}_o, \underline{u}_o) + [\frac{\partial f}{\partial x}\delta\underline{x} + \frac{\partial f}{\partial u}\delta\underline{u}]. \tag{32}$$

The change in $\underline{u}$, $\delta\underline{u}$ is defined as

$$\delta\underline{u} = \underline{u} - \underline{u}_o \tag{33}$$

Substituting equation (33) for $\delta\underline{u}$ in equation (32) yields

$$\delta\dot{\underline{x}}(t) = f(\underline{x}_o, \underline{u}_o) + [\frac{\partial f}{\partial x}\delta\underline{x} + \frac{\partial f}{\partial u}(\underline{u} - \underline{u}_o)] \tag{34}$$

Equation (34) was employed in deriving the linearized error state equation defined below.

1. Lift

$$L = .5\rho\, v^2\, (.1 + 2.5\alpha)\, A + u_3\, MT\, \alpha$$

$$\delta L = \rho\, v_o\, (.1 + 2.5\alpha_o)\, A\, \delta v + 1.25\, \rho\, v_o^2\, A\, \delta\alpha \tag{35}$$

$$+ u_{3_o}\, MT\, \delta\alpha + MT\, \alpha_o\, \delta u_3.$$

2. Drag

$$D = .5\rho v^2 [.0327 + .135\alpha + 1.6875\alpha^2] A$$

$$\delta D = \rho v_o [.0327 + .135\alpha_o + 1.6875\alpha_o^2] A \delta v + .5 \rho v_o^2 [.135 + 3.375\alpha_o] A \delta\alpha \quad (36)$$

3. Altitude

$$\dot{z} = v \sin\gamma$$

$$\delta\dot{z} = (v_o \cos\gamma_o)\delta\gamma + (\sin\gamma_o)\delta v$$

$$= a_1 \delta\gamma + a_2 \delta v \quad (37)$$

4. Roll

$$\dot{\phi} = u_2$$

5. Heading

$$\dot{\psi} = \frac{L \sin\phi}{mv \cos\gamma} \quad (38)$$

$$\delta\dot{\psi} = \frac{\sin\phi_o}{mv_o \cos\gamma_o}\delta L + \frac{L_o \cos\phi_o}{mv_o \cos\gamma_o}\delta\phi - \frac{L_o \sin\phi_o}{mv_o^2 \cos\gamma_o}\delta v + \frac{L_o \sin\phi_o \sin\gamma_o}{mv_o (\cos^2\gamma_o)}\delta\gamma$$

$$= \frac{L_o \cos\phi_o}{mv_o \cos\gamma_o}\delta\phi + \frac{L_o \sin\phi_o \sin\gamma_o}{mv_o (\cos^2\gamma_o)}\delta\gamma + \frac{(1,25\rho v_o^2 A + u_{3_o} MT) \sin\phi_o}{mv_o \cos\gamma_o}\delta\alpha$$

$$+\left[\frac{-L_o \sin\phi_o}{m\cos\gamma_o v_o^2} + \frac{\rho v_o\,(.1 + 2.5\alpha_o)\,A\sin\phi_o}{mv_o\cos\gamma_o}\right]\delta v$$

$$+\frac{\sin\phi_o\,MT\,\alpha_o}{mv_o\cos\gamma_o}u_3 - \frac{\sin\phi_o\,MT\,\alpha_o}{mv_o\cos\gamma_o}u_{3_o}$$

$$= a_3\delta\phi + a_4\delta\gamma + a_5\delta\alpha + a_6\delta v + b_1u_3 + e_1u_{3_o} \qquad (39)$$

6. Flight path angle

$$\dot{\gamma} = \frac{L\cos\phi - W\cos\gamma}{mv}$$

$$\delta\dot{\gamma} = \frac{\cos\phi_o}{mv_o}\delta L - \frac{L_o\sin\phi_o}{mv_o}\delta\phi + \frac{W\sin\gamma_o}{mv_o}\delta\gamma$$

$$-\frac{L_o\cos\phi_o}{mv_o^2}\delta v + \frac{W\cos\gamma_o}{mv_o^2}\delta v$$

$$= \frac{-L_o\sin\phi_o}{mv_o}\delta\phi + \frac{W\sin\gamma_o}{mv_o}\delta\gamma$$

$$+\frac{(1.25\rho v_o^2 A + u_{3_o}MT)\cos\phi_o}{mv_o}\delta\alpha$$

$$+\left[\frac{-L_o\cos\phi_o + W\cos\gamma_o}{mv_o^2} + \frac{\rho v_o\,(.1 + 2.5\alpha_o)\,A\cos\phi_o}{mv_o}\right]\delta v$$

$$+\frac{\cos\phi_o\,MT\,\alpha_o}{mv_o}u_3 - \frac{\cos\phi_o\,MT\,\alpha_o}{mv_o}u_{3_o}$$

$$= a_7\delta\dot{\phi} + a_8\delta\gamma + a_9\delta\alpha + a_{10}\delta v + b_2u_3 + e_2u_{3_o} \qquad (40)$$

7. Angle of attack

$$\dot{\alpha} = u_1 + (L/W - 1)\,(AL1)$$

$$\delta\dot{\alpha} = u_1 + \left[\frac{L_o}{W} - 1\right] AL1 + \left[\frac{\delta L}{W}\right] AL1$$

$$= -.06\left[\frac{1.25\,\rho v_o^2\,A + u_{3_o}\,MT}{W}\right]\delta\alpha$$

$$-.06\left[\frac{\rho\, v_o\,(.1 + 2.5\,\alpha_o)\,A}{W}\right]\delta v + u_1 - \frac{.06\,MT\,\alpha_o}{W}\,u_3$$

$$+\frac{.06\,MT\alpha_o}{W}\,u_{3_o} + \left[\left(\frac{L_o}{W} - 1\right) AL1\right]$$

$$= -.06\,a_{11}\delta\alpha - .06\,a_{12}\delta v + u_1 - .06\,b_3 u_3$$

$$+ .06\,e_3 u_{3_o} + \left[\frac{L_o}{W} - 1\right] AL1 \qquad (41)$$

8. Velocity

$$\dot{v} = \frac{u_3\,(MT)\cos\alpha - D - W\sin\gamma}{m}$$

$$\delta\dot{v} = \frac{-u_{3_o}\,(MT)\sin\alpha_o}{m}\,\delta\alpha + \frac{MT\cos\alpha_o}{m}\,\delta u_3$$

$$-\frac{\delta D}{m} - \frac{W\cos\gamma_o}{m}\,\delta\gamma$$

$$= \frac{-W\cos\gamma_o}{m}\,\delta\gamma - \left[\frac{u_{3_o}MT\sin\alpha_o + .5\rho v_o^2(.135+3.375\,\alpha_o)A}{m}\right]\delta\alpha$$

$$-\left[\frac{\rho v_o\,(.0327 + .135\,\alpha_o + 1.6875\,\alpha_o^2)A}{m}\right]\delta v$$

$$+ \frac{MT \cos \alpha_o}{m} u_3 - \frac{MT \cos \alpha_o}{m} u_{3_o}$$

$$= a_{13}\delta\gamma + a_{14}\delta\alpha + a_{15}\delta v + b_4 u_3 + e_4 u_{3_o} \qquad (42)$$

In reality the pilot more likely controls in terms of the "error" states and not the actual or absolute state values. That is, he is concerned with the difference or error (δ) between the actual state variable values and the command or desired values. Let $\underline{x}$ be redefined in terms of the error states

$$\underline{x} = \begin{bmatrix} \delta z \\ \delta\phi \\ \delta\psi \\ \delta\gamma \\ \delta\alpha \\ \delta v \end{bmatrix} = \begin{bmatrix} z - z_o \\ \phi - \phi_o \\ \psi - \psi_o \\ \gamma - \gamma_o \\ \alpha - \alpha_o \\ v - v_o \end{bmatrix} \qquad (43)$$

The error state variable relation can now be expressed in the following linear form

$$\dot{\underline{x}}(t) = A\underline{x}(t) + B\underline{u}(t) + E\underline{w}(t) \qquad (44)$$

where A, B, and E are constant matrices, and $\underline{w}$ is the vector of nominal disturbances. The entries of A, B, E, and $\underline{w}$ are determined by equations (36) to (41).

$$A = \begin{bmatrix} 0 & 0 & 0 & a_1 & 0 & a_2 \\ 0 & 0 & 0 & 0 & 0 & 0 \\ 0 & a_3 & 0 & a_4 & a_5 & a_6 \\ 0 & a_7 & 0 & a_8 & a_9 & a_{10} \\ 0 & 0 & 0 & 0 & -.06a_{11} & -.06a_{12} \\ 0 & 0 & 0 & a_{13} & a_{14} & a_{15} \end{bmatrix} ; \qquad (45)$$

$$B = \begin{bmatrix} 0 & 0 & 0 \\ 0 & 1 & 0 \\ 0 & 0 & b_1 \\ 0 & 0 & b_2 \\ 1 & 0 & -.06b_3 \\ 0 & 0 & b_4 \end{bmatrix} \quad ; \tag{46}$$

$$E = \begin{bmatrix} 0 & 0 & 0 \\ 0 & 0 & 0 \\ e_1 & 0 & 0 \\ e_2 & 0 & 0 \\ .06e_3 & 0 & 1 \\ e_4 & 0 & 0 \end{bmatrix} \quad ; \tag{47}$$

$$\underline{w} = \begin{bmatrix} u_{3_o} \\ 0 \\ \left(\frac{L_o}{W} - 1\right) AL1 \end{bmatrix} \quad ; \tag{48}$$

where,

$a_1 = v_o \cos \gamma_o$

$a_2 = \sin \gamma_o$

$a_3 = \dfrac{L_o \cos \phi_o}{m v_o \cos \gamma_o}$

$a_4 = \dfrac{L_o \sin \phi_o \sin \gamma_o}{m v_o (\cos \gamma_o)^2}$

$$a_5 = \frac{(1.25\rho v_o^2 A + u_{3_o} MT) \sin \phi_o}{m v_o \cos \gamma_o}$$

$$a_6 = \frac{-L_o \sin \phi_o}{m v_o^2 \cos \gamma_o} + \frac{\rho v_o (.1 + 2.5 \alpha_o) A \sin \phi_o}{m v_o \cos \gamma_o}$$

$$a_7 = \frac{-L_o \sin \gamma_o}{m v_o}$$

$$a_8 = \frac{W \sin \gamma_o}{m v_o}$$

$$a_9 = \frac{(1.25\rho v_o^2 A + u_{3_o} MT) \cos \phi_o}{m v_o}$$

$$a_{10} = \frac{-L_o \cos \phi_o}{m v_o^2} + \frac{W \cos \gamma_o}{m v_o^2} + \frac{\rho v_o (.1 + 2.5 \alpha_o) A \cos \phi_o}{m v_o}$$

$$a_{11} = \frac{1.25\rho v_o^2 A + u_{3_o} MT}{W}$$

$$a_{12} = \frac{\rho v_o (.1 + 2.5 \alpha_o) A}{W}$$

$$a_{13} = \frac{-W \cos \gamma_o}{m}$$

$$a_{14} = \frac{-u_{3_o} MT \sin \alpha_o - .5\rho v_o^2 (.135 + 3.375 \alpha_o) A}{m}$$

$$a_{15} = \frac{-\rho v_o (.0327 + .135 \alpha_o + 1.6875 \alpha_o^2) A}{m}$$

$$b_1 = \frac{\sin \phi_o \, MT \alpha_o}{m v_o \cos \gamma_o}$$

$$b_2 = \frac{\cos \phi_o \, MT \, \alpha_o}{mv_o}$$

$$b_3 = \frac{MT \, \alpha_o}{W}$$

$$b_4 = \frac{MT \cos \alpha_o}{m}$$

$$e_1 = \frac{-\sin \phi_o \, MT \, \alpha_o}{mv_o \cos \gamma_o} = -b_1$$

$$e_2 = \frac{-\cos \phi_o \, MT \, \alpha_o}{mv_o} = -b_2$$

$$e_3 = \frac{-MT \, \alpha_o}{W} = -b_3$$

$$e_4 = \frac{-MT \cos \alpha_o}{m} = -b_4$$

In addition to the error states, $\underline{x}(t)$, the pilot also tends to utilize the rate of change of the control states, $\dot{\underline{u}}(t)$, in determining his control inputs. Thus it is desirable to include $\dot{\underline{u}}(t)$ in the control formulation. Let

$$\dot{\underline{u}}(t) = \underline{n}(t) \tag{49}$$

where $\underline{n}(t)$ is a manipulated variable representing the derivative of $\underline{u}(t)$.

Then augmenting equation (44) to include $\dot{\underline{u}}(t)$ yields

$$\begin{bmatrix} \dot{\underline{x}}(t) \\ \dot{u}(t) \end{bmatrix} = \begin{bmatrix} A & B \\ 0 & 0 \end{bmatrix} \begin{bmatrix} x(t) \\ u(t) \end{bmatrix} + \begin{bmatrix} 0 \\ I \end{bmatrix} \underline{n}(t) + \begin{bmatrix} E \\ 0 \end{bmatrix} \underline{w}(t), \tag{50}$$

where I represents the identity matrix.

However, the state vector $\underline{x}$ does not include all the displayed variables utilized by the pilot. Vertical velocity and g-load are both critical variables in that they are the defining parameters of the maneuvers. On the other hand, the pilot infrequently uses flight path angle and angle of attack. Therefore, it is desirable to form an equivalent set of states by replacing these two variables with vertical velocity and g-load in the state vector. This places the state vector $\underline{x}$ in a display variable frame of reference. Both vertical velocity and g-load can be expressed as a function of the original six state variables.

Equation (3) defines vertical velocity as

$$\dot{z} = v \sin \gamma.$$

Assuming $\sin \gamma \approx \gamma$, and using the nominal value for v, δ vertical velocity can be derived from equation (3).

$$\delta \text{ vertical velocity} = v_o \, \delta\gamma. \tag{51}$$

δ g-load is determined in a similar manner. From equation (14)

$$\text{g-load} = L/W.$$

Then,

$$\delta \text{ g-load} = \delta L/W. \tag{52}$$

Substituting equation (35) for δL yields

$$\delta \text{ g-load} = [(1.25\rho v_o^2 A + u_{3_o} MT)\, \delta\alpha + \rho v_o (.1 + 2.5\, \alpha_o) A\, \delta v + (MT\, \alpha_o)\, (u_3 - u_{3_o})]/W \tag{53}$$

$$= a_{11}\delta\alpha + a_{12}\delta v + b_3 u_3 - b_3 u_{3_o}. \tag{54}$$

Let $\underline{e}$ represent the error state vector of displayed variables utilized by the pilot in making flight control decisions. Then $\underline{e}$ is defined as:

$$\underline{e} = \begin{bmatrix} \delta z \\ \delta\phi \\ \delta\psi \\ v_o\,\delta\gamma \\ \delta L/W \\ \delta v \end{bmatrix} = \delta \begin{bmatrix} \text{altitude} \\ \text{roll angle} \\ \text{heading} \\ \text{vertical velocity} \\ \text{g-load} \\ \text{velocity} \end{bmatrix} \tag{55}$$

By making a coordinate change and translation in accordance with equations (51) to (54), the system states $\underline{x}$, displayed errors $\underline{e}$, and controls $\underline{u}$ can be represented by the following linear expression:

$$\begin{bmatrix} e \\ u \end{bmatrix} = \underline{C}_x \begin{bmatrix} x \\ u \end{bmatrix} - \underline{C}_w \underline{w}. \tag{56}$$

where

$$\underline{C}_x = \left[\begin{array}{cccccc:ccc} 1 & 0 & 0 & 0 & 0 & 0 & 0 & 0 & 0 \\ 0 & 1 & 0 & 0 & 0 & 0 & 0 & 0 & 0 \\ 0 & 0 & 1 & 0 & 0 & 0 & 0 & 0 & 0 \\ 0 & 0 & 0 & v_o & 0 & 0 & 0 & 0 & 0 \\ 0 & 0 & 0 & 0 & a_{11} & a_{12} & 0 & 0 & b_3 \\ 0 & 0 & 0 & 0 & 0 & 1 & 0 & 0 & 0 \\ \hdashline 0 & 0 & 0 & 0 & 0 & 0 & 1 & 0 & 0 \\ 0 & 0 & 0 & 0 & 0 & 0 & 0 & 1 & 0 \\ 0 & 0 & 0 & 0 & 0 & 0 & 0 & 0 & 1 \end{array}\right] = \begin{bmatrix} C_{11} & C_{12} \\ 0 & I \end{bmatrix}$$

in partitioned format;

$$\underline{C}_w = \begin{bmatrix} C_{12} \\ 0 \end{bmatrix}$$

Then,

$$\begin{bmatrix} x \\ u \end{bmatrix} = \underline{C}_x^{-1} \begin{bmatrix} e \\ u \end{bmatrix} + \underline{C}_x^{-1} \underline{C}_w \underline{w}, \tag{57}$$

$$\frac{d}{dt} \begin{bmatrix} e \\ u \end{bmatrix} = \underline{C}_x \begin{bmatrix} \dot{x} \\ \dot{u} \end{bmatrix}$$

$$= \underline{C}_x \left[\begin{pmatrix} A & B \\ 0 & 0 \end{pmatrix} \begin{pmatrix} x \\ u \end{pmatrix} + \begin{pmatrix} 0 \\ I \end{pmatrix} \underline{\eta} + \begin{pmatrix} E \\ 0 \end{pmatrix} \underline{w} \right]. \tag{58}$$

Substituting equation (57) for $\begin{pmatrix} x \\ u \end{pmatrix}$ yields

$$\begin{bmatrix} \dot{e} \\ \dot{u} \end{bmatrix} = \underline{C}_x \left[\begin{pmatrix} A & B \\ 0 & 0 \end{pmatrix} \left[\underline{C}_x^{-1} \begin{pmatrix} e \\ u \end{pmatrix} + \underline{C}_x^{-1} \underline{C}_w \underline{w} \right] + \begin{pmatrix} 0 \\ I \end{pmatrix} \underline{\eta} + \begin{pmatrix} E \\ 0 \end{pmatrix} \underline{w} \right] \tag{59}$$

$$= \begin{bmatrix} C_{11} & C_{12} \\ 0 & I \end{bmatrix} \begin{bmatrix} A & B \\ 0 & 0 \end{bmatrix} \begin{bmatrix} C_{11}^{-1} & -C_{11}^{-1} C_{12} \\ 0 & I \end{bmatrix} \begin{bmatrix} e \\ u \end{bmatrix} +$$

$$\left[\begin{pmatrix} C_{11} & C_{12} \\ 0 & I \end{pmatrix} \begin{pmatrix} A & B \\ 0 & 0 \end{pmatrix} \begin{pmatrix} C_{11}^{-1} & -C_{11}^{-1} C_{12} \\ 0 & I \end{pmatrix} \begin{pmatrix} C_{12} \\ 0 \end{pmatrix} + \right.$$

$$\left. \begin{pmatrix} C_{11} & C_{12} \\ 0 & I \end{pmatrix} \begin{pmatrix} -B \\ 0 \end{pmatrix} \right] \underline{w} + \begin{bmatrix} C_{11} & C_{12} \\ 0 & I \end{bmatrix} \begin{bmatrix} 0 \\ I \end{bmatrix} \underline{\eta} \tag{60}$$

which reduces to

$$\begin{bmatrix} \dot{e} \\ \dot{u} \end{bmatrix} = \left[\begin{array}{c|c} C_{11} A C_{11}^{-1} & -C_{11} A C_{11}^{-1} C_{12} + C_{11} B \\ \hline 0 & 0 \end{array} \right] \begin{bmatrix} e \\ u \end{bmatrix}$$

$$+ \left[\begin{array}{c|c} C_{11} A C_{11}^{-1} C_{12} - C_{11} B \\ \hline 0 \end{array} \right] \underline{w} + \begin{bmatrix} 0 \\ I \end{bmatrix} \underline{\eta} \tag{61}$$

In order to simplify notation let

$$\hat{A} = C_{11} A C_{11}^{-1}$$

$$\hat{B} = -C_{11} A C_{11}^{-1} C_{12} + C_{11} B$$

Then equation (55) can be rewritten as

$$\begin{bmatrix} \dot{e} \\ \dot{u} \end{bmatrix} = \begin{bmatrix} \hat{A} & \hat{B} \\ 0 & 0 \end{bmatrix} \begin{bmatrix} e \\ u \end{bmatrix} + \begin{bmatrix} -\hat{B} \\ 0 \end{bmatrix} \underline{w} + \begin{bmatrix} 0 \\ I \end{bmatrix} \underline{\eta}. \tag{62}$$

In order to "close" the system, that is, to make $\underline{w}$ an endogenous state of the system as opposed to being an exogenous variable, the following state augmentation is made:

$$\begin{bmatrix} \dot{e} \\ \dot{u} \\ \dot{w} \end{bmatrix} = \begin{bmatrix} \hat{A} & \hat{B} & -\hat{B} \\ 0 & 0 & 0 \\ 0 & 0 & 0 \end{bmatrix} \begin{bmatrix} e \\ u \\ w \end{bmatrix} + \begin{bmatrix} 0 \\ I \\ 0 \end{bmatrix} \underline{\eta}. \tag{63}$$

$\dot{\underline{w}}$ is assumed to be zero since $\underline{w}$ is constant over any interval of interest (see equation 48). Now let

$$\underline{v} = \underline{u} - \underline{w}.$$

Then,

$$\dot{\underline{v}} = \dot{\underline{u}} = \underline{\eta}, \text{ since } \dot{\underline{w}} = 0.$$

Therefore,

$$\frac{d}{dt} \begin{bmatrix} e \\ v \\ w \end{bmatrix} = \frac{d}{dt} \begin{bmatrix} e \\ u \\ w \end{bmatrix}$$

$$= \begin{bmatrix} \hat{A} & \hat{B} & -\hat{B} \\ 0 & 0 & 0 \\ 0 & 0 & 0 \end{bmatrix} \begin{bmatrix} e \\ v + w \\ w \end{bmatrix} + \begin{bmatrix} 0 \\ I \\ 0 \end{bmatrix} \underline{\eta} \tag{64}$$

which reduces to

$$\begin{bmatrix} \dot{e} \\ \dot{v} \\ \dot{w} \end{bmatrix} = \begin{bmatrix} \hat{A} & \hat{B} & 0 \\ 0 & 0 & 0 \\ 0 & 0 & 0 \end{bmatrix} \begin{bmatrix} e \\ v \\ w \end{bmatrix} + \begin{bmatrix} 0 \\ I \\ 0 \end{bmatrix} \underline{\eta} \tag{65}$$

Because equation (65) indicates that $\underline{e}$ and $\underline{v}$ are not functions of $\underline{w}$, $\underline{w}$ need not be considered with $\underline{e}$ and $\underline{v}$.* Therefore, for purposes of the control problem, the following system representation will be employed:

$$\begin{bmatrix} \dot{e} \\ \dot{v} \end{bmatrix} = \begin{bmatrix} \hat{A} & \hat{B} \\ 0 & 0 \end{bmatrix} \begin{bmatrix} e \\ v \end{bmatrix} + \begin{bmatrix} 0 \\ I \end{bmatrix} \underline{\eta} \tag{66}$$

letting

$$\tilde{A} = \begin{bmatrix} \hat{A} & \hat{B} \\ 0 & 0 \end{bmatrix}, \quad \tilde{B} = \begin{bmatrix} 0 \\ I \end{bmatrix}, \text{ and } \underline{\tilde{X}} = \begin{bmatrix} e \\ v \end{bmatrix}$$

equation (66) can now be written as:

$$\frac{d}{dt} \underline{\tilde{X}}(t) = \tilde{A} \underline{\tilde{X}}(t) + \tilde{B} \underline{\eta}(t) \tag{67}$$

The system is now in the standard, well-known linear system form.

The objective now is to find a control input $\underline{\eta}(t)$ which minimizes the system error without the excessive use of control energy. The attempt is to represent the behaviors of the operator who is solving

---

* $\underline{w}$ influences the initial conditions of $\underline{v}$, but nothing else.

the control problem. These considerations, plus mathematical tractability requirements, lead to a performance function to be minimized of the form

$$J = \tfrac{1}{2}\int_0^\infty (\tilde{\underline{X}}(t)^T Q\, \tilde{\underline{X}}(t) + \underline{n}^T(t)\, R\, \underline{n}(t))\, dt \tag{68}$$

where Q and R are weighting matrices which take on the same meaning here as in the optimal control model described earlier.

It is desirable to optimize the system over the indefinite future since it is assumed that the control problem will not change over the interval of interest. Therefore, the integration interval ranges from $t = t_o$ (the present) to $t \to \infty$ (the future). The infinite optimization interval results in a time invariant control policy, not constant control inputs. It assures that if the control problem is well-posed, the system error will remain near zero after the initial transient response.

Solution to the Control Problem

Since the system describing equations are in the standard form, the performance function J is minimized by a control of the form (see Athans and Falb, 1966).

$$\underline{n}(t) = -R^{-1}\, \tilde{B}^T\, K\, \tilde{\underline{X}}(t) \tag{69}$$

where K satisfies the following algebraic Riccati equation

$$K\tilde{A} + \tilde{A}^T K - K\tilde{B}R^{-1}\, \tilde{B}^T K + Q = 0. \tag{70}$$

If K is partitioned as

$$K = \begin{bmatrix} K_{11} & K_{12} \\ K_{21} & K_{22} \end{bmatrix}$$

Then,

$$\underline{n}(t) = R^{-1} [0\ I] \begin{bmatrix} K_{11} & K_{12} \\ K_{21} & K_{22} \end{bmatrix} \begin{bmatrix} e\ (t) \\ v\ (t) \end{bmatrix} \tag{71}$$

$$= (-R^{-1}K_{21} \quad -R^{-1}K_{22}) \begin{bmatrix} e\ (t) \\ v\ (t) \end{bmatrix} \tag{72}$$

$$= (K_1\ K_2) \begin{bmatrix} e\ (t) \\ v\ (t) \end{bmatrix} \tag{73}$$

where $K_1 = -R^{-1}K_{21}$ and

$$K_2 = -R^{-1}K_{22}.$$

Substituting equation (74) for $\underline{n}(t)$ in equation (67) yields

$$\dot{\underline{\tilde{X}}}(t) = \tilde{A}\,\underline{\tilde{X}}(t) + \tilde{B}\,\underline{n}(t)$$

$$= \tilde{A}\,\underline{\tilde{X}}(t) + \begin{bmatrix} 0 \\ I \end{bmatrix} (K_1\ K_2) \begin{bmatrix} e\ (t) \\ v\ (t) \end{bmatrix}$$

$$= \left[\tilde{A} + \begin{pmatrix} 0 & 0 \\ K_1 & K_2 \end{pmatrix}\right] \underline{\tilde{X}}(t). \tag{74}$$

Then, substituting the original values for $\tilde{A}$ and $\tilde{X}$ into equation (74) produces

$$\frac{d}{dt} \begin{bmatrix} e \\ v \end{bmatrix} = \begin{bmatrix} \hat{A} & \hat{B} \\ 0 & 0 \end{bmatrix} \begin{bmatrix} e \\ v \end{bmatrix}. \tag{75}$$

Returning to the full augmented system formulation, the closed-loop optimal response solution can be written as

$$\frac{d}{dt}\begin{bmatrix} e \\ v \\ w \end{bmatrix} = \begin{bmatrix} \hat{A} & \hat{B} & 0 \\ K_1 & K_2 & 0 \\ 0 & 0 & 0 \end{bmatrix} \begin{bmatrix} e \\ v \\ w \end{bmatrix}. \tag{76}$$

The objective now is to have a control law dependent only on displayed variables and in the form least sensitive to "errors" (bias, or constant disturbances). The following change of variable and translation accomplishes this objective.

Define a new variable $\underline{y}$ as

$$\begin{aligned} \underline{y} &= -G\underline{e} + \underline{u} \\ &= -G\underline{e} + \underline{v} + \underline{w}. \end{aligned} \tag{77}$$

Then, in augmented form,

$$\begin{bmatrix} e \\ y \\ w \end{bmatrix} = \begin{bmatrix} I & 0 & 0 \\ -G & I & I \\ 0 & 0 & I \end{bmatrix} \begin{bmatrix} e \\ v \\ w \end{bmatrix}. \tag{78}$$

Equivalently,

$$\begin{bmatrix} e \\ v \\ w \end{bmatrix} = \begin{bmatrix} I & 0 & 0 \\ G & I & -I \\ 0 & 0 & I \end{bmatrix} \begin{bmatrix} e \\ y \\ w \end{bmatrix}. \tag{79}$$

Then,

$$\frac{d}{dt}\begin{bmatrix} e \\ y \\ w \end{bmatrix} = \begin{bmatrix} I & 0 & 0 \\ -G & I & I \\ 0 & 0 & 0 \end{bmatrix} \begin{bmatrix} \dot{e} \\ \dot{v} \\ \dot{w} \end{bmatrix}. \tag{80}$$

Substituting in equations (76) and (79) yields

$$\begin{bmatrix} \dot{e} \\ \dot{y} \\ \dot{w} \end{bmatrix} = \begin{bmatrix} I & 0 & 0 \\ -G & I & I \\ 0 & 0 & 0 \end{bmatrix} \begin{bmatrix} \hat{A} & \hat{B} & 0 \\ K_1 & K_2 & 0 \\ 0 & 0 & 0 \end{bmatrix} \begin{bmatrix} I & 0 & 0 \\ G & I & -I \\ 0 & 0 & I \end{bmatrix} \begin{bmatrix} e \\ y \\ w \end{bmatrix} \tag{81}$$

$$= \begin{bmatrix} \hat{A} & \hat{B} & 0 \\ -G\hat{A}+K_1 & -G\hat{B}+K_2 & 0 \\ 0 & 0 & 0 \end{bmatrix} \begin{bmatrix} I & 0 & 0 \\ G & I & -I \\ 0 & 0 & I \end{bmatrix} \begin{bmatrix} e \\ y \\ w \end{bmatrix} \tag{82}$$

$$= \begin{bmatrix} \hat{A}+\hat{B}G & \hat{B} & -\hat{B} \\ -G\hat{A}+K_1+(-G\hat{B}+K_2)G & -G\hat{B}+K_2 & G\hat{B}-K_2 \\ 0 & 0 & 0 \end{bmatrix} \begin{bmatrix} e \\ y \\ w \end{bmatrix}. \tag{83}$$

At this point, it is desirable to solve for G such that

$$-G\hat{B} + K_2 = 0. \tag{84}$$

This reduces the second part of the (2,1) entry as well as the (2,2) and (2,3) entries of the coefficient matrix in equation (50) to zero. This is advantageous in that now y is a function of only e, and not y and w. Therefore, only an initial value of y is required, and without the need for measurement, less error is introduced into the model and a "proportional and integral" control law results.

The optimal solution which satisfies equation (84) is defined by

$$G = K_2 (\hat{B}^T\hat{B})^{-1} \hat{B}^T. \tag{85}$$

Equation (83) then reduces to

$$\frac{d}{dt} \begin{bmatrix} e \\ y \\ w \end{bmatrix} = \begin{bmatrix} \hat{A}+\hat{B}G & \hat{B} & -\hat{B} \\ -G\hat{A}+K_1 & 0 & 0 \\ 0 & 0 & 0 \end{bmatrix} \begin{bmatrix} e \\ y \\ w \end{bmatrix}, \tag{86}$$

which is clearly in proportional and integral form.

Equation (86) provides a deterministic representation of the optimally controlled system, including the perfect human operator. However, this model assumes that the pilot has both perfect information about system states and that he executes control inputs with perfect accuracy. This is unrealistic, and an attempt will be made to represent uncertainties in the system by adding zero mean Gaussian-distributed white noise terms. Thus a stochastic process model is introduced which includes the above model plus three noise terms.

$$\text{Let } \underline{X} = \begin{bmatrix} e \\ y \\ w \end{bmatrix} \quad \text{and} \quad A = \begin{bmatrix} \hat{A}+\hat{B}G & \hat{B} & \hat{B} \\ -G\hat{A}+K_1 & 0 & 0 \\ 0 & 0 & 0 \end{bmatrix}. \tag{87}$$

Then, adding a noise term, $\underline{\varepsilon}_e$, to represent the error in the linearization process, equation (86) becomes

$$\dot{\underline{X}} = A\,\underline{X} + \underline{\varepsilon}_e, \tag{88}$$

The covariance statistics over any two time points s and t for the linearization error $\underline{\varepsilon}_e$ are defined as

$$E\left[\underline{\varepsilon}_e(s)\,\underline{\varepsilon}_e^{T}(t)\right] = \tfrac{1}{2}\,\underline{V}_{\varepsilon_e}(t)\,\delta(t-s). \tag{89}$$

A second error, $\underline{\varepsilon}_d$, is introduced by the reading error in updating the displayed variables. Let $\hat{\underline{e}}$ represent the best estimate of $\underline{e}$. Then

$$\hat{\underline{e}} = \underline{e} + \underline{\varepsilon}_d. \tag{90}$$

The mean statistics for $\underline{\varepsilon}_d$ are assumed to be zero and the covariance statistics are defined in similar fashion to those of $\underline{\varepsilon}_e$.

$$E\left[\underline{\varepsilon}_d(s)\,\underline{\varepsilon}_d^{T}(t)\right] = \tfrac{1}{2}\,\underline{V}_{\varepsilon_d}(t)\,\delta(t-s). \tag{91}$$

A third error term, $\underline{\varepsilon}_u$, is required to represent the pilot's control input errors. It too is assumed to be zero-mean Gaussian distributed. Then,

$$\underline{u} = G(\underline{e} + \underline{\varepsilon}_d) + \underline{y} + \underline{\varepsilon}_u. \tag{92}$$

The control input error covariance statistics are defined as

$$E\left[\underline{\varepsilon}_u(s)\ \underline{\varepsilon}_u^T(t)\right] = \tfrac{1}{2}\ \underline{V}_{\underline{\varepsilon}_u}(t)\ \delta(t-s). \tag{93}$$

Equations (88) through (93) completely define the closed-loop control solution. A Kalman filter estimator of state variable values was deemed beyond the scope of this problem, and therefore was not constructed.

The Open-Loop, Closed-Loop Control System

Typically, one would stop at this point in the development, having presented a control model and its closed-loop solution. However, in contrast to the traditional optimal control model, it is assumed that information about the system states is available only periodically to the pilot; continuous sampling is not an option. In between samples, the control system operates open-loop. Estimates of the mean and covariance statistics of the error states are made by a "forecasting" system. The open-loop, closed-loop control system should not be confused with a sampled-data control system. In sampled-data systems, a discrete control input is computed from each sample of the displayed state variables and held at the same value for the whole interval. In this system, the pilot continues to make control inputs between samples based upon the best available estimate of the state of the aircraft. If the control model were to include an isomorphic model of the aircraft,

$$\frac{-4}{mv_o (\cos \gamma_o)^2}$$

and if the forecasting system could make perfect predictions of future states, then there would be no need for sampling. This open-loop, closed-loop type of control system has been successfully employed by Willke and Miller (1974) in a production planning and control system model.

Because in the DAIS system the pilot has other tasks such as MFK switching to perform in addition to his flight control, he cannot continuously sample the system status displays. The pilot reads the state variable displays only as time permits and operates in a so-called open-loop preprogrammed fashion between sampling. Thus, between samples, updated conditional estimates of $\underline{e}$ and $\underline{y}$ (termed $\underline{m}_e$ and $\underline{m}_y$, respectively), as well as the state variable covariance statistics $\underline{V}(t)$, are determined by the forecasting system.

This forecasting system is based on the stochastic process model defined by equations (88) to (93). The density function of a Gauss-markov process is completely described by two deterministic functions, the mean value vector $\underline{x}(t) = E[\underline{x}(t)]$, and the covariance matrix $\underline{V}(t) = E\{[\underline{x}(t)-E(\underline{x}(t))][\underline{x}(t)-E(\underline{x}(t))]^T\}$. The derivations of these two functions follow.

1. Mean

Writing equation (88) in system transition matrix format yields

$$\underline{x}(t) = \Phi(t)\,\underline{x}_o + \int_o^t \Phi(t, s)\,\underline{\varepsilon}_e(s)\,ds \qquad (94)$$

where $\underline{x}_o$ indicates the known initial values of the state vector $\underline{x}$.

Then the expected value of $\underline{x}(t)$ conditioned on the value of $\underline{x}_0$ can be expressed as

$$E\,[\underline{x}(t)|\,\underline{x}_0] = E\,[\Phi(t)\,\underline{x}_0 + \int_0^t \Phi\,(t,\,s)\,\underline{\varepsilon}_e(s)\,ds] \tag{95}$$

$$= E\,[\Phi(t)\,\underline{x}_0] + E\,[\int_0^t \Phi\,(t,\,s)\,\underline{\varepsilon}_e(s)\,ds] \tag{96}$$

$$= \Phi(t)\,E(\underline{x}_0) + \int_0^t [\Phi(t,\,s)\,E(\underline{\varepsilon}_e(s)\,ds]. \tag{97}$$

The error term $\underline{\varepsilon}_e$ is assumed to have a zero mean Gaussian distribution. Thus, $E\,[\underline{\varepsilon}_e(s)] = 0$. Therefore, equation (97) is reduced to

$$E\,[\underline{x}(t)|\,\underline{x}_0] = \Phi(t)\,E\,(\underline{x}_0). \tag{98}$$

However, since $\underline{x}_0$ is a constant,

$$E\,[\underline{x}(t)|\,\underline{x}_0] = \Phi(t)\,\underline{x}_0. \tag{99}$$

Define

$$E\,[\underline{x}(t)|\,\underline{x}_0] = \underline{m}(t). \tag{100}$$

This equation coupled with equation (99) implies that the conditional mean of $\underline{x}(t)$ satisfies the equation

$$\dot{\underline{m}}(t) = A\,\underline{m}(t) \tag{101}$$

where A is defined as in equation (87).

Assume that state variable samples are taken at time points $t_{s_1}, t_{s_2}, \ldots t_{s_n}$. Then the observed states can be represented

where I represents the identity matrix.

as $\underline{x}(t_{s_1})$, $\underline{x}(t_{s_2})$, . . . $\underline{x}(t_{s_n})$. In between samples, equation (101) is used to determine the current best estimate of $\underline{m}(t)$. That is, for

$$t_{s_i} \leq t < t_{s_{i+1}},$$

$$\underline{m}(t) = \Phi(t-t_{s_i})\ \underline{x}(t_{s_i}). \tag{102}$$

Figure 10 illustrates an example time history of the forecasting process where state variables are sampled every n time units. At time zero, the state variable takes on a value of x_0. For $0 < t < n$, equation (101) determines m(t). At time n, a new state variable sample x_1 is taken. The forecasting system then adjusts itself and makes x_1 its best estimate of m. This process continues with new samples being taken every n time units and conditional estimates being computed between samples. Figure 10 also displays the true state trajectory over time.

2. Covariance

This section derives the covariance relationship for the displayed state variable vector $\underline{e}$, where $\underline{e}$ is defined as in equation (55). In general, the covariance of any vector $\underline{x}(t)$ is defined as

$$\underline{V}\ [\underline{x}(t)] \doteq E\ \{[\underline{x}(t) - E\ (\underline{x}(t)]\ [\underline{x}(t) - E\ (\underline{x}(t))]^T\}. \tag{103}$$

Recall that from equation (62)

$$\dot{\underline{e}}(t) = \hat{A}\ \underline{e}(t) + \hat{B}\ \underline{u}(t) + \underline{\varepsilon}_e(t). \tag{104}$$

Substituting conditional estimates of the means for $\underline{e}$ and $\underline{y}$ into equation (92) yields

$$\underline{u}(t) = G\underline{m}_e(t) + \underline{m}_y(t) + \underline{\varepsilon}_u(t). \tag{105}$$

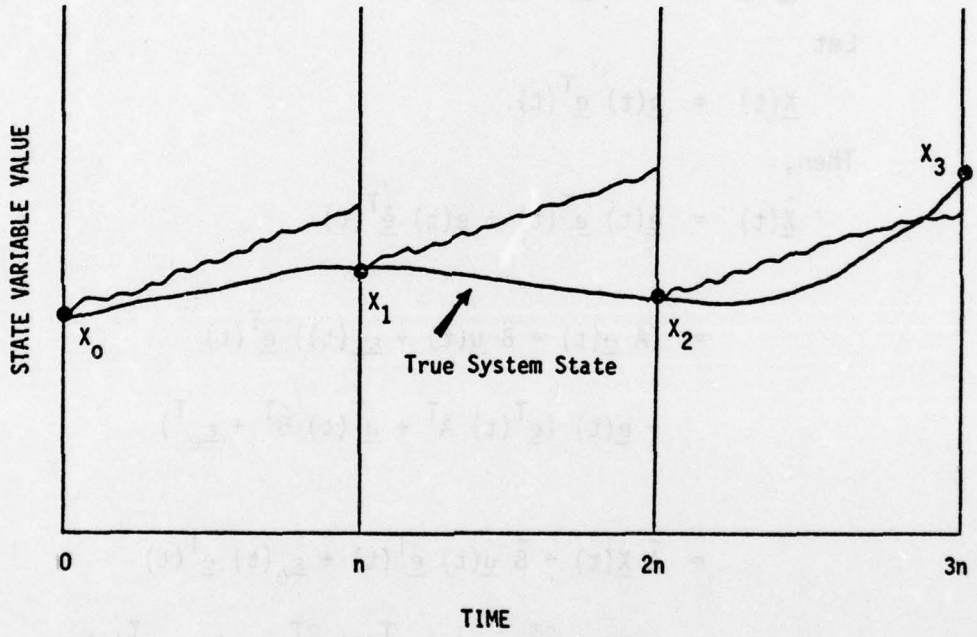

FIGURE 10. STATE VARIABLE SAMPLING AND FORECASTING SYSTEM

Then

$$\underline{V}\,[\underline{e}(t)] = E\,\{\underline{e}(t) - E\,(\underline{e}(t))]\,[\underline{e}(t) - E\,(\underline{e}(t))]^T\}. \tag{106}$$

However, the expected values of the error states are zero. Thus,

$$E\,[\underline{e}(t)] = 0. \tag{107}$$

Equation (106) then reduces to

$$\underline{V}\,[\underline{e}(t)] = E\,[\underline{e}(t)\,\underline{e}^T(t)]. \tag{108}$$

Let

$$\underline{X}(t) = \underline{e}(t)\,\underline{e}^T(t). \tag{109}$$

Then,

$$\dot{\underline{X}}(t) = \dot{\underline{e}}(t)\,\underline{e}^T(t) + \underline{e}(t)\,\dot{\underline{e}}^T(t) \tag{110}$$

$$= (\hat{A}\,\underline{e}(t) + \hat{B}\,\underline{u}(t) + \underline{\varepsilon}_e(t))\,\underline{e}^T(t)$$

$$+ \underline{e}(t)\,(\underline{e}^T(t)\,\hat{A}^T + \underline{u}^T(t)\,\hat{B}^T + \underline{\varepsilon}_e{}^T) \tag{111}$$

$$= \hat{A}\,\underline{X}(t) + \hat{B}\,\underline{u}(t)\,\underline{e}^T(t) + \underline{\varepsilon}_e(t)\,\underline{e}^T(t)$$

$$+ \underline{X}(t)\,\hat{A}^T + \underline{e}(t)\,\underline{u}^T(t)\,\hat{B}^T + \underline{e}(t)\,\underline{\varepsilon}_e{}^T(t). \tag{112}$$

From equations (108) and (109)

$$\dot{\underline{V}}(t) = E\,[\underline{X}(t)]. \tag{113}$$

A theorem from probability theory (see Parzen, 1962) states that

$$E\,[\dot{\underline{X}}(t)] = \frac{d}{dt}\,E\,[\underline{X}(t)]. \tag{114}$$

Using equations (112) to (114) the covariance derivative can be expressed as

$$\dot{\underline{V}}(t) = \hat{A}\,\underline{V}(t) + \hat{B}\,E\,[\underline{u}(t)\,\underline{e}^T(t)] + E\,[\underline{\varepsilon}_e(t)\,\underline{e}^T(t)]$$

$$+ \underline{V}(t)\,\hat{A}^T + E\,[\underline{e}(t)\,\underline{u}(t)^T]\,\hat{B}^T + E\,[\underline{e}(t)\underline{\varepsilon}_e{}^T(t)]. \qquad (115)$$

$E\,[\underline{\varepsilon}_e(t)\,\underline{e}^T(t)]$ and $E\,[\underline{e}(t)\,\underline{u}(t)^T]$ need to be determined.

Using transition matrix notation, $\underline{e}(t)$ can be rewritten as

$$\underline{e}(t) = \Phi(t, t_o)\,\underline{e}\,(t_o)$$

$$+ \int\Phi(t, s)\,\hat{B}\,(G\underline{m}_e(s) + \underline{m}_y(s) + \underline{\varepsilon}_u(s))\,ds$$

$$+ \int\Phi(t, s)\,\underline{\varepsilon}_e(s)\,ds \qquad (116)$$

Then,

$$E\,[\underline{e}(t)\,\underline{\varepsilon}_e{}^T(t)] = E\,[\Phi(t, t_o)\,\underline{e}(t_o)\,\underline{\varepsilon}_e{}^T(t)]$$

$$+ E\,[\int\Phi(t, s)\,\hat{B}\,[G\,\underline{m}_e(t) + \underline{m}_y(t)]\underline{\varepsilon}_u{}^T(t)ds$$

$$+ E\,[\int\Phi(t, s)\,\hat{B}\,\underline{\varepsilon}_u(s)\,\underline{\varepsilon}_e{}^T(t)ds$$

$$+ \int E\,[\Phi(t, s)\,\underline{\varepsilon}_e(s)\,\underline{\varepsilon}_e{}^T(t)ds. \qquad (117)$$

If the noise on $\underline{u}(t)$ is independent of the noise on $\underline{e}(t)$, and if $\underline{e}(t_o)$ is assumed to be zero, then the first three terms of equation (117) go to zero. Then,

$$E\,[\underline{e}(t)\,\underline{\varepsilon}_e{}^T(t)] = \int\Phi(t, s)\,E\,[\underline{\varepsilon}_e(s)\,\underline{\varepsilon}_e{}^T(t)]\,ds \qquad (118)$$

Substituting equation (89) for $E\,[\underline{\varepsilon}_e(s)\,\underline{\varepsilon}_e{}^T(t)]$ yields

$$E\,[\underline{e}(t)\,\underline{\varepsilon}_e{}^T(t)] = \int \tfrac{1}{2}\Phi(t, s)\,\underline{V}_{\varepsilon_e}(t)\,\delta(t-s)\,ds \tag{119}$$

$$= \tfrac{1}{2}\,\underline{V}_{\varepsilon_e}(t). \tag{120}$$

The next step is to determine $E\,[\underline{e}(t)\,\underline{u}(t)^T]$.

$$\underline{e}(t)\,\underline{u}^T(t) = \Phi(t, t_o)\,\underline{e}(t_o)\,\underline{u}^T(t)$$

$$+ \int \Phi(t, s)\,\hat{B}\,(\underline{u}(s))\,\underline{u}^T(t)\,ds$$

$$+ \int \Phi(t, s)\,\underline{\varepsilon}_e(s)\,\underline{u}^T(t)\,ds. \tag{121}$$

From equation (105)

$$\underline{u}(s)\,\underline{u}^T(t) = (G\underline{m}_e(s) + \underline{m}_y(s) + \underline{\varepsilon}_u(s))\,(\underline{m}_e{}^T(t)G^T$$

$$+ \underline{m}_y{}^T(t) + \underline{\varepsilon}_u{}^T(t)) \tag{122}$$

$$= G\underline{m}_e(s)\,\underline{m}_e{}^T(t)G^T + G\underline{m}_e(s)\,\underline{m}_y{}^T(t) + G\underline{m}_e(s)\underline{\varepsilon}_u{}^T(t)$$

$$+ \underline{m}_y(s)\,\underline{m}_e{}^T(t)G^T + \underline{m}_y(s)\,\underline{m}_y{}^T(t) + \underline{m}_y(s)\underline{\varepsilon}_u{}^T(t)$$

$$+ \underline{\varepsilon}_u(s)\,\underline{m}_e{}^T(t)G^T + \underline{\varepsilon}_u(s)\,\underline{m}_y{}^T(t) + \underline{\varepsilon}_u(s)\underline{\varepsilon}_u{}^T(t) \tag{123}$$

Taking the expected value of equation (123), all but the last term go to zero. That is,

$$E\,[\underline{u}(s)\,\underline{u}^T(t)] = E\,[\underline{\varepsilon}_u(s)\,\underline{\varepsilon}_u{}^T(t)] \tag{124}$$

AD-A071 574 AEROSPACE MEDICAL RESEARCH LAB WRIGHT-PATTERSON AFB OH F/G 5/8
COMBINED DISCRETE NETWORK--CONTINUOUS CONTROL MODELING OF MAN-M--ETC(U)
MAR 79 D J SEIFERT

UNCLASSIFIED AMRL-TR-79-34 NL

2 OF 3
AD
A071574

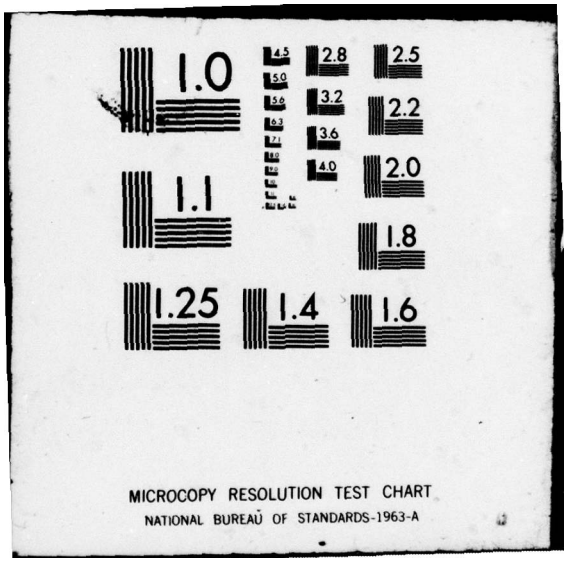
1.0
1.1
1.25
1.4
1.6
1.8
2.0
2.2
2.5
2.8
3.2
3.6
4.0
4.5
5.0
5.6
6.3
7.1
MICROCOPY RESOLUTION TEST CHART
NATIONAL BUREAU OF STANDARDS-1963-A

$$= \int \tfrac{1}{2}\Phi(t,s)\, \underline{V}_{\varepsilon_u}(t)\, \delta(t-s)\, ds \tag{125}$$

$$= \tfrac{1}{2}\, \underline{V}_{\varepsilon_u}(t). \tag{126}$$

From equation (121),

$$E\,[\underline{e}(t)\, \underline{u}^T(t)] = E\,[\underline{e}(t_o)\, \underline{u}^T(t)]$$

$$+ E\,[\hat{B}\,(\underline{u}(s)\, \underline{u}^T(t)]$$

$$+ E\,(\underline{\varepsilon}_e(s)\, \underline{u}^T(t)]. \tag{127}$$

However, $E\,[\underline{e}(t_o)]$ and $E\,[\underline{\varepsilon}_e(s)]$ are both zero. Therefore,

$$E\,[\underline{e}(t)\, \underline{u}^T(t)] = \hat{B}\, E\,[\underline{u}(s)\, \underline{u}^T(t)]. \tag{128}$$

Substituting equation (126) for $E\,[\underline{u}(s)\, \underline{u}^T(t)]$ yields

$$E\,[\underline{e}(t)\, \underline{u}^T(t)] = \tfrac{1}{2}\, \hat{B}\, \underline{V}_{\varepsilon_u}(t). \tag{129}$$

Plugging the results of equations (120) and (129) into equation (115) produces

$$\dot{\underline{V}}(t) = \hat{A}\, \underline{V}(t) + \tfrac{1}{2}\, \hat{B}\, \underline{V}_{\varepsilon_u}{}^T(t)\, \hat{B}^T + \tfrac{1}{2}\, \underline{V}_{\varepsilon_e}{}^T(t)$$

$$+ \underline{V}(t)\, \hat{A}^T + \tfrac{1}{2}\, \hat{B}\, \underline{V}_{\varepsilon_u}(t)\, \hat{B}^T + \tfrac{1}{2}\, \underline{V}_{\varepsilon_e}(t). \tag{130}$$

Combining terms,

$$\dot{\underline{V}}(t) = \hat{A}\, \underline{V}(t) + \underline{V}(t)\, \hat{A}^T + \hat{B}\, \underline{V}_{\varepsilon_u}(t)\, \hat{B}^T + \underline{V}_{\varepsilon_e}(t). \tag{131}$$

Between samples equation (131) serves the same purpose for the covariance propagation as equation (101) does for generating the mean. The computed value of the covariance in equation (131) forms the new best estimate for the next update. This is an attempt to model a situation in which the pilot has some knowledge of the system status and aircraft behavior even though he is not sampling continuously due to other task demands.

Upon taking a sample of one or more state variables, the mean value vector $\underline{m}(t)$ of the displayed variable(s) just read is re-initialized to the sampled values. Similarly, the covariance matrix $\underline{V}(t)$ is also re-initialized. Since the pilot has perfect information about the state variables sampled, with the exception of the display reading error, the covariance terms of these variables are set to the variance of this display error, $\underline{V}_{\epsilon_d}$. Until the next sample occurs, the state variable means and covariances are conditionally updated. The flowchart in Figure 11 summarizes the implementation in the program software.

The aircraft state variable equations, along with the logic for updating mean and covariance estimates, are programmed in subroutine STATE. A detailed description of the task network model and how it interacts with subroutine STATE is included in the next chapter.

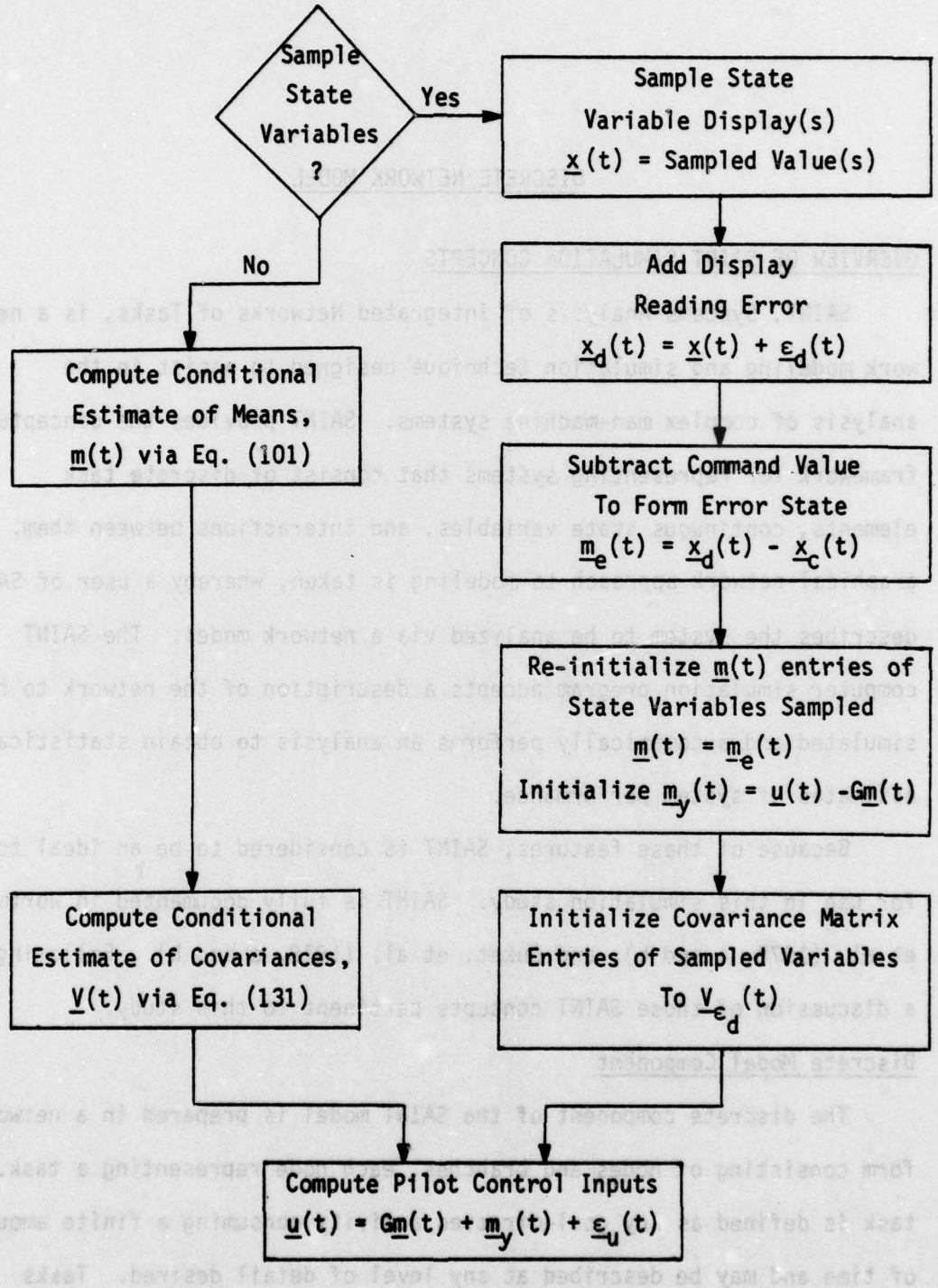

FIGURE 11. FLOWCHART OF STATE VARIABLE MEAN AND COVARIANCE COMPUTATIONS

DISCRETE NETWORK MODEL

OVERVIEW OF SAINT SIMULATION CONCEPTS

SAINT, Systems Analysis of Integrated Networks of Tasks, is a network modeling and simulation technique designed to assist in the analysis of complex man-machine systems. SAINT provides the conceptual framework for representing systems that consist of discrete task elements, continuous state variables, and interactions between them. A graphical-network approach to modeling is taken, whereby a user of SAINT describes the system to be analyzed via a network model. The SAINT computer simulation program accepts a description of the network to be simulated and automatically performs an analysis to obtain statistical estimates of system performance.

Because of these features, SAINT is considered to be an ideal tool for use in this simulation study. SAINT is fully documented in Wortman, et al. (1978, a and b), and Duket, et al. (1978, a and b). Following is a discussion of those SAINT concepts pertinent to this study.

Discrete Model Component

The discrete component of the SAINT model is prepared in a network form consisting of nodes and branches, each node representing a task. A task is defined as any goal-directed activity consuming a finite amount of time and may be described at any level of detail desired. Tasks are described by a set of characteristics (e.g., performance time duration, priority, resource requirements). Branches connecting the

nodes indicate precedence relations and are used to model the sequencing and looping requirements among the tasks. Complex precedence relations have been designed into SAINT to allow predecessor-successor relationships which are deterministic, probabilistic, and conditional. Resources, either human operator or hardware equipment, perform the tasks in accordance with the prescribed precedence relations, subject to resource availability. In addition to specifying predecessor-successor requirements among tasks, the precedence relations indicate the flow of information through the network. Information is organized into packets with each information packet containing attributes that characterize the information being carried. The information packet can characterize items flowing through the network, signals being processed by the network, or any other concept related to network flow. Information attribute values can be assigned or modified at any task in the network and can influence both task performance times and task branching relations. Other attribute types include those used to describe resource characteristics and system attributes, which are global in nature.

Each task in a SAINT network has two requirements which must be satisfied before the task can be performed. First, a specified number of predecessor tasks must be completed before the task is released. Second, once the task has been released, the resource required to perform the task must be available (i.e., they are not busy performing other tasks). All tasks which have been released (all predecessor requirements have been satisfied) but whose required resources are not available are ranked in a queue according to their priority. Task

priority may be assigned at the start of the simulation and may change dynamically as a function of system parameters and contingencies. When the required resources are made available due to task completions, the tasks in the waiting queue are started. The time to perform a task may be specified as a random variable defined by a probability distribution. SAINT supplies the user with eleven different distributions (Normal, Gamma, Beta, Weibull, etc.).

Frequently the task performance time is also a function of the type of task, the resource or resources performing the task, the status of the system, or the condition of the environment at the time the task is executed. SAINT provides for the specification of factors which influence task performance via user-written moderator functions. Examples of such factors include fatigue, operator proficiency, and hardware reliability. In addition to moderator functions, user-written functions (subroutine USERF) can be developed for specifying attribute assignments. Both types of functions are written in FORTRAN or a FORTRAN-compatible language.

Thus SAINT provides for the development of dynamic and realistic system simulation models. Contingencies, decision-making, and emergency conditions can be represented via SAINT's flexible attribute assignment and branching logic.

The basic symbol used to model a task in a SAINT network is illustrated in Figure 12. The input side of the node reflects the precedence requirements for releasing a task. The number of requirements for

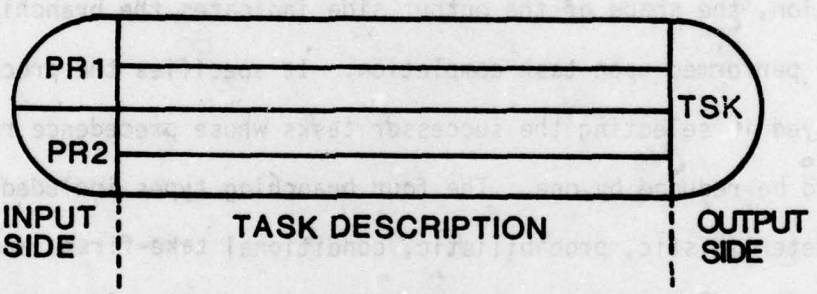

PR1 number of predecessor completions required for first release of the task

PR2 number of predecessor completions required for subsequent release of the task

TSK task number

FIGURE 12. SAINT TASK SYMBOL

releasing a task the first time is on the top (PR1) and the number of requirements for releasing a task on subsequent times is on the bottom (PR2).

The center portion of the task symbol shown in Figure 12 contains all task description information, such as performance time characteristics, statistics to be collected, and attributes to be assigned. It is subdivided into rows, with each row containing a specific type of descriptive information about the task.

The output side of the node contains the task number (TSK). In addition, the shape of the output side indicates the branching operation to be performed upon task completion. It specifies the process to be employed in selecting the successor tasks whose precedence requirements should be reduced by one. The four branching types included in SAINT are deterministic, probabilistic, conditional take-first, and conditional take-all. Their shapes are depicted in Figure 13. Conditions may be based on task completion, simulated time, or attribute values.

Continuous State Variable Model Component

The second component of a SAINT model is the state variable description. While variables describing the task-oriented model component, such as resource busy/idle status, change values at discrete points in time, state variables change values continuously over time. The SAINT user defines these state variables by writing the algebraic, difference, or differential equations that govern their time-dependent behavior. The SAINT user writes the state variable equations in a FORTRAN subroutine (subroutine STATE). SAINT employes a Runge-Kutta-England (RKE) numerical algorithm to integrate the differential equations of subroutine

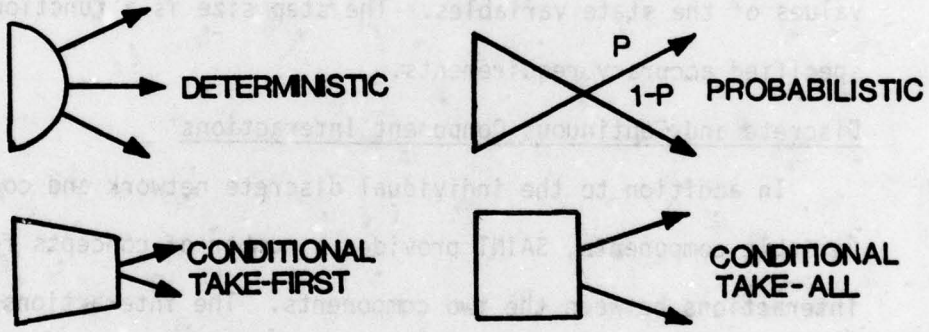

FIGURE 13. TASK BRANCHING SYMBOLISM

STATE. The RKE algorithm obtains a solution to a set of simultaneous first order ordinary differential equations. Higher order differential equations can be modeled by placing the equations in canonical form.

In SAINT, simulated time is advanced in accordance with the type of system being modeled. If no state variables are included, simulated time is advanced from one task completion to the next. When state variables are included in the model, time is also incremented in steps between scheduled task completions for the purpose of updating the values of the state variables. The step size is a function of user-specified accuracy requirements.

Discrete and Continuous Component Interactions

In addition to the individual discrete network and continuous state variable components, SAINT provides a number of concepts for modeling interactions between the two components. The interactions between tasks and state variables are initiated either by tasks being completed or by state variables crossing specified threshold values. Upon the completion of a task, state variables may be discretely regulated by increasing or decreasing their values. In addition, task completions can change the values of logical variables which can be used to alter state variable equation forms or the network structure. In this manner the discrete task-oriented component of the model affects the continuous state variable component.

Threshold crossings by state variables can signal or initiate tasks. Thus the values of state variables can influence task

performance characteristics and precedence relations. Threshold crossings can also change the values of logical variables which, in turn, can be used to alter equation forms or change task precedence.

Many of these SAINT concepts will be illustrated in the following sections which present a detailed description of the SAINT network model constructed for the DAIS system.

DAIS NETWORK DESCRIPTION

A discrete task network was constructed for the DAIS system employing the SAINT symbol set. The network is used to represent several concepts within the model. First of all, it designates the timing and sequencing of the maneuver segments. That is, it models the time duration of the flight control alone segment, followed by the switching instruction, and finally, the MFK task sequence. Secondly, it is used to model the discrete activities of the pilot, which at this time are the MFK switching tasks. These task times are based on the empirical button-push time statistics collected in the DAIS man-in-the-loop simulation. A third role of the network is to represent different state variable display sampling algorithms. The network models the execution of these algorithms and initiates the interaction with the state variable module. The final function of the network is to access the scoring, statistical collection, and plotting routines at the proper intervals.

The baseline SAINT diagram is portrayed in Figure 14. Recall that the numbers at the left of each node represent task precedence requirements and that the number at the right of each node is the task number

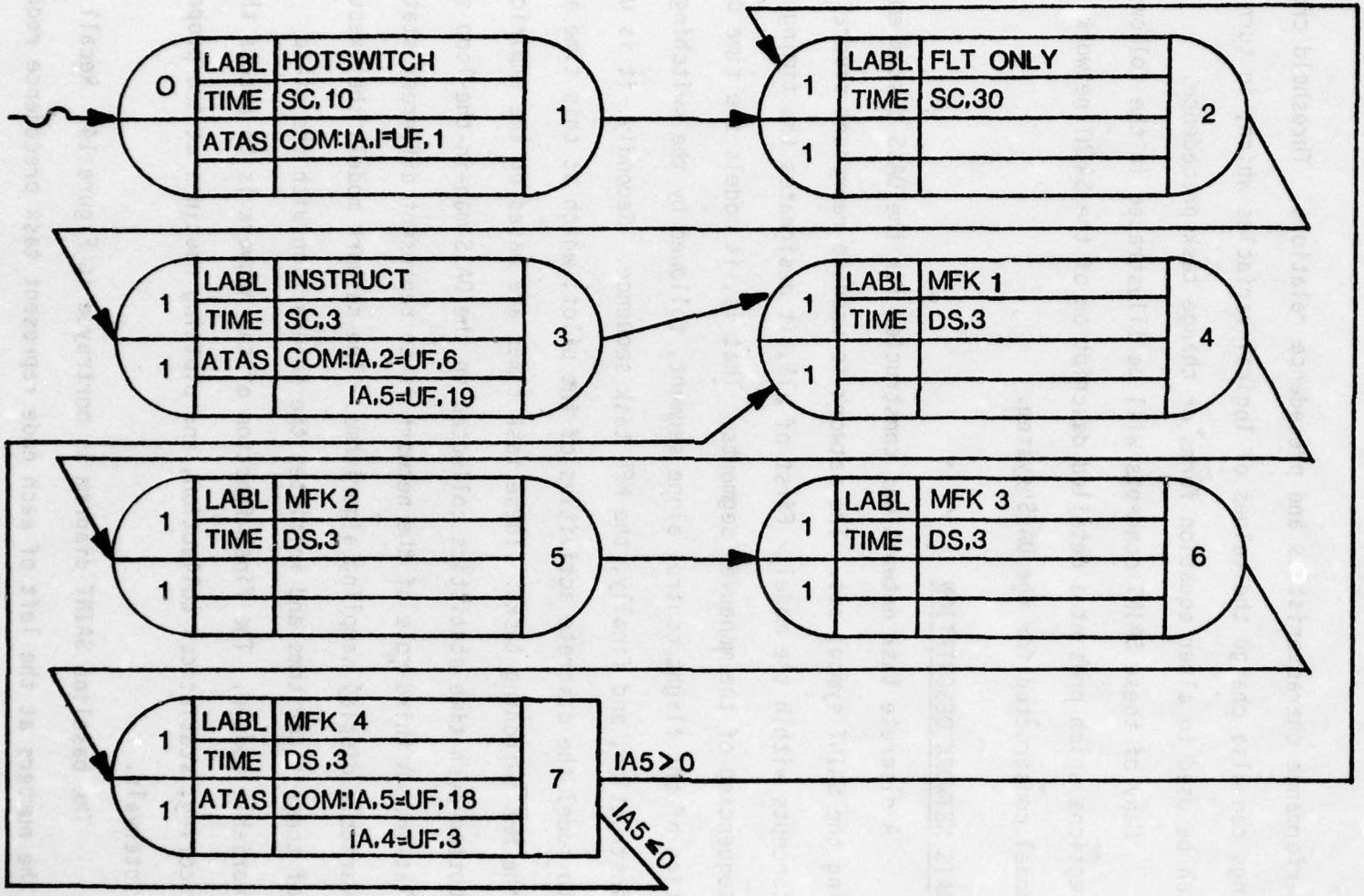

FIGURE 14. DAIS NETWORK DIAGRAM FOR CASE 1

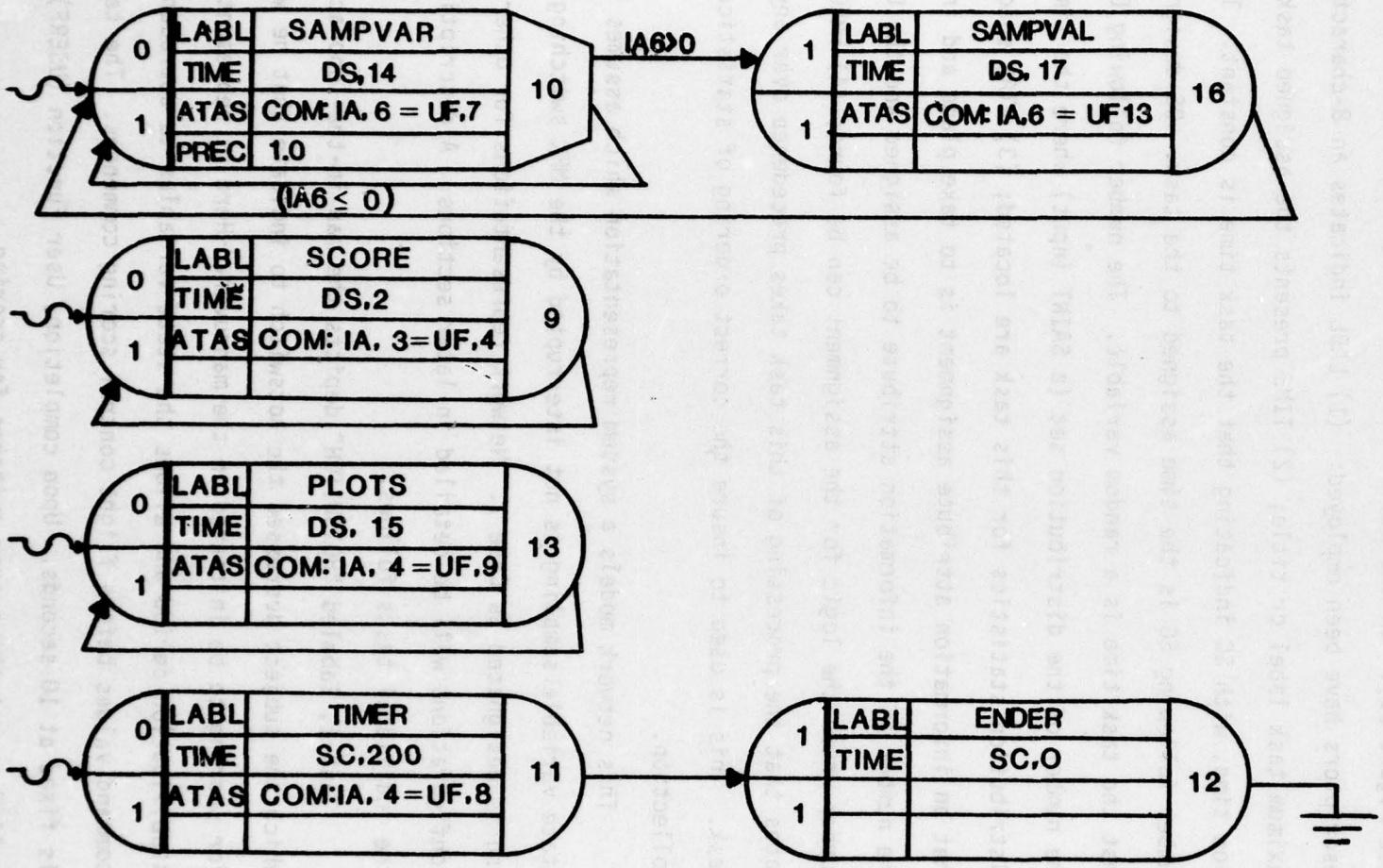

FIGURE 14. CONTINUED

(see Figure 12). In the center portion of the node, four of the SAINT descriptors have been employed: (1) LABL indicates an 8-character maximum task label or title; (2) TIME presents the assigned task execution time, with SC indicating that the task time is constant. The number following SC is the time assigned to the task. DS designates that the task time is a random variable. The number following DS is the number of the distribution set (a SAINT input) where the time distribution statistics for this task are located; (3) ATAS specifies that an information attribute assignment is to take place and includes the number of the information attribute to be assigned and the USERF number where the logic for the assignment can be found; (4) PREC designates that the processing of this task takes precedence over any other task. This is used to insure the correct ordering of statistical collection.

This network models a system representation which assumes that state variable sampling is not interrupted by the MFK switching tasks and is designated as Case 1. Network representations for other system configurations will be detailed in later sections. A description of the individual tasks follows:

Task 1, labeled "HOTSWITCH" depicts the man-in-the-loop action in which the subject depressed the hotswitch to indicate that he was ready for scoring to be initiated on the maneuver. Here it represents a stabilization period and allows the state variables to approach the command values before flight control scoring commences. The task time is fixed at 10 seconds. Upon completion, User Function (USERF) is called to set the proper switches for scoring.

The flight control alone segment of the mission is represented by Task 2 (FLT ONLY). As in the real-time simulation, its duration is 30 seconds. At the start of this task, USERF designates to the scoring routine to begin collecting data in the "flight control alone" mode.

Upon completion of this 30 second segment, the pilot is issued an MFK switching instruction. In the DAIS simulation this instruction averaged three seconds, and thus this is the time assigned to Task 3. While this task time could have been modeled using a probability distribution rather than a constant, it was not deemed to be an important parameter of the model. At the completion of the task, USERF is called to initiate the computation of the score for the "flight alone" phase and to indicate that the multi-function switching task sequence is about to begin.

This MFK sequence is modeled by Tasks 4 through 7. These tasks are repeated for a total of eight switching tasks. In the real-time simulation, the weighted average number of switch closings, pooled over the four task difficulty levels and subjects, was 7.59. Thus eight was chosen as a representative number. The mean and standard deviation for an individual switch closure pooled over maneuvers, subjects, and MFK difficulty levels, were found to be $\bar{X} = 1.08$ and $\sigma = 0.93$ (see Table 7). A normal distribution with these values as the parameters is used for all the switching tasks. Both the number of tasks and the parameters employed could easily be changed to reflect variations in the switching sequence caused by such things as the type of instruction, the level of difficulty, and individual differences. In many instances, these differences would be extremely important for evaluating design variations

and different system configurations. At this point in the DAIS modeling exercise, it was not considered to be a critical issue.

At the second completion of task 7, USERF is called to induce scoring of the switching sequence. Information attribute 5 (IA 5) is updated in USERF to indicate the number of times task 7 has been performed. IA 5 is set to 0 if the sequence of four tasks has been performed only once, and in this case task 7 branches back to task 4 for another performance of these four tasks. A value of 1 in IA 5 indicates that the MFK switching sequence has been completed and task 7 branches back to task 2, "FLT ONLY," for another cycle in the maneuver.

Tasks 10 and 11, which appear on the second page of Figure 14, are used to implement the state variable sampling algorithms and rules. Task 10 specifies a code that determines which variable or set of variables is to be sampled. This code is placed in IA 6 by USERF. If no variables are to be sampled, the code is set to zero, time advances, and task 10 is repeated. If IA 6 is non-zero, task 16 is started. The variable(s) indicated by the code in IA 6 are sampled by calling the appropriate sampling routine indicated in USERF. The specifics of the sampling algorithms employed will be described in detail in later sections. Task 16 branches back to task 10 to determine the next state variable sample to be taken. The time distributions of these two tasks are parameters of the model and are varied as a function of the type of maneuver. Sensitivity analysis was performed on these parameters and will be described in later discussions.

Task 9 triggers the collection of flight parameter data used in the formulas for scoring flight control performance. Subroutine SCORER is

called from USERF and computes the differences between the actual and the command values for the pertinent variables. As in the real-time simulation, these measures are taken every .2 seconds. Thus task 9 has a time duration of .2 seconds and continually repeats itself in cyclic fashion.

The SAINT simulation package contains a plotting routine which facilitates the user in obtaining graphical and tabular output of system variables over time. Task 13 collects and stores flight variables such as altitude, velocity, g-load, vertical velocity, etc. in a format compatible with the plotting routine. Task 13 cycles every .2 seconds and employs USERF to call the plotting routine.

A maneuver lasts 200 seconds. Task 11 is used to implement this timing requirement. At the completion of this task, USERF calls the routines which compute mission statistics (histograms, means, standard deviations) and initiates the state variable plots. Task 11 branches to task 12, a sink task, which signals the end of the simulation.

SAINT/DAIS MODULES

The NETWORK is only one of several modules in the combined discrete/continuous DAIS simulation model. Figure 15 presents an overview of the functions of the modules and their interactions. At the beginning of the simulation, SAINT calls INTLC to initialize the run conditions and program variables. The aircraft equations of motion are initialized, the command values for the maneuver parameters are defined, and starting values for state variable variances and means are specified. In addition, all statistical variables, such as those used in scoring, are initialized.

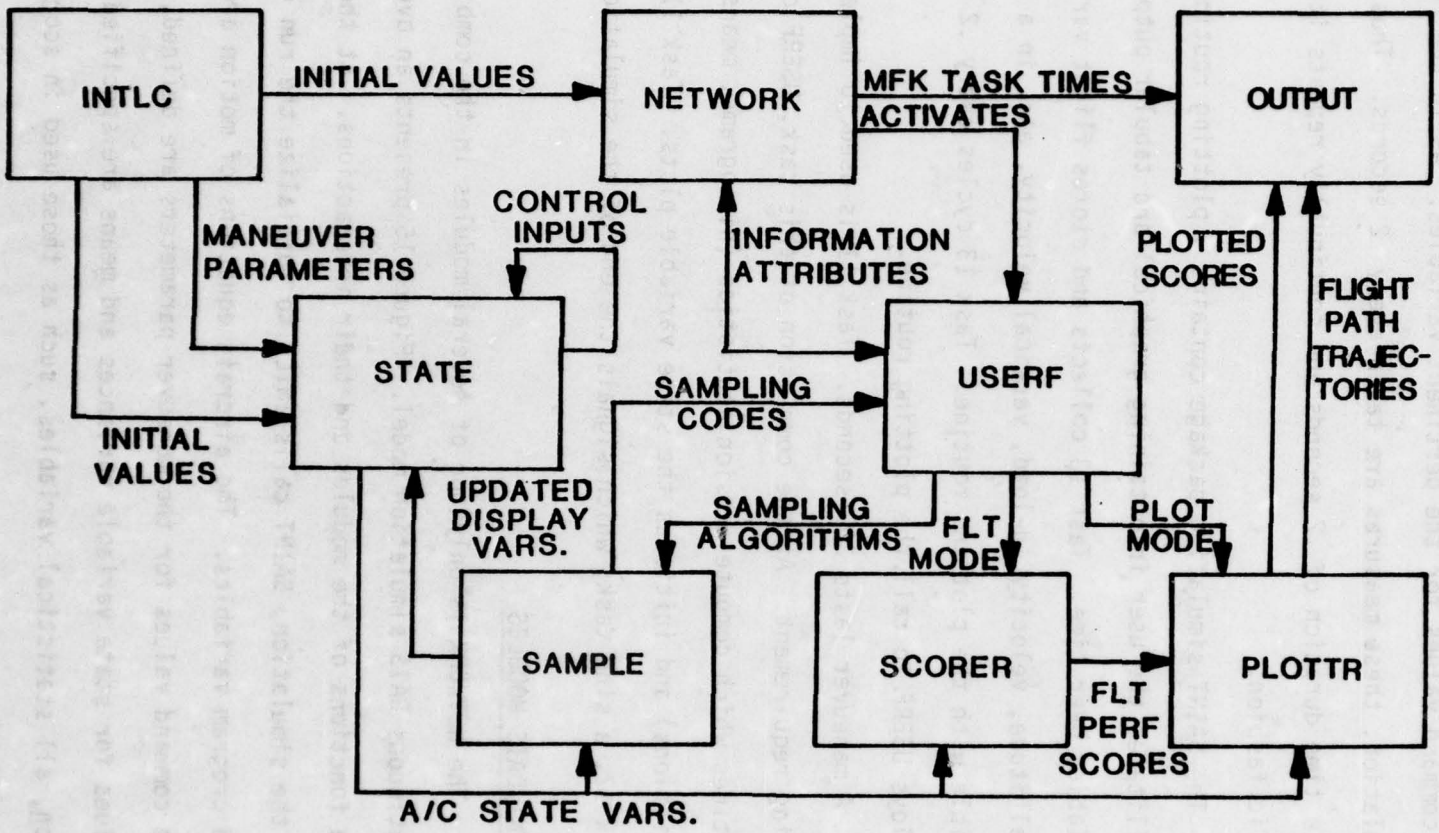

FIGURE 15. STRUCTURE OF SAINT/DAIS MODULES

At this point, both the NETWORK and the STATE modules are initiated. STATE operates in parallel with the NETWORK, with interaction occurring in the form of updated samples of displayed state variables (from SAMPLE). In between samples, STATE computes conditional estimates of the mean and variances of the state variables. From these parameters, the control model determines the "optimal" control inputs for the stick and throttle (u_1, u_2, u_3). These control inputs are then used to update the aircraft equations of motion. This process is repeated every 200 milliseconds.

The NETWORK controls the timing and sequencing of the discrete activities and decisions. It employs USERF to determine and transfer information attribute values and to activate support modules such as SAMPLE, SCORER, and PLOTTR. SAMPLE contains a series of sub-modules, different ones being employed for the various sampling algorithms. The type of sampling to be performed is communicated by the NETWORK via USERF. Sampling is typically performed in two phases; the first phase involves the determination of which variable(s) are to be sampled; the second entails actually taking the sample. Most of the algorithms for determining what samples to take are encoded in FORTRAN, while some, such as in the probability transition matrix approach, are represented by the NETWORK. In either case, communication occurs between the NETWORK and SAMPLE in the form of codes transmitted via information attributes.

SAMPLE employs the current estimates of the aircraft state variables (from STATE) in computing the difference between the actual state variables and their respective command values. A

Gaussian-distributed noise term is added to this term to reflect display reading errors. The updated estimates of the displayed state variables along with their error variances are passed to STATE.

Task 9 ("SCORE") of the NETWORK calls USERF to initiate the scoring routine, SCORER. Other tasks in the NETWORK set codes within USERF which designate the phases of the maneuver, such as the "flight alone" segment. This information is communicated to the SCORER module. SCORER computes and stores the appropriate flight performance scoring statistics in accordance with the flight mode indicator passed to it. Certain codes specify that statistics are to be summarized according to the scoring formulas and printed or passed on to the plotting routine (PLOTTR).

PLOTTR may be activated by Task 13 of the NETWORK. In this case, USERF calls PLOTTR in the data collection mode. PLOTTR stores the aircraft state variables (from STATE), along with the current time, in a format compatible with the SAINT plotting routines. SCORER may also activate PLOTTR and pass it flight performance scores to be plotted as a function of time. At the end of the maneuver (Task 12), USERF calls PLOTTR in the output mode, which designates that both the performance scores and the state variable plots are to be printed.

Thus, similar to the man-in-the-loop simulation, outputs of the SAINT/DAIS model include flight performance scores, flight path trajectories, and MFK task times. There is continual interaction between the discrete network and supporting modules and the continuous state optimal control model. More details on the model parameters and sampling algorithms employed will be discussed in the following two chapters.

BASELINE MODEL CONSTRUCTION

PARAMETER ESTIMATION

A number of model parameters must be quantified for both the straight and level and turning dive maneuvers. These parameters include the quadratic cost function weighting terms for the state variables and controls (Q and R), the state variable display sampling error distributions, and the motor-noise distributions on the control inputs. The following discussion presents the rationale for the selection of these terms.

Quadratic Cost Function Weights

Determination of the state variable weights for the OCM is still considered to be more of an "art" than a science. However, Baron and Levison suggest some heuristic rules for estimating these weights which have been demonstrated to be fairly successful (see, e.g., Baron and Levison, 1973). Maximum allowable deviations, or limits, are determined for each problem variable partly from performance specifications, partly from physical limitations, and partly from a knowledge of human preference and capabilities. The weighting for each quadratic term is then simply the inverse of the square of the corresponding limit.

Kuperman et al. (1977) developed a model of the DAIS system which employed thresholds as the primary impetus for determining when to make control input adjustments. These thresholds were applied as first approximations to the state variable weights. Per the algorithm, the

weights were computed as the inverse of the square of these limits and are displayed in Table 9. In both the straight and level and turning dive maneuvers, the weights on the control variables (n_1, n_2, and n_3) were initially all estimated to be 1.0. The weights on u_1, u_2, and u_3 were set to zero for both maneuvers. Also presented in Table 9 are the "actual" weights employed in the models. These weights evolved over a series of "trial and error" runs in which sensitivity analysis was performed, and the weights were varied until the aircraft appeared to "fly" in a reasonable fashion.

In the straight and level case, the basic problem with employing the original estimates for the weights is that they produce flight performance which is much too good. That is, all the state variables were in much tighter control than indicated in the DAIS experiment. G-load was particularly well behaved. Lowering the weight on g-load did produce some excursions in that variable but did nothing to perturb any of the other variables. Altitude appeared to be the next candidate for examination -- its range was only ±15 ft. of the command value, whereas the threshold was ±75 ft. Variations in the altitude weight proved to be fruitless. There was little sensitivity to the weight, even across different sample intervals. Similarly, variations in the weight on the variable controlling angle of attack (u_1) proved to be somewhat insensitive. Reducing the weight on vertical velocity did produce noticeable results, however. With vertical velocity so tightly controlled, it was only natural that excursions in altitude would be limited. Reducing this weight to .0002 resulted in more reasonable aircraft performance.

TABLE 9

ESTIMATED AND ACTUAL QUADRATIC COST FUNCTION WEIGHTS

STATE VARIABLES	STRAIGHT AND LEVEL		TURNING DIVE	
	ESTIMATED	ACTUAL	ESTIMATED	ACTUAL
Altitude	.000178	.000178	0.0	0.0
Roll	0.0	0.0	.16	.16
Heading	.16	.16	0.0	0.0
Vert. Vel.	.001	.0002*	.001	.0001*
G-load	100	.01*	44.44	10.0*
Velocity	.017778	.017778	.001	1.0*
CONTROL VARIABLES				
n_1	1.0	1000.*	1.0	100.*
n_2	1.0	1.0	1.0	100.*
n_3	1.0	1.0	1.0	1000.*

* Indicates weights that were changed from original estimates.

The turning dive maneuver exhibited the reverse of the straight and level problem -- using the estimated weights, the simulated aircraft crashed into the ground. (Actually, since negative altitudes were not restricted by the model, the vehicle appeared to more closely resemble a submarine than a plane.) Initial attempts to rectify the situation were made by increasing the weights on velocity, vertical velocity, and all three control variables. The u_3 variable, throttle, was still very erratic, and its weight was increased to 1000. These changes helped considerably, but now the model began to abnormally terminate due to extremely small values in lift. Since lift is a function of g-load, its weight was altered next. Intuition suggests increasing the weight to correct the control problems of a given variable. The g-load weight was increased from 44.44 to 100. and resulted in even worse performance. Closer examination revealed that g-load was being over-controlled not under-controlled. The resulting gain matrix produced performance which was continually over-compensating for errors in g-load. Reducing the weight on g-load to 10. resulted in representative values for g-load. Now flight performance was too good; the rate of descent was too slow. Reducing the weight on vertical velocity produced acceptable results.

While these weights are for the most part intuitively pleasing and acceptable in terms of which variables are important within each maneuver, the extreme sensitivity of some weights is of concern. Slight changes in vertical velocity weight in both maneuvers, and g-load in turning dive, produced significant changes in flight performance. In this case, appropriate system behavior was known <u>a priori</u>, and the weights could easily be manipulated to match this performance. Since in general this

is not true, one must question the validity of employing Baron and Levison's algorithm for determining quadratic cost function weights. At a minimum, sensitivity analysis of the weights should be performed.

Display and Motor-Noise Error Distributions

There are at least two different approaches to quantifying these assumed zero-mean Gaussian noise processes. Optimal control theory practitioners advocate a heuristic algorithm based on the "noise/signal ratio" of the displayed variable. Display error distributions are computed using past performance histories. Another approach, which is perhaps more appealing, would be to use more generic estimates of observation error, based on empirical studies of display reading errors while engaged in flight control activities. These distributions would then truly represent observation errors and not just the remnant terms that could not be explained by the optimal control model. In this combined formulation, the additional "remnant" human behaviors would hopefully be represented in the network and sampling models.

An extensive review of the "display" literature was made. Many of the empirical studies in this area have been performed by AMRL, or in close conjunction with AMRL. Most of this work took place in the early fifties. While a large number of studies have been performed on displays and display errors, they unfortunately do not apply to the problem at hand. The majority of the studies were not performed under flight control conditions. The displayed variables the subjects were to read differed from trial to trial, and thus did not reflect the same errors as would occur in a continuous monitoring mode. Some empirical research was performed in a tracking mode. In these experiments, they

were typically comparing flight performance as a function of different types of displays (circular dial displays vs. tape displays, e.g.). Individual display reading errors were not recorded. Because of this failure to find any empirical data on display observation errors, it was decided to use the optimal control algorithm estimates as a first approximation. A summary of the approach follows.

Each of the displayed variables utilized by the human is assumed to be perturbed by a zero-mean Gaussian noise process that is linearly uncorrelated with other such noise processes and with system input noise disturbances. Therefore, each noise process can be quantified by a single parameter; namely, its autocovariance. The autocovariance of each observation noise component appears to vary proportionately with the mean squared signal level. Thus,

$$E\{v_{y_i}(t)\, v_{y_i}(s)\} = V_{y_i}(t)\, \delta(t-s)$$

$$V_{y_i}(t) = \pi P_i E\{y_i^2(t)\}$$

$$= \pi P_i y_i^2(t)$$

where P_i is the noise/signal ratio and has units of normalized power per rad/sec. Numerical values for P_i of .01 (i.e., -20 dB) have been employed successfully (Baron, 1976).

Estimates of the variance of the display error noise term were computed from the DAIS empirical data base employing this algorithm

$$\sigma_y^2 = (.01)(\pi)(\text{MEAN SQUARE ERROR}_y).$$

A similar heuristic rule is recommended for the motor noise terms. In this case, the suggested value for P_i is .003 (i.e., -25 dB). Thus,

$$\sigma_u^2 = (.003)(\pi)(\text{MEAN SQUARE ERROR}_u).$$

The resulting parameters for the error distribution terms for straight and level are contained in Table 10. Similarly, Table 11 lists the parameters for the turning dive maneuver. The minimum and maximum values of the distributions (required by SAINT), are set to three times the standard deviation.

BASELINE MODEL RUNS

Case 1

A series of model runs were made in the Case 1 configuration employing the parameter values defined in the previous section. Recall that Case 1 specifies that all state variable displays are to be sampled every n time units. The assumption is made that the multi-function switching tasks do not interfere with the flight control variable sampling. The flight control display variable sampling interval was varied over a range of 1. to 10. seconds for straight and level, and .5 to 2. seconds for turning dive. The resulting overall scores for three different initial random number seeds are displayed in Tables 12 and 13. Each random number seed corresponds to a new sample from the ensemble of mission scores. A graphical representation of the data appears in Figures 16 and 17. The three symbols displayed on the graph denote the three different samples taken at that sample interval.

Several things are apparent. Variations in model scores do occur as a function of the initial random number seed chosen. However, with

TABLE 10

STRAIGHT AND LEVEL DISTRIBUTION PARAMETERS FOR OBSERVATION AND MOTOR NOISE TERMS

VARIABLE	MEAN SQUARE ERROR	STD. DEV. $\sigma = \sqrt{P_i \pi \text{ MSE}}$	MINIMUM	MAXIMUM
Altitude	2269.	8.44	-25.33	25.33
Velocity	56.98	1.34	-4.01	4.01
G-load	.01657	.0228	-.068	.068
u_1	$.534 \times 10^{-3}$	.0022	-.007	.007
u_2	.910 E-4	.0093*	-	-
u_3	.007662	.0085	-.025	.025

* Assumed zero.

TABLE 11

TURNING DIVE DISTRIBUTION PARAMTERS FOR OBSERVATION AND MOTOR NOISE TERMS

VARIABLE	MEAN SQUARE ERROR	STD. DEV. $\sigma = \sqrt{P_{i\pi}\ MSE}$	MINIMUM	MAXIMUM
Vertical Vel.	511.3889	4.008	-12.02	12.02
G-load	.0847	.052	-.155	.155
Velocity	154.3	2.202	-6.6	6.6
u_1	.0098	.0096	-.029	.029
u_2	.797	.0867	-.26	.26
u_3	.038	.0189	-.057	.057

TABLE 12

STRAIGHT AND LEVEL CASE 1 SCORES

SAMPLE INTERVAL (SEC)	RANDOM NUMBER SEED		
	1	2	3
1	.1228	.1217	.1227
2	.1745	.1658	.1598
3	.2105	.2107	.2037
4	.2529	.3237	.2601
4.5	.5389	.6241	.3600
5	.8483	.8913	.5772
6	.3594	.4828	.3562
7	.4068	.4253	.4094
10	.6056	.5075	.5161

TABLE 13

TURNING DIVE CASE 1 SCORES

SAMPLE INTERVAL (SEC)	RANDOM NUMBER SEED		
	1	2	3
.5	3.259	2.564	2.810
.6	3.146	3.332	2.402
.75	2.940	2.134	2.859
.8	2.578	2.097	2.997
1.0	9.915	8.892	9.660
1.4	4.515	4.716	7.646
1.6	5.980	3.652	5.945
1.8	8.825	7.101	9.399
2.0	11.510	17.680	11.810

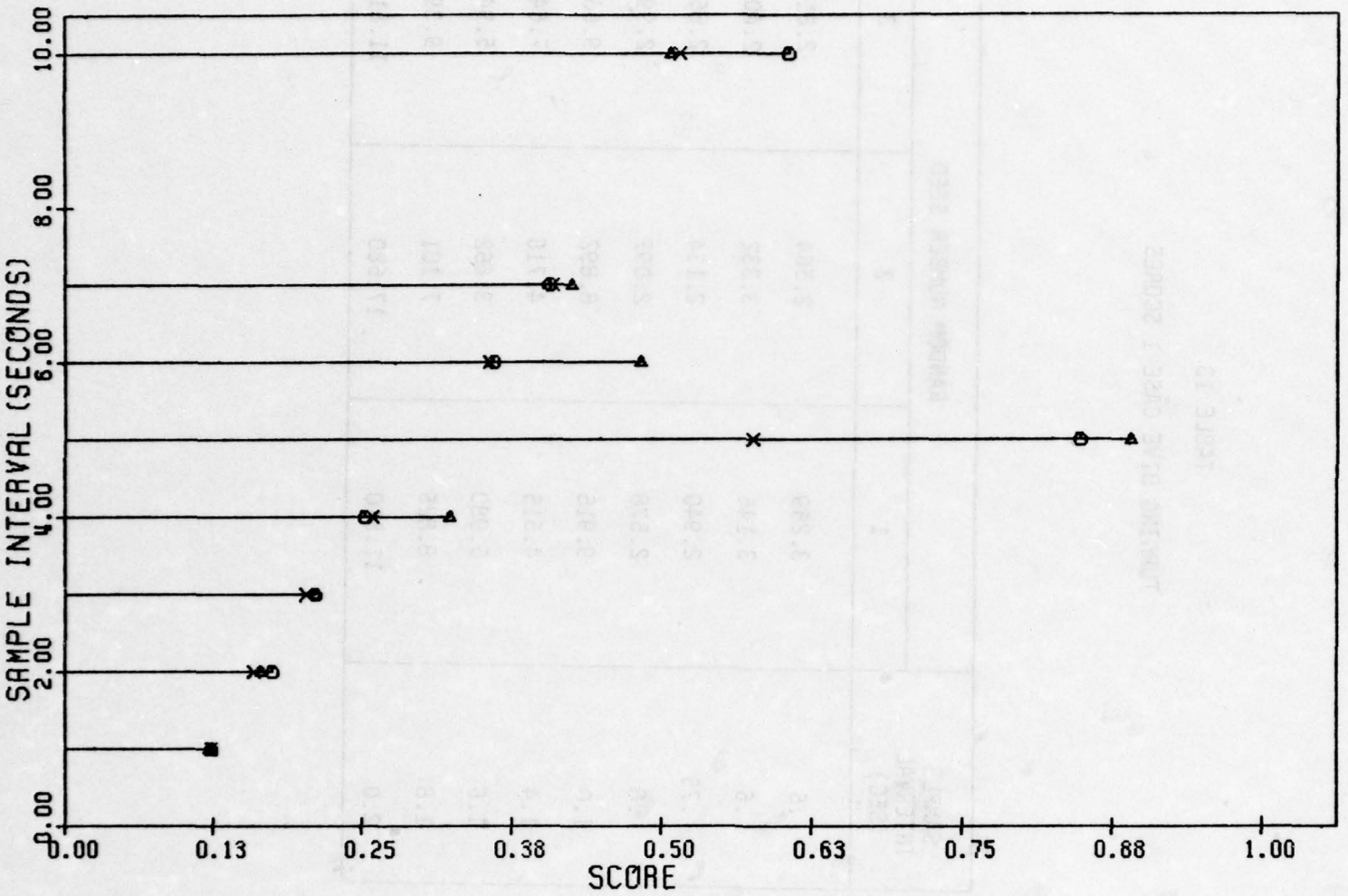

FIGURE 16. STRAIGHT AND LEVEL CASE 1 SCORES AS A FUNCTION OF THE SAMPLE INTERVAL

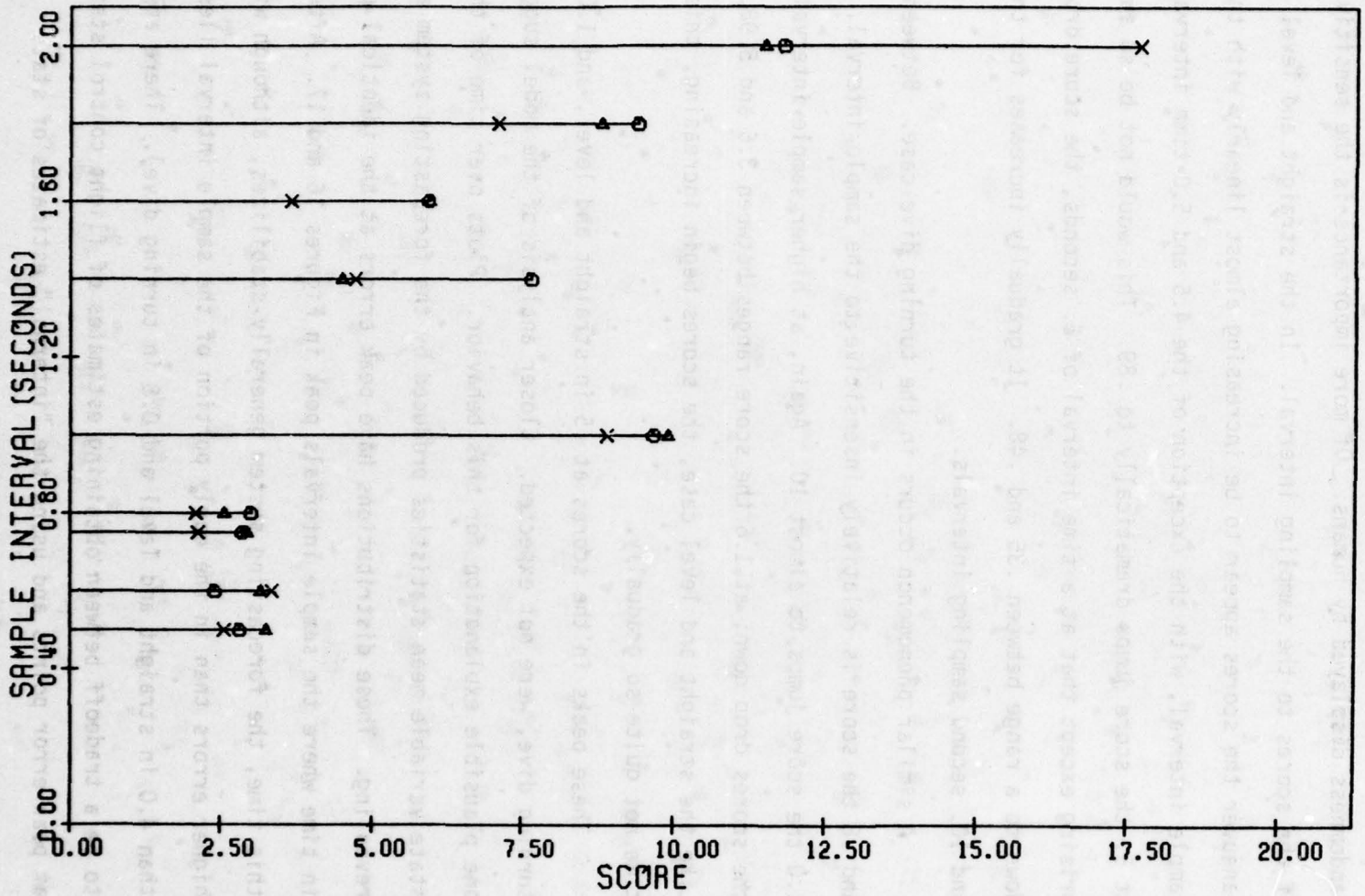

FIGURE 17. TURNING DIVE CASE 1 SCORES AS A FUNCTION OF THE SAMPLE INTERVAL

a couple exceptions, these do not appear extreme and are not unlike the randomness displayed by humans. Of more importance is the sensitivity of the scores to the sampling interval. In the straight and level maneuver the scores appear to be increasing almost linearly with the sample interval, with the exception of the 4.5 and 5.0 time intervals. At 5. the score jumps dramatically to .89. This would not be so surprising except that at a time interval of 6. seconds, the score drops down to a range between .35 and .48. It gradually increases for the 7. and 10. second sampling intervals.

A similar phenomenon occurs in the turning dive case. Between .5 and .8 the score is relatively insensitive to the sample interval. At 1.0 the score jumps to almost 10. Again, at higher sample intervals the scores drop down; at 1.6 the score ranges between 3.6 and 5.98. Like the straight and level case, the scores begin increasing, this time not quite so gradually.

These peaks in the scores at .5 in straight and level, and 1.0 in turning dive, were not expected. Closer analysis of the model suggests one plausible explanation for this behavior. Plots over time of the state variable mean statistics produced by the forecasting system are revealing. These distributions have peak errors at the identical points in time where the sample intervals peak in Figures 16 and 17. After this time, the forecasting system generally stabilizes, although with higher errors than in the early portion of the sample interval (less than 4.0 in straight and level and 0.8 in turning dive). There appears to be a tradeoff between obtaining estimates of flight control states at peak error points and using the "internal" estimates of state

variable values. This suggests in the turning dive case that if samples cannot be taken before .8 second intervals, that perhaps it would be better to wait until around 1.6 secs. A similar case can be made for the straight and level maneuver.

Comparison to DAIS Results

The objective of this study effort is to demonstrate the feasibility of employing combined modeling approaches for exploring such things as alternate sampling rules, priority schemes, and system configurations, many of which extend far beyond the scope of the DAIS man-in-the-loop studies. Therefore, the intent here was not to try to "match" the DAIS experimental results precisely, but rather to use it as a baseline departure point for examining alternate issues.

Results of the Case 1 runs for both maneuvers appear to reflect fairly well the performance of the DAIS subjects. In the straight and level flight alone maneuver, DAIS subjects averaged a score of .727 with a standard deviation of .219. Experimenters indicated that the highly motivated pilots consistently performed at the .5 level. Figure 16 suggests that the sampling interval could span up to 10 seconds and still maintain scores within one standard deviation of the DAIS subjects. Likewise, comparable scores can be obtained in the turning dive maneuver with sample intervals up to 1.6 seconds. The DAIS experimental results produced a mean score of 5.495 with a 1.135 standard deviation. Thus the model results appear to be in agreement with the DAIS man-in-the-loop study scores.

Cases 2 and 3

It is probably quite unrealistic to assume that the MFK tasks do not interfere with the flight control variable sampling; nor is it apparent that the pilot operates in a strict priority mode. He more likely "time shares" between flight control and switching, appearing to operate almost in parallel. This behavior is difficult to represent in a simulation model. One possible approach is to use an interleave scheme during the switching task period in which the pilot alternates between an MFK subtask and a flight control display update. This sampling scheme has been termed Case 2, and a graph of the network model description is contained in Figure 18. Tasks 14, 15, 17, and 19 have been added to represent the "between MFK task" display sampling activities. No sampling is permitted during the individual MFK tasks. The rest of the network is identical to Case 1.

An alternate sampling scheme, which is the counterpart to Case 1, gives switching priority over flight control. In this formulation (Case 3), the pilot would under no condition interrupt a keyboard task to update his control task. This represents an extreme or "worst" case in terms of the amount of time devoted to flight control. Figure 19 displays the SAINT network for Case 3. No sampling is performed during or between tasks 4-7. At the end of the second completion of task 7, task 14 is performed. Task 14 samples all of the flight control variables before returning to the flight alone segment of the maneuver.

Models of Cases 2 and 3 were exercised for both maneuvers. Graphs of the straight and level scores resulting from 3 different initial random number seeds appear in Figures 20 and 21. Table 14 contains a

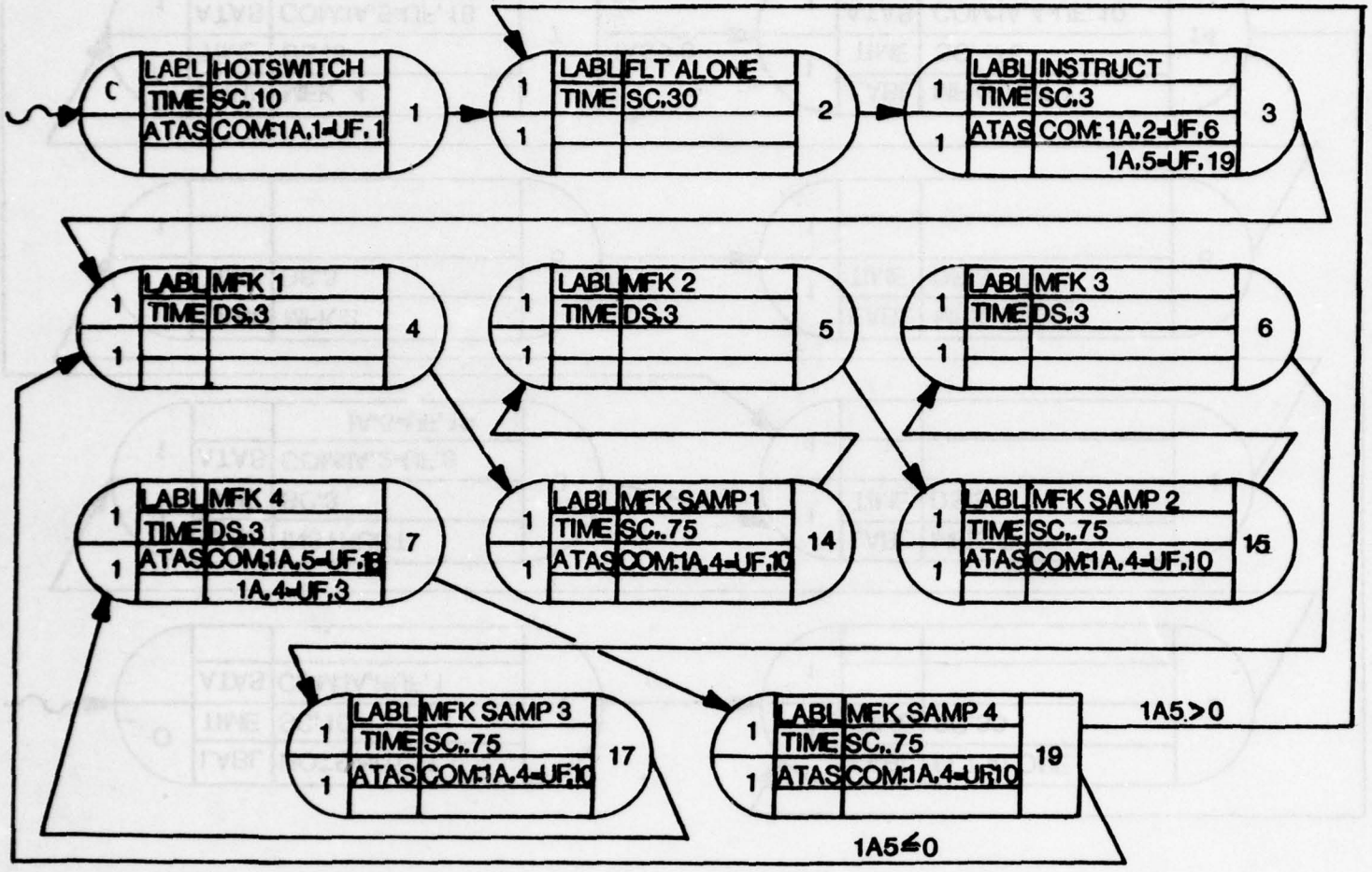

FIGURE 18. CASE 2 NETWORK

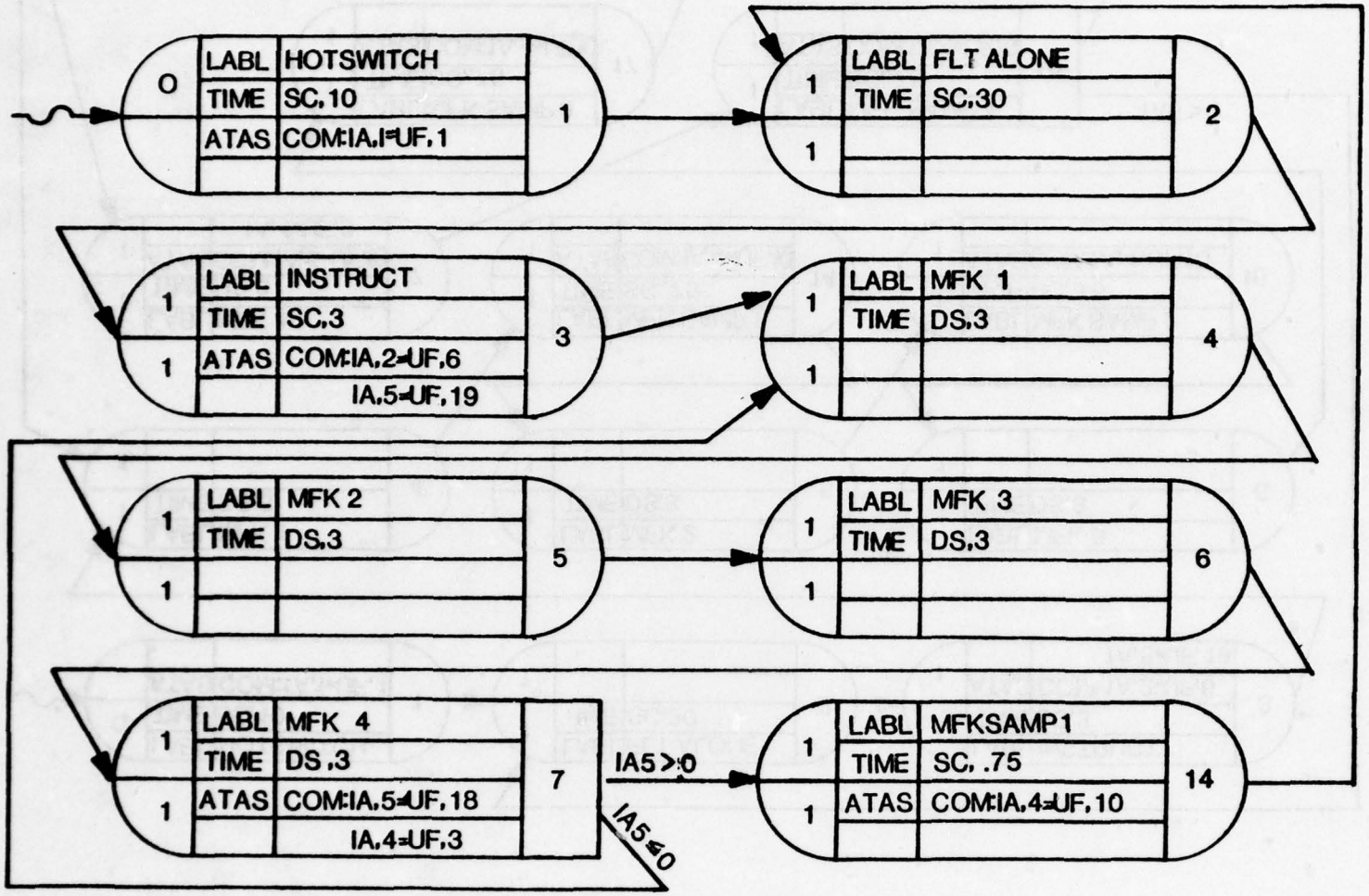

FIGURE 19. CASE 3 NETWORK

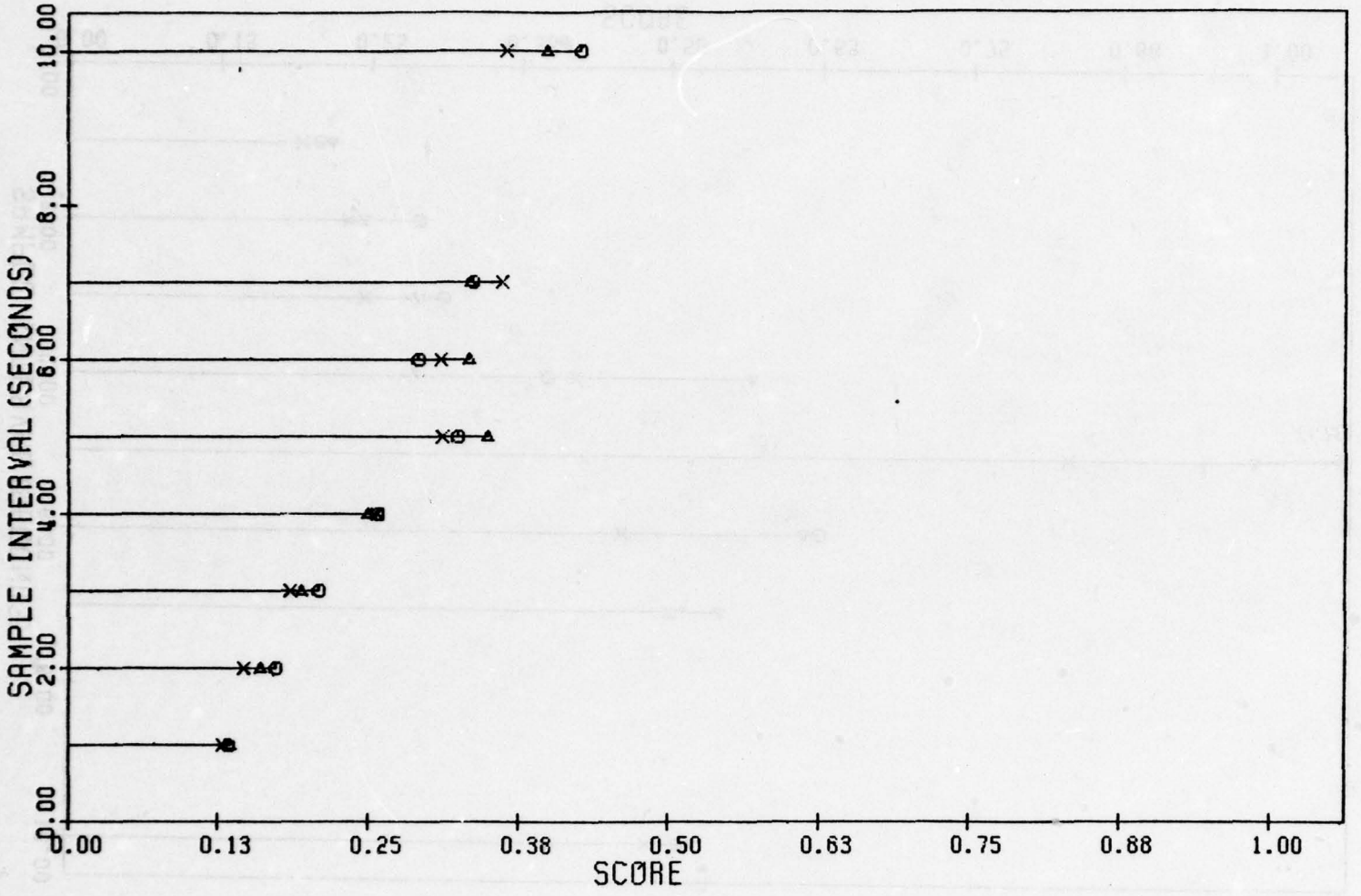

FIGURE 20. STRAIGHT AND LEVEL CASE 2 SCORES AS A FUNCTION OF THE SAMPLE INTERVAL

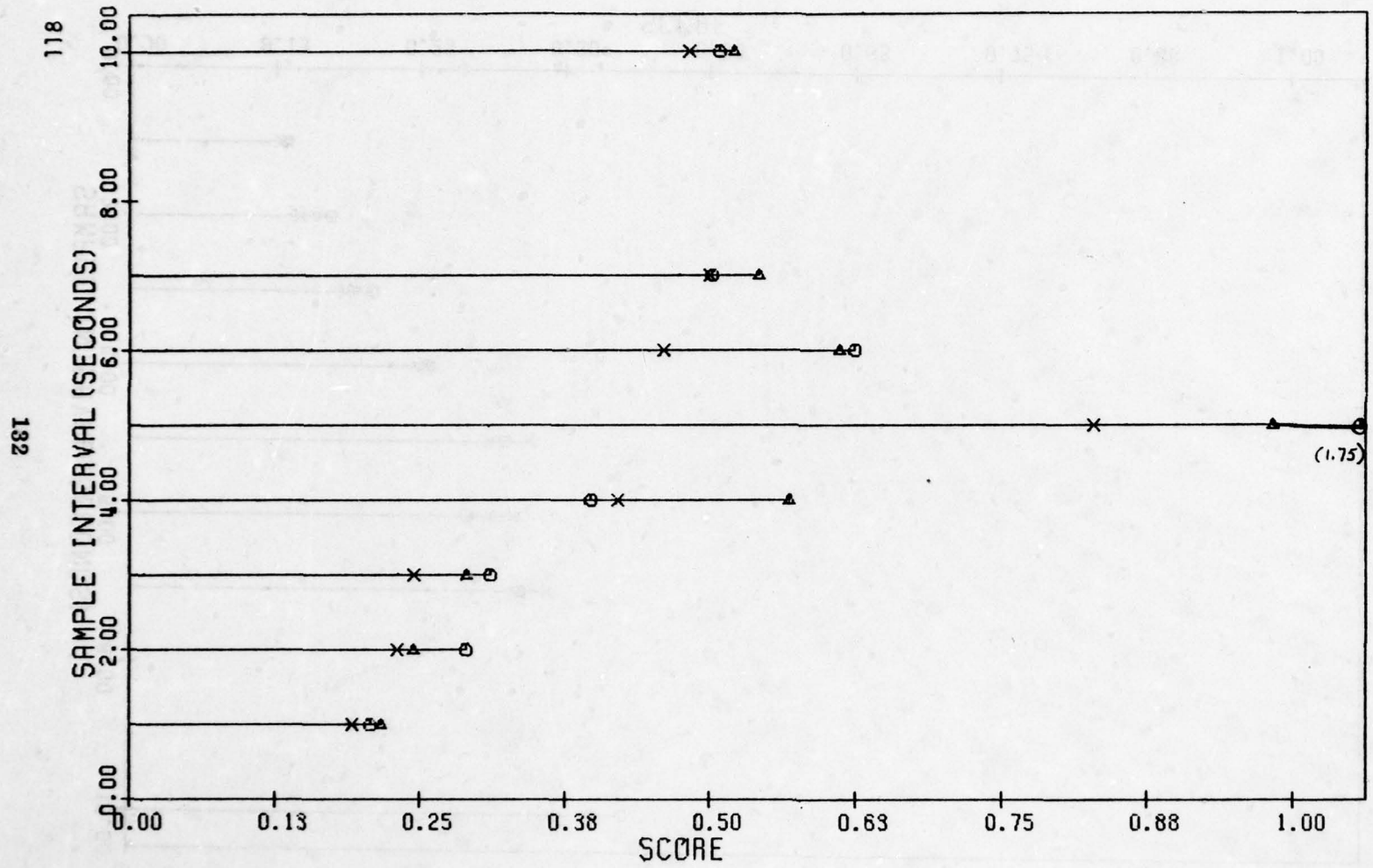

FIGURE 21. STRAIGHT AND LEVEL CASE 3 SCORES AS A FUNCTION OF THE SAMPLE INTERVAL

TABLE 14

STRAIGHT AND LEVEL AVERAGE SCORES

SAMPLE INTERVAL (SEC)	CASE 1 (AVERAGE)	CASE 2 (AVERAGE)	CASE 3 (AVERAGE)
1	.1224	.1330	.2059
2	.1667	.1599	.2553
3	.2083	.1972	.2819
4	.2789	.2551	.4618
5	.7723	.3293	1.1880
6	.3995	.3127	.5549
7	.4138	.3451	.5148
10	.5431	.3976	.5028

summary of the score statistics for all three cases. In Case 2, state variable sampling is performed between each of the eight MFK tasks, each of which have mean durations of 1.08 seconds. During the "flight alone" segments of the mission, sampling is performed at the regular specified interval. Thus for intervals greater than 1.08, Case 2 sampling would actually occur more frequently than in the Case 1 condition, and lower scores would be expected. This is precisely what occurred. At the 1 sec. sample interval, the Case 2 average score of .1330 is higher than the Case 1 score of .1224. At all the other intervals (2 through 10), the Case 2 score is lower, as anticipated. It is also of interest to note that the peak at 5 sec. is barely noticeable due to the increased sampling.

In Case 3 no sampling is performed during the MFK switching sequence, which has an average duration of 8.64 secs. The Case 3 results for sample intervals between 1 and 7 secs. indicate scores which in all instances are higher than the Case 1 scores. The results of a 1-way ANOVA determined that Case 3 scores are significantly different from those of Case 1 at the $\alpha = .0014$ level. It is to be noted, however, that all Case 3 scores, with the exception of the 5 second interval, are well within acceptable behavior. For the 10 second interval, sampling actually occurs more in Case 3 than in Case 1 since the average duration of the switching sequence is 8.64. As expected, the Case 3 score is slightly better.

Graphs for the turning dive Cases 2 and 3 scores are displayed in Figures 22 and 23. Summary statistics for all three cases can be found in Table 15. Peaks in the scores at 1.0 are still quite evident in both

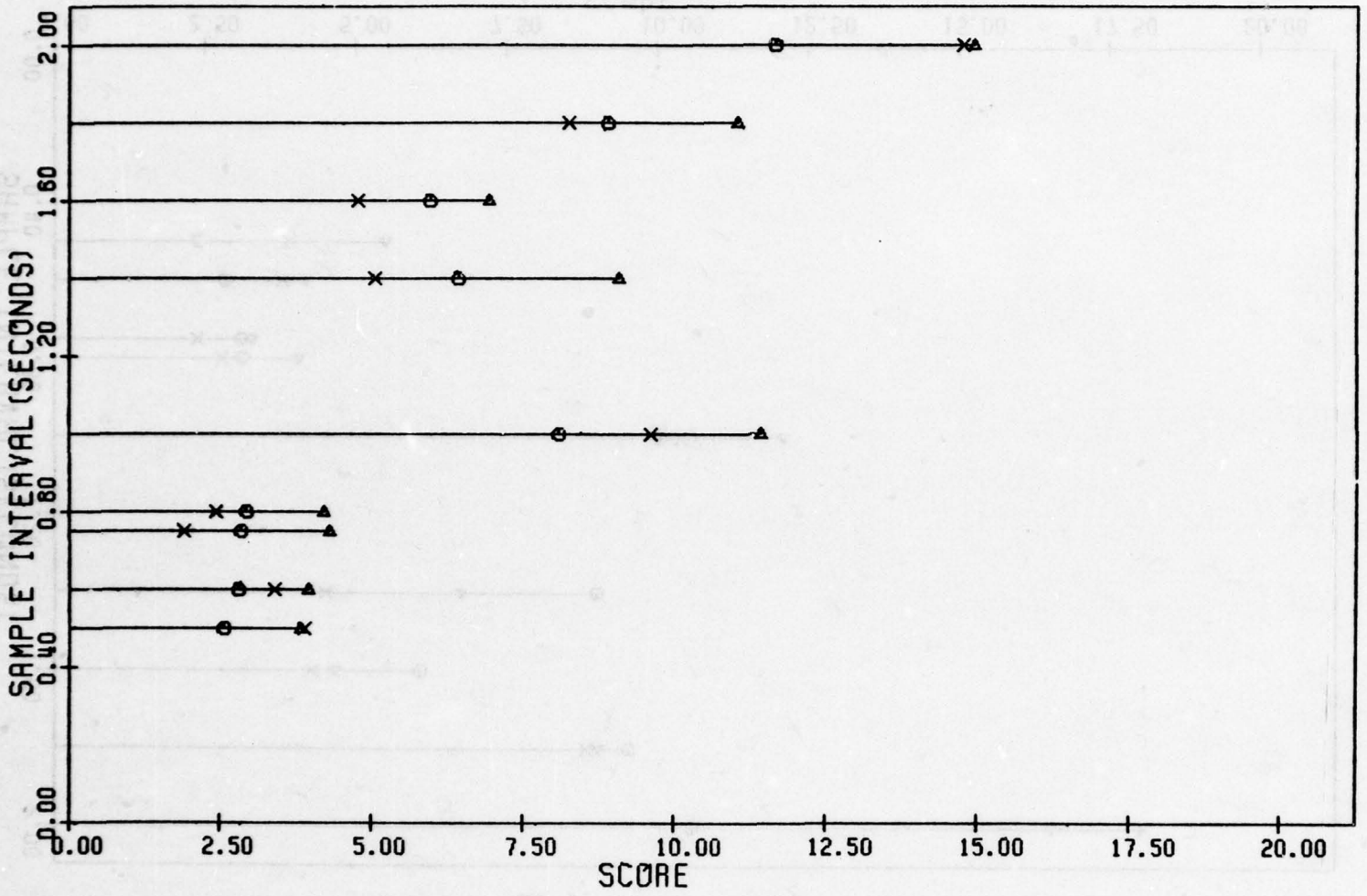

FIGURE 22. TURNING DIVE CASE 2 SCORES AS A FUNCTION OF THE SAMPLE INTERVAL

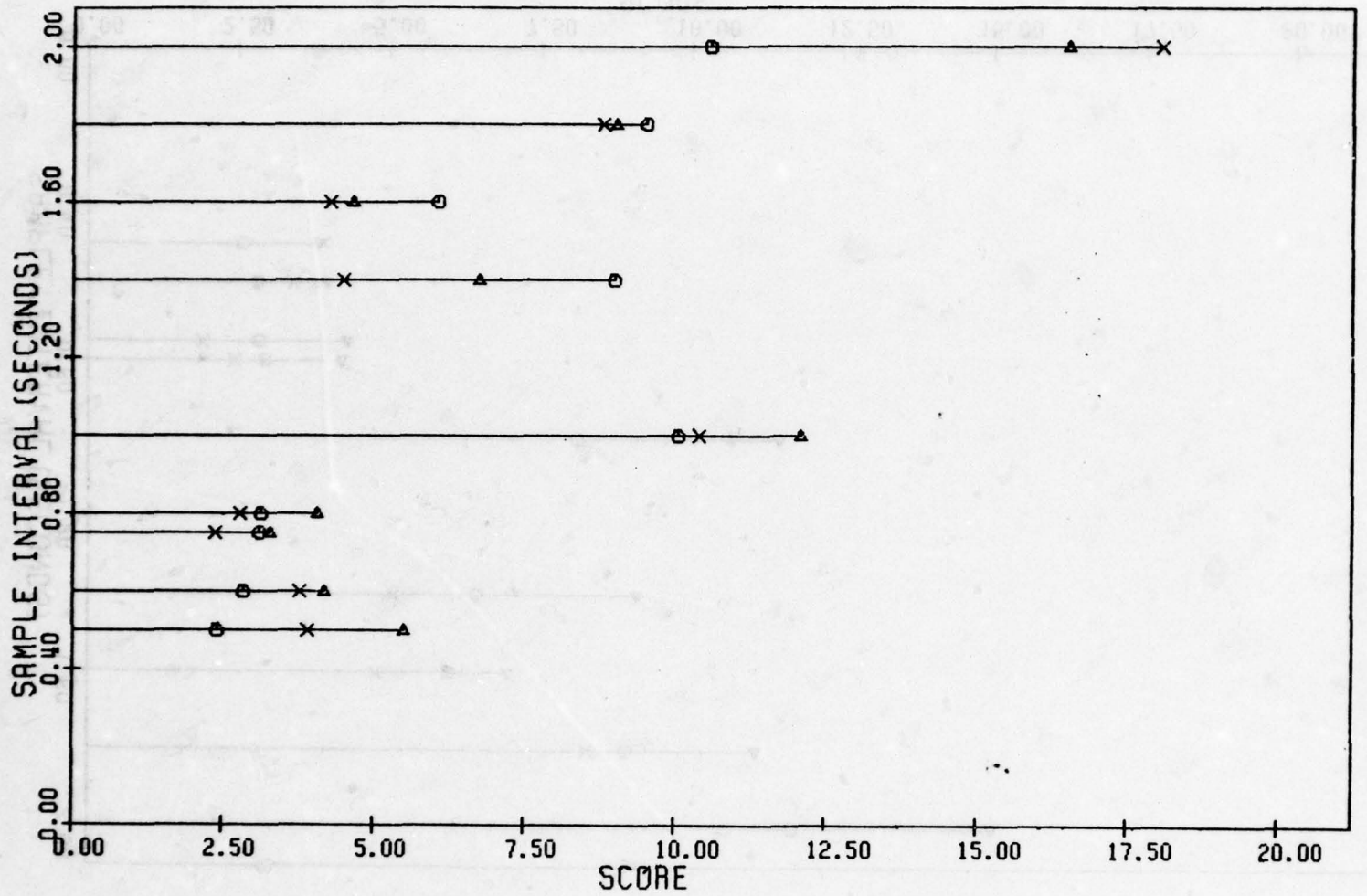

FIGURE 23. TURNING DIVE CASE 3 SCORES AS A FUNCTION OF THE SAMPLE INTERVAL

TABLE 15

TURNING DIVE AVERAGE SCORES

SAMPLE INTERVAL (SEC)	CASE 1 (AVERAGE)	CASE 2 (AVERAGE)	CASE 3 (AVERAGE)
.5	2.878	3.434	3.936
.6	2.961	3.396	3.598
.75	2.644	3.021	2.915
.8	2.557	3.198	3.316
1.0	9.489	9.714	10.853
1.4	5.626	6.857	6.754
1.6	5.192	5.886	5.004
1.8	8.442	9.388	9.128
2.0	13.667	13.783	15.063

cases. A 1-way ANOVA across the three cases only showed an overall conservative significant difference (using a mean squared error across sample intervals) at the $\alpha = .10$ level. Further analysis, via planned comparisons of the individual cases taken in pairs, resulted in the significance levels displayed in Table 16.

TABLE 16
SIGNIFICANCE LEVELS OF PLANNED COMPARISONS

CASES	SIGNIFICANCE LEVEL
1, 2	$\alpha = .1076$
1, 3	$\alpha = .0543$
2, 3	$\alpha = .5964$

The only cases which can be considered significantly different are 1 and 3. It was anticipated that this difference would have been more highly significant. A detailed analysis of the Case 3 model was performed and the results are described in the following section.

SENSITIVITY ANALYSIS ON COMPONENTS OF ERROR

Three separate flight performance scores are recorded for each mission: (1) flight alone phase, (2) flight and MFK switching phase, and (3) overall mission scores. In Case 3 the intuitive notion was that the scores would be much worse (higher) during the combined flight control and switching segments than during the flight alone segments, since no sampling was permitted during these sequences. However, this was not generally true. It was decided to examine flight performance in more detail than that afforded by the three "averaged" scores. A

new task was added to the network which activated the scoring routine every 1.4 time units. Thus, after every 7 update points, a new score is computed. The selection of 7 points was somewhat arbitrary, although any less than this number would have probably been too short a time span. This new scoring scheme was then applied to the Case 3 turning dive maneuver. Turning dive was selected because of its complexity, difficulty, and its resulting sensitivity to sampling interruptions. Also of concern is the great deal of variability in scores that it demonstrates, often with illogical results.

A graph of the scores for the turning dive, Case 3, appear in Figure 24. The Δ's indicate when MFK switching is occurring. No clear patterns or trends exist. There appears to be a great deal more variability in the scores than was expected, certainly more than can be ascertained from "mean" data. The extreme range of the scores is also of concern. At some instances the vehicle is very well controlled; at other points in time, control is much less well established.

In an attempt to determine if these characteristics were just anomalies of the simulation model, a similar graph was prepared for a "typical" turning dive maneuver from the real-time experiment (see Figure 25). It shows the same degree of variability as the model outputs and also indicates approximately the same range of scores. It appears that the model is duplicating fairly well the performance of the DAIS subjects.

An attempt was made to determine the nature of this variability. The same turning dive Case 3 condition as depicted in Figure 24 was rerun with all the display and control input error distributions

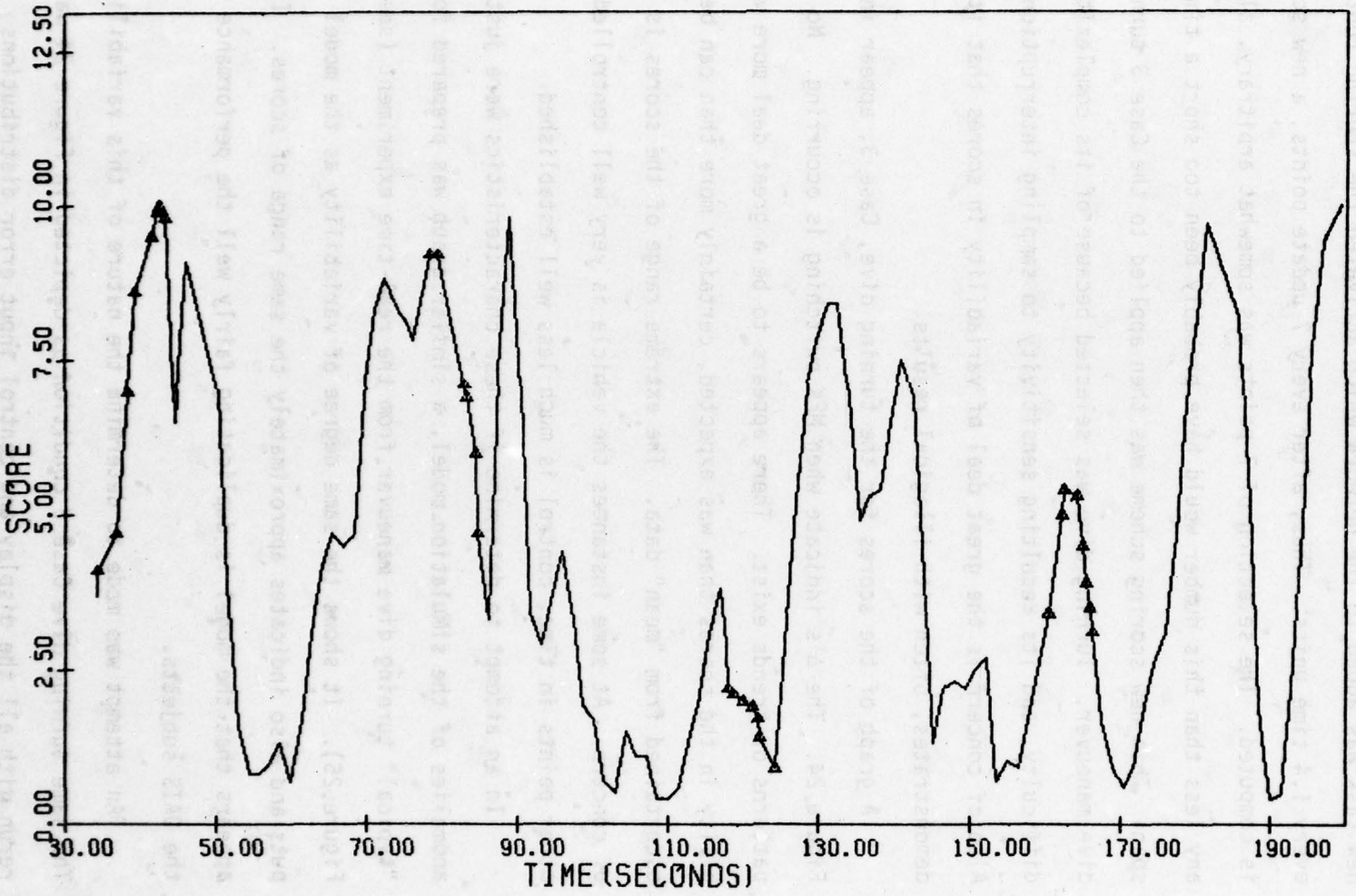

FIGURE 24. TURNING DIVE CASE 3 SCORES

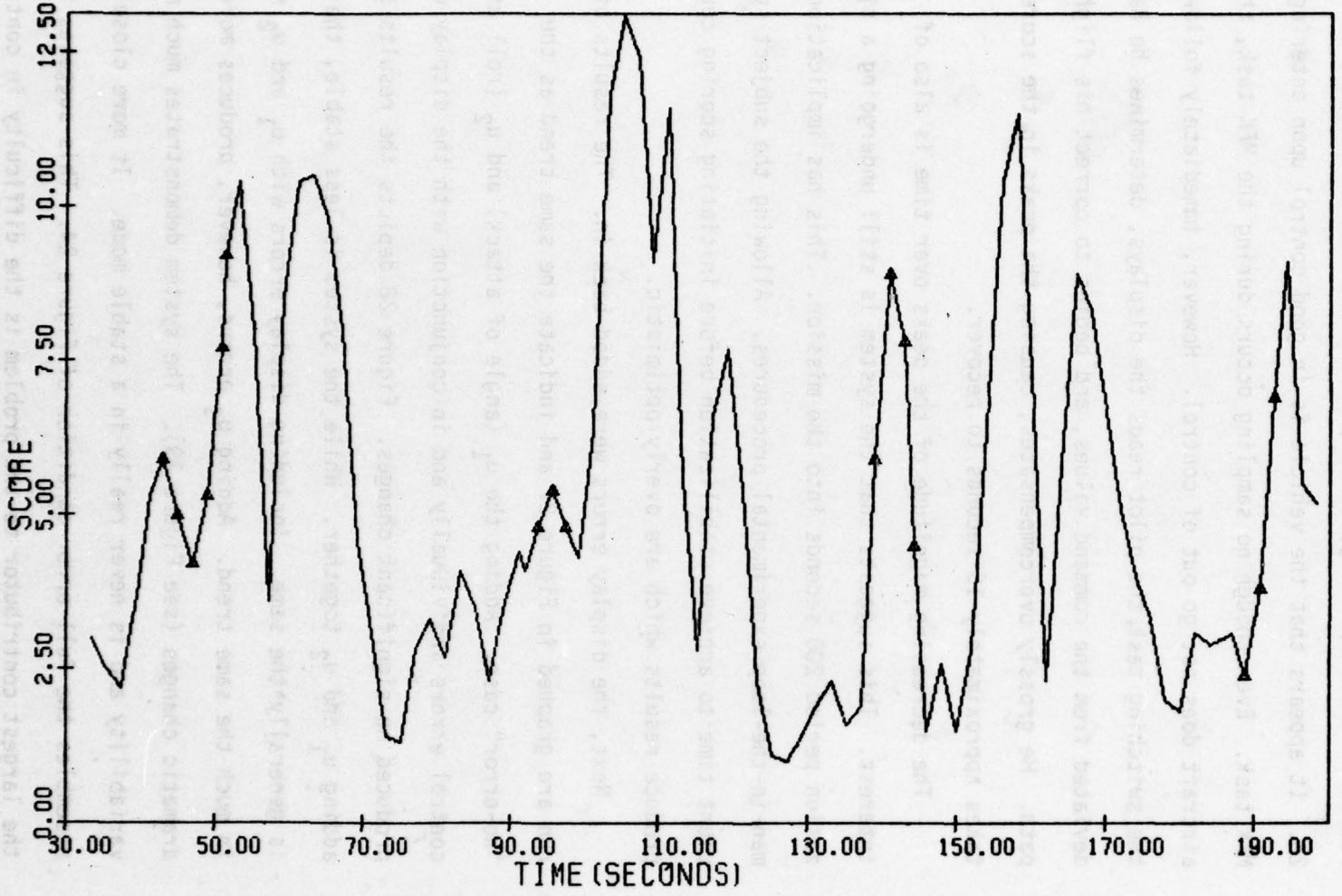

FIGURE 25. "TYPICAL" TURNING DIVE SCORES FROM REAL-TIME EXPERIMENT

removed. The surprising, but logical, results are contained in Figure 26. It appears that the vehicle is in good control upon entering the MFK task. Even though no sampling occurs during the MFK task, the aircraft does not go out of control. However, immediately following the switching task, the pilot reads the displays, determines he has deviated from the command values, and begins to correct his flight path. He grossly overcompensates, causing the peaks in the score, and takes approximately 10 seconds to recover.

The decreasing magnitude of the peaks over time is also of interest. This suggests that the system is still undergoing a stabilization period 200 seconds into the mission. This has implications on man-in-the-loop experimental procedures. Allowing the subject sufficient time to achieve stabilization before initiating scoring could produce results which are overly optimistic.

Next, the display errors were added back in. The results of this run are graphed in Figure 27 and indicate the same trend as the "no-error" case. Adding the u_1 (angle of attack) and u_2 (roll angle) control errors individually and in conjunction with the display errors produced no significant changes. Figure 28 depicts the results of adding u_1 and u_2 together. While the system is less stable, the trend is generally the same. Including display errors with u_1 and u_2 results in much the same trend. Adding u_3 errors, however, produces more dramatic changes (see Figure 29). The system demonstrates much more variability and is never really in a stable mode. It more closely resembles the full error condition of Figure 24. This suggests that the largest contributor to the problem is the difficulty in controlling

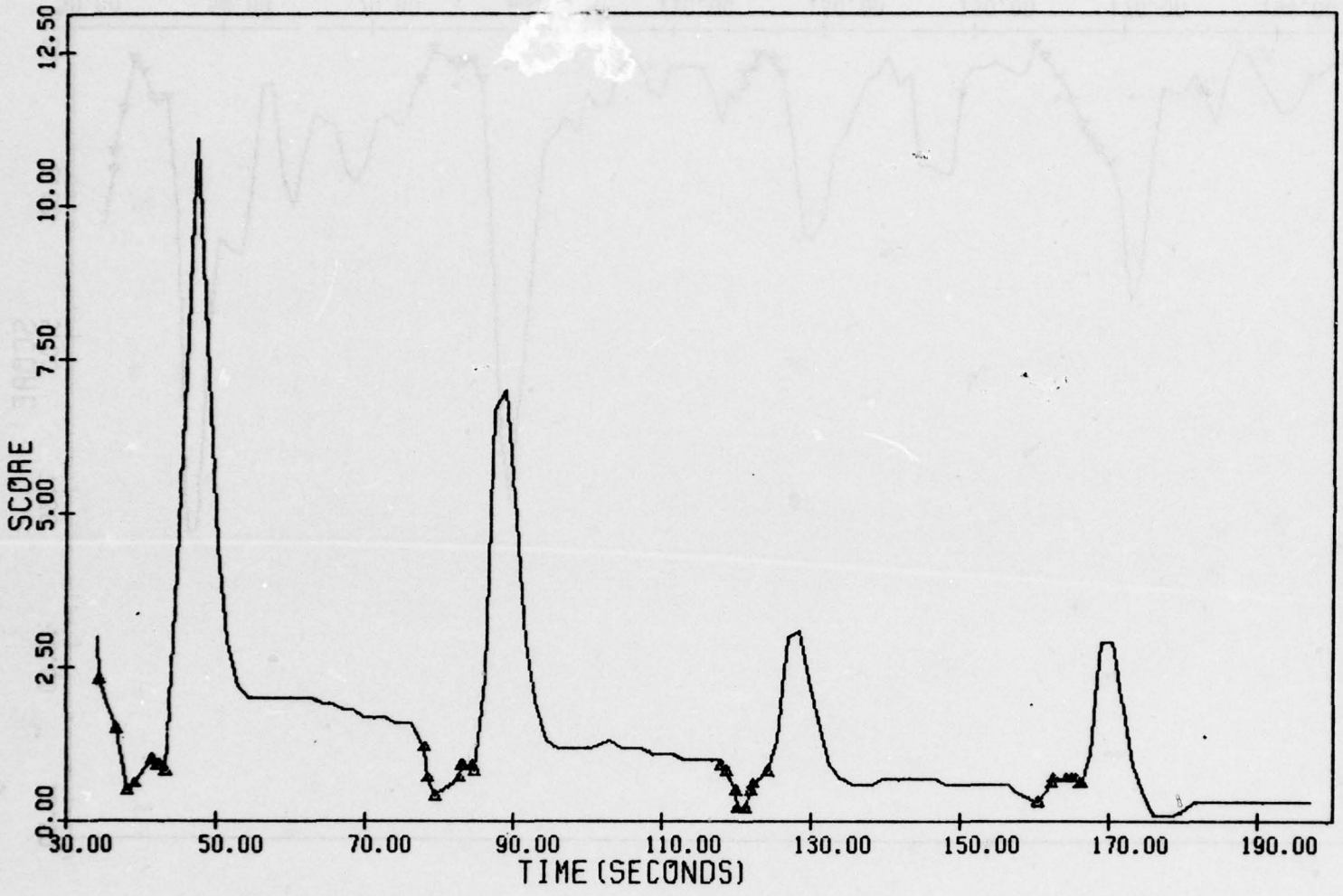

FIGURE 26. TURNING DIVE CASE 3 SCORES (NO DISPLAY OR CONTROL ERRORS)

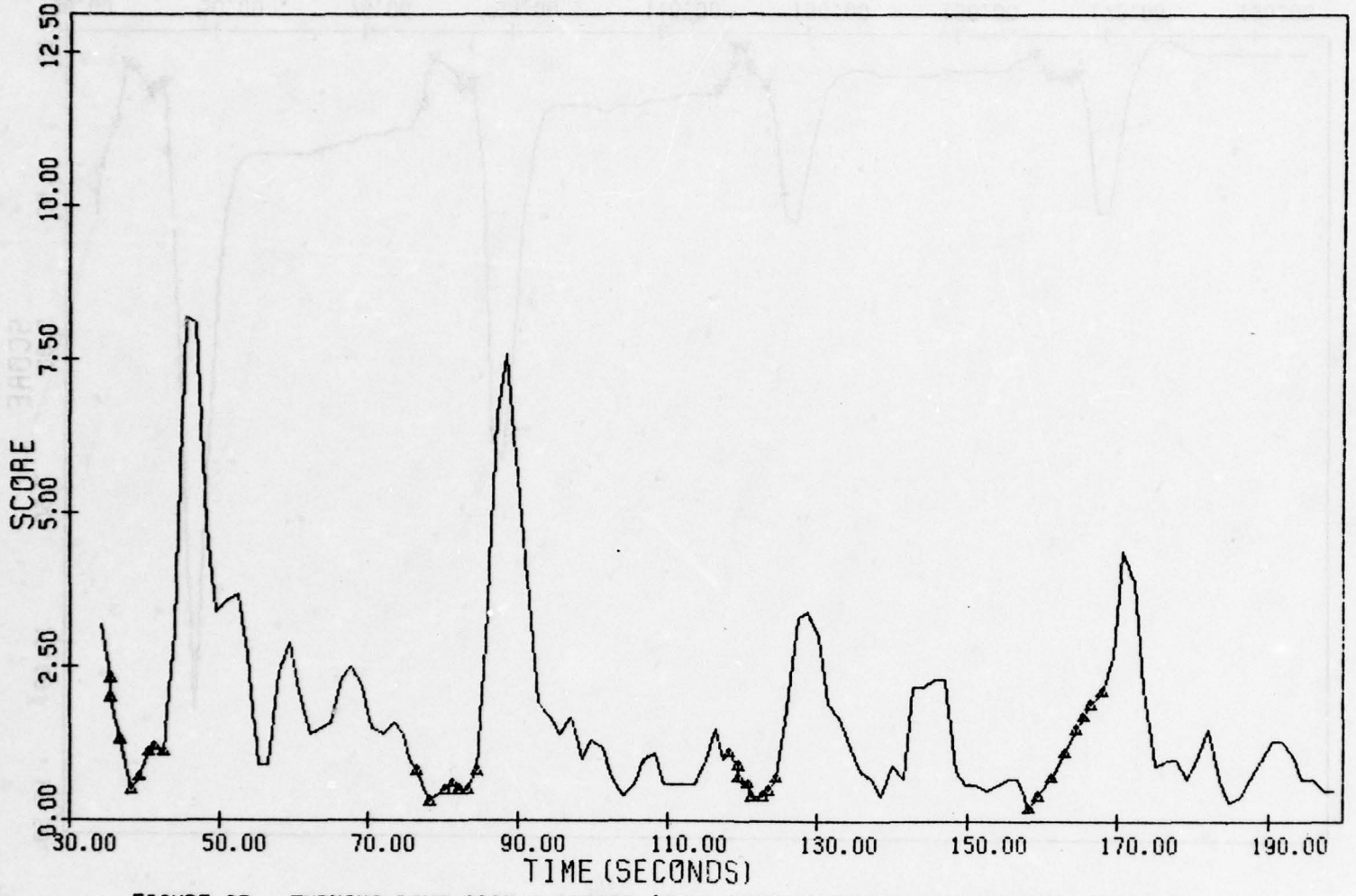

FIGURE 27. TURNING DIVE CASE 3 SCORES (FULL DISPLAY ERRORS, NO CONTROL ERRORS)

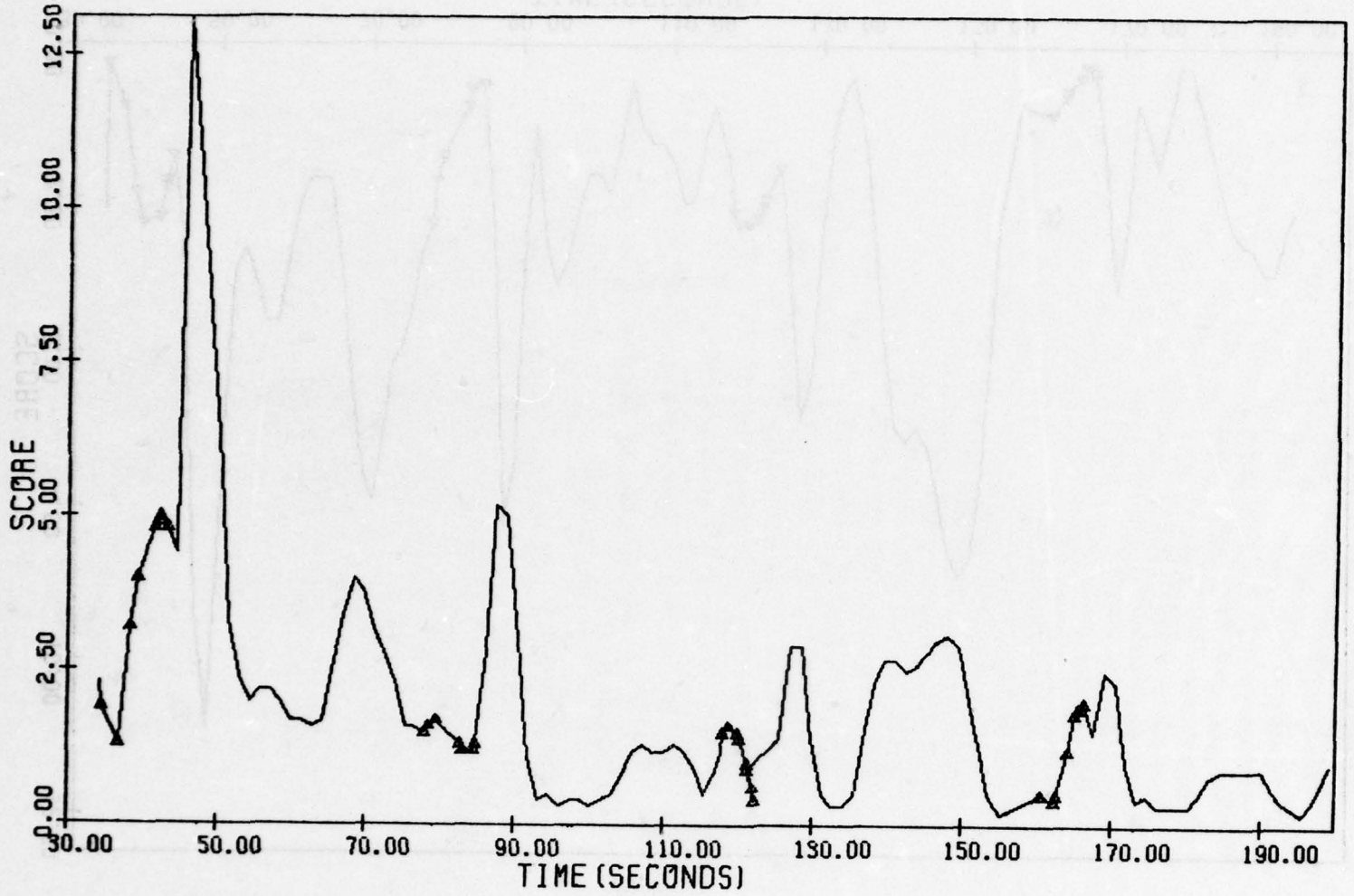

FIGURE 28. TURNING DIVE CASE 3 SCORES (u_1 AND u_2 ERRORS ONLY)

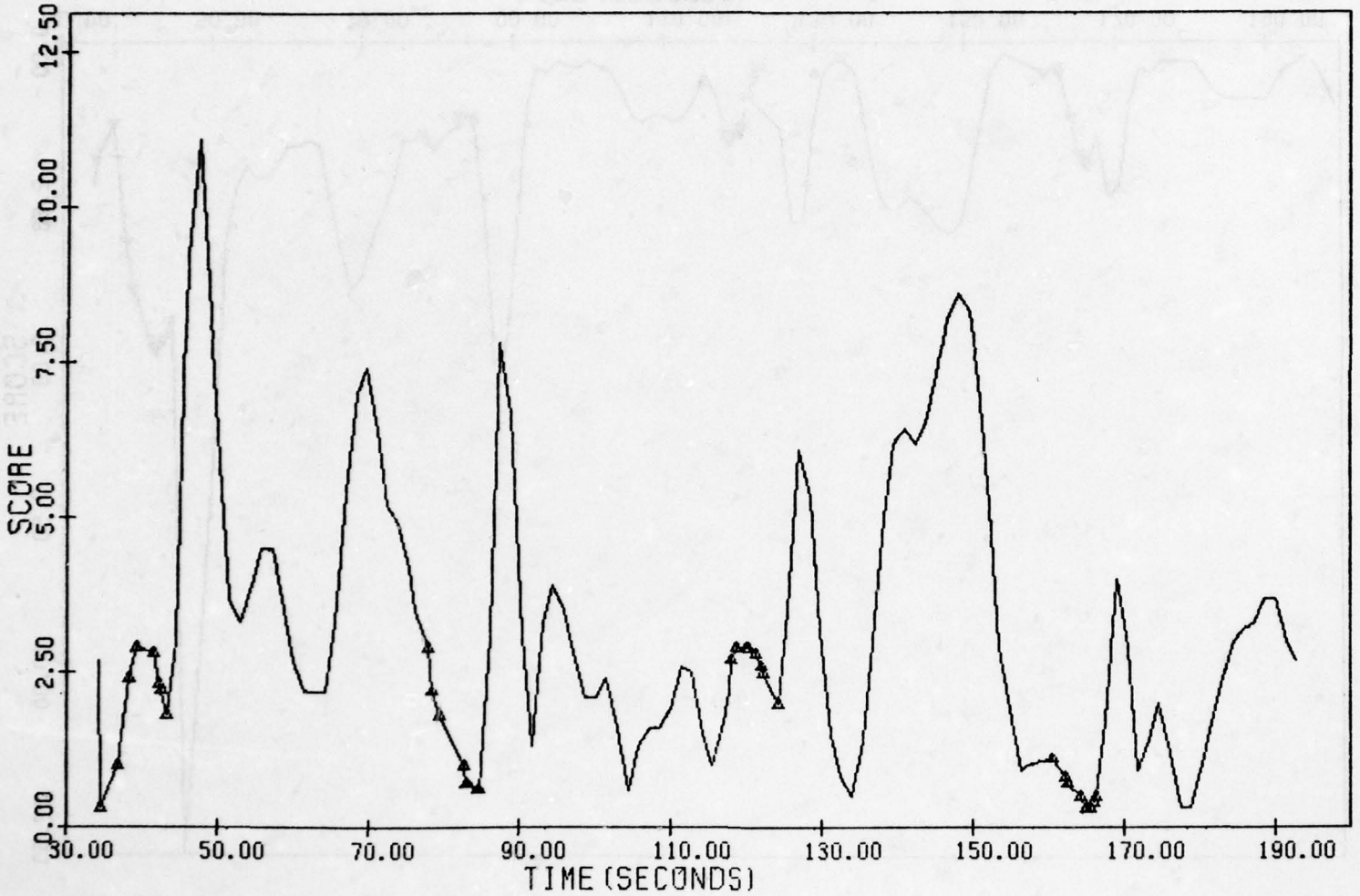

FIGURE 29. TURNING DIVE CASE 3 SCORES (u_3 ERROR ONLY)

throttle (u_3), with some additional problems with the other two control variables, u_1 and u_2. Discussions with DAIS experimenters and more detailed examination of the data proved this to be true. It was apparent that vertical velocity was not well controlled in either maneuver, but particularly not in turning dive. While vertical velocity is a function of all three control variables, it is most heavily determined by throttle. It was known for some time that there were physical problems with the response characteristics of both the stick and the throttle. The stick in particular had an extensive amount of "dead space" around the center point. It is hypothesized, based on the above results and conversations with DAIS experimenters, that the DAIS subjects had an exceptionally difficult time controlling the stick and throttle, resulting in extensive variability of flight parameters, vertical velocity in particular. This could very well be the reason why no significant effects were reported between the "flight alone" and "flight plus MFK" conditions. The high variability caused by poor stick and throttle hardware, coupled with inadequate scoring techniques based on averages, may have masked the true effects.

Performance measurement, as represented by the overall flight scores, appears to be a critical issue. Moray (1976) addresses the importance of the measurement problem.

> A search through the literature can provide roughly equal numbers of papers asserting, for example, that secondary discrete tasks do or do not affect the information transmission rate of a tracking task. The reason may be connected with the nature of the tasks, the difficulty of the discrimination required, the order of the control and bandwidth of the tracking task, etc. But equally it may simply be due to the nature of measurement.

In many experiments the significant events are few, and if all data are lumped together, the overall change is too slight to be readily observed. This may in fact be what has occurred in this case.

REINVESTIGATION OF CASE DIFFERENCES WITH REDUCED ERRORS

At this time, the more overriding problem appears to lie in the large control errors. In an attempt to represent more realistic system conditions, display and control input noise distributions were reduced. The standard deviations of all three control input error distributions were reduced to 1/3 of their original values. Likewise, the standard deviations of all the display error distribution were cut in half, with the exception of vertical velocity, which was set to 1/6 its original value. The model was rerun under these reduced error conditions, coupled with the more frequent scoring procedure. The results with no display errors, only control errors, are displayed in Figure 30. A graph of the scores adding the display errors back in is shown in Figure 31. The trend is again very evident. A sharp peak in the score immediately follows the MFK task sequence. This suggests that now the system may be more sensitive to different sampling strategies and procedures. In an attempt to investigate more thoroughly the effects of reducing the error distribution on overall performance scores, a complete set of runs was made across the three cases and all the sample intervals for both maneuvers. The results for one replication of the straight and level maneuver are displayed in Table 17. In general, the scores are somewhat lower, with much less sensitivity being exhibited among the different cases.

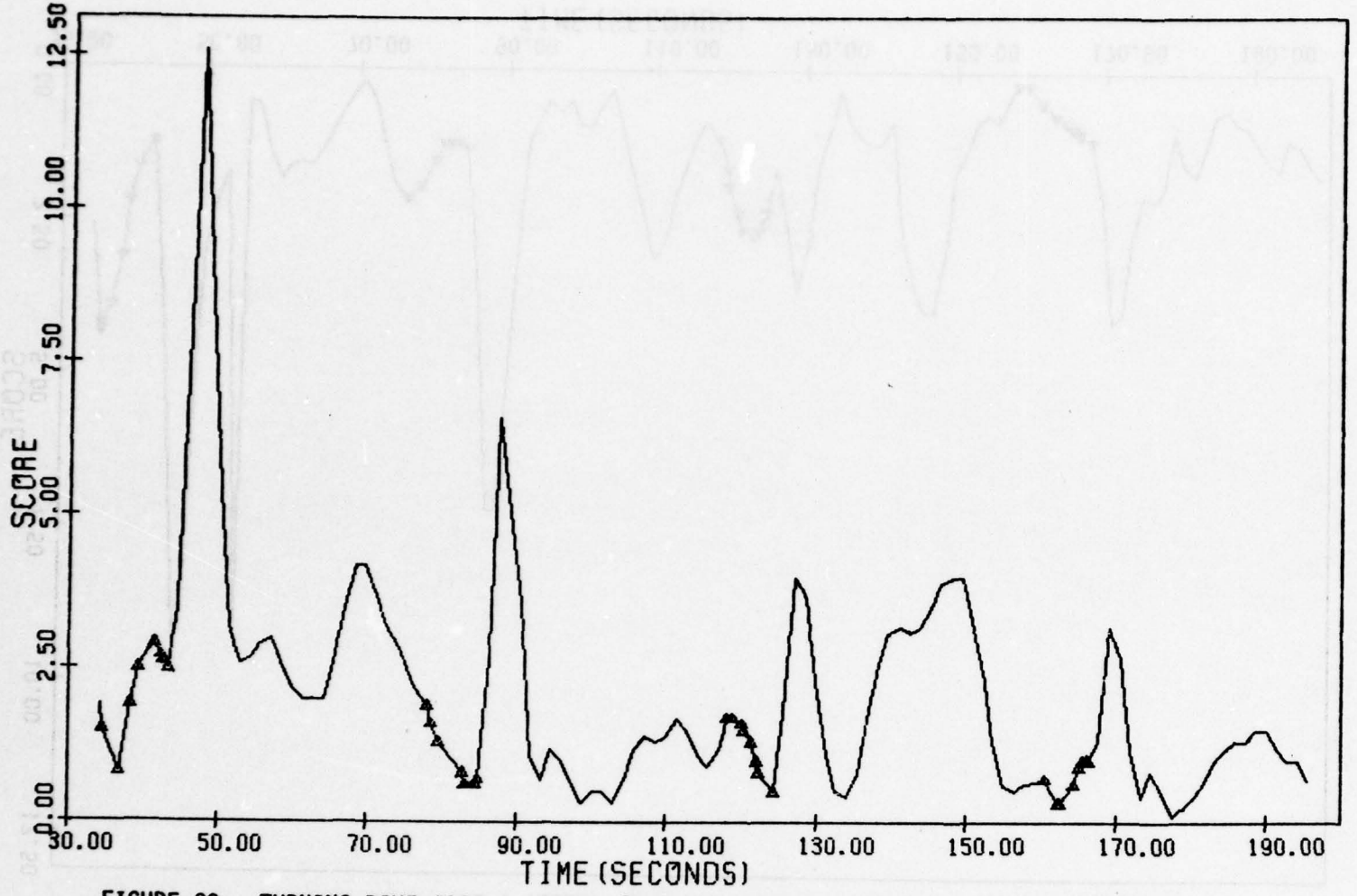

FIGURE 30. TURNING DIVE CASE 3 SCORES (REDUCED CONTROL ERRORS, NO DISPLAY ERRORS)

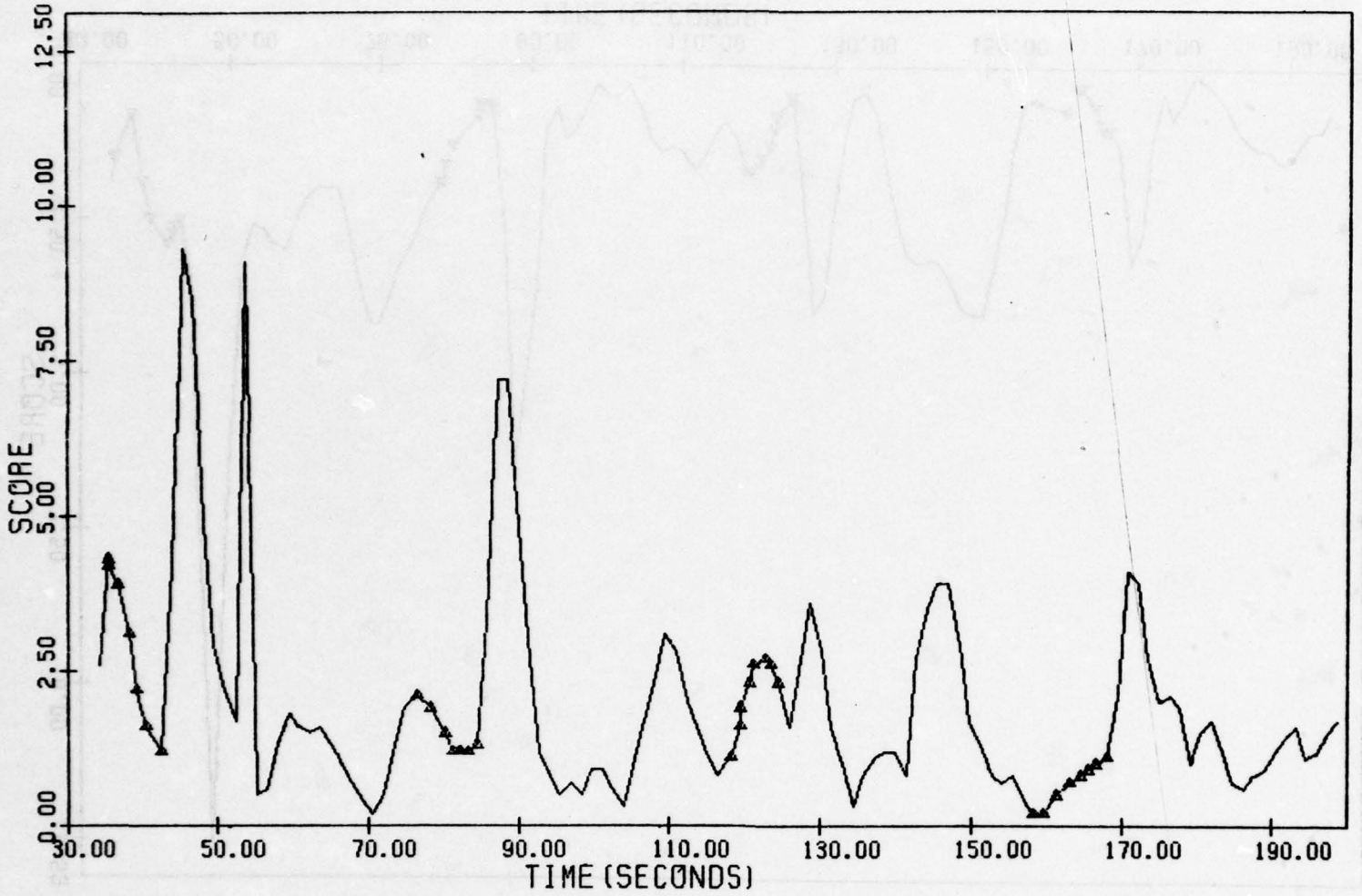

FIGURE 31. TURNING DIVE CASE 3 SCORES (REDUCED CONTROL AND DISPLAY ERRORS)

TABLE 17

SCORES FOR THE STRAIGHT AND LEVEL MANEUVER
WITH REDUCED ERROR DISTRIBUTIONS

SAMPLE INTERVAL	CASE 1	CASE 2	CASE 3
1.0	.1114	.1140	.1662
2.0	.1423	.1345	1.978
3.0	.1761	.1622	.2127
4.0	.2557	.2133	.3502
5.0	.5830	.2607	.7522
6.0	.3045	.2604	.3857
7.0	.3142	.2926	.3895
10.0	.3911	.3192	.4224

A similar set of runs was made for turning dive, only this time three replications across all conditions were made. The average scores are contained in Table 18. The performance scores still contain a large peak at a sample interval of 1.0. Beyond this point the scores are somewhat erratic, with Case 3 performance actually appearing to be better than Case 1 performance. Because of this erratic behavior, which probably indicates that these sampling intervals are unrealistic and beyond the acceptable confines of the state model, values above the 0.8 sample interval were discarded. A 1-way ANOVA across cases performed on this reduced performance set resulted in an overall conservative significant difference between cases at the $\alpha = .0119$ level. The individual pairwise planned comparisons resulted in the following significant levels displayed in Table 19. The difference between Case 1 and Case 3 is now highly significant with $\alpha = .0020$. Rerunning the ANOVA of the full error cases on the sample intervals less than 1.0 produces a difference between Case 1 and Case 3 at the $\alpha = .0263$ level. However, the reduced error case is still greater than an order of magnitude more significant.

While these runs certainly do not "prove" that significant differences would have been found in the real-time man-in-the-loop experiment had the stick and throttle been better engineered, it does demonstrate the extreme sensitivity of the system to these parameters, and indicates how main effects may very well have been hidden by their variability. It makes a case for employing a model such as this one for determining how "well-behaved" such system components must be constructed to perform in order to produce desired system characteristics.

TABLE 18

AVERAGE SCORES FOR THE TURNING DIVE MANEUVER
WITH REDUCED ERROR DISTRIBUTIONS

SAMPLE INTERVAL	CASE 1	CASE 2	CASE 3
.2	2.000	2.316	2.729
.4	1.402	1.614	2.153
.6	1.404	1.548	1.993
.8	.989	1.560	1.762
1.0	10.330	10.790	8.856
1.4	5.199	6.131	4.693
1.6	4.434	4.968	3.930
1.8	8.255	8.654	7.103
2.0	16.147	15.760	12.827

TABLE 19

SIGNIFICANCE LEVELS OF PLANNED COMPARISONS (REDUCED ERROR CASES)

CASES	SIGNIFICANCE LEVEL
1, 2	$\alpha = .1859$
1, 3	$\alpha = .0020$
2, 3	$\alpha = .1313$

This analysis also points to the need for examining alternate scoring formulations other than the "overall" mission score employed. Ignoring the peaks in the scores immediately following the MFK switching sequence, and using only "averaged" scores, necessarily mask the true effects due to the secondary tasks. One cannot help but to postulate that the outcome of the man-in-the-loop experiment would have been different had the controls been better and the scoring been more sensitive.

ALTERNATE SAMPLING SCHEMES

INTRODUCTION

The optimal control model approach has traditionally assumed that all state variables displayed to the pilot would be read each time sampling occurs. In the model runs described in the previous chapter, this assumption was adhered to. Even in Cases 2 and 3 where sampling was disallowed during certain segments, when sampling did occur, it included all six state variables. It is not clear that pilots actually perform in this manner.

This notion is not a new one. Milton et al. (1949) and Senders (1955, 1964) conducted experimental research on fixations on instruments of a panel. Based on these experiments, Senders proposed a model which postulates a simple information-rate periodical sampling such that instruments are sampled at regular intervals at rates proportional to their bandwidths. Later, Senders (1965) proposed the notion of "the probability of exceeding a threshold" as the basis for the evident aperiodicity of a pilot's sampling behavior. In 1966, Carbonell introduced a queueing model of visual sampling based on the concept of different instruments competing for the attention of the pilot. Costs are assigned to each instrument. At each sampling instant, the decision as to what instruments to look at is based on comparing the combined effect of both the probability of exceeding the threshold and a cost of exceeding that threshold. Effectively,

the instruments queue for the pilots attention; the instrument with the highest priority at each instant is then served (looked at). Sheridan (1970) also ascribes cost functional parameters in a model based upon Bayesian preposterior information analysis. This model specifies how long a supervisor or monitor of a process should wait between input samples to maximize a given value or payoff function, assuming he resets the controls with each sample as a function of the best available information.

While the above discussion of sampling algorithms is certainly not exhaustive, it does appear to be representative. Many of these approaches could be used as they stand, or with slight modification, in models of systems comprised of monitoring and supervisory control activities. The following sections describe the results of applying different sampling schemes, some of which are variations of the above, to the DAIS model. The intent is not to advocate or validate any particular sampling algorithm; rather, it is to be considered a demonstration of the feasibility of exploring alternative sampling behavior with this combined modeling approach.

SAMPLING ALGORITHM BASED ON EYE MOVEMENT DATA

Spicuzza, Pinkus, and O'Donnell (1974) performed experiments employing the DAIS simulator in an attempt to develop, instrument, and test a series of human performance assessment measures to be used as standard evaluation tools in future advanced digital avionics information systems. As part of the analysis process, they collected eye

movement data while the subject was flying the simulated DAIS aircraft. Their rationale for collecting the data is stated in the following excerpt from their report.

> . . . Since the DAIS systems which have been proposed will incorporate extremely novel display configurations, it is necessary to determine precisely how skilled pilots use the new displays. Their utilization of information presented on CRT displays may be entirely different than it was with traditional display formats. Some method is therefore necessary to determine how long a pilot's eyes remain on displays of various types, and the sequence of transitions from one type of display to another. Such information will be of value not only in determining the proper cockpit lay-out and the most efficient design for a given display, but more importantly, will provide information about the types and duration of displays needed to fly a mission. This will allow maximum utilization of the DAIS capability to selectively present data to the pilot by emphasizing relevant and eliminating redundant information.

To collect the eye movement data they employed a system which involves the use of a light beam reflected off the subject's cornea and into a videcon tube which displays the reflected light as a spot on a TV screen. The subject's field-of-view can then be displayed on a TV screen with the flying dot superimposed. The position of the dot indicates the precise point at which the subject is looking. A series of runs was made across different maneuvers and conditions. The eye movements made by the subjects were recorded on video tape. Analysis was performed which determined time histories of the six sectors of the CRT the subject was fixating on. These were digitally recorded at 0.1 second intervals. Thus if the subject's eyes remained in a given sector of the screen for one second, 10 entries representing that sector would be digitized on the tape. While this study employed six sectors of the CRT, only three of these sectors are pertinent to the

current DAIS configuration. A representation of these three sectors, designated as A, B, and C, is contained in Figure 32. In the baseline control cases of interest here, subjects seldom looked at the remaining three sectors, and thus little accuracy is sacrificed by ignoring them.

Frequency and probability of use statistics for each sector were developed for each maneuver type as well as the frequency of all sequences of two eye movements. These sequences were easily converted into a probability transition structure amenable to a network formulation. The finite state markov chain representations of the transition sequences of two eye movements for the straight and level and turning dive maneuvers are portrayed in Figures 33 and 34, respectively. Nodes A, B, and C represent those respective sectors, and node N indicates that the subject is looking at none of these three sectors.

Since the eye movement data indicate that all state variable displays are not read simultaneously, this data base provided an excellent starting point for examining alternate sampling schemes. State variables can now be sampled in accordance with the sector currently being viewed. A SAINT network model was constructed to represent both the sampling of a given sector along with the transition probabilities between sectors. These diagrams are contained in Figures 35 and 36. Various sampling algorithms within each sector can now readily be explored.

The concept of using probability sequences for determining state variable sampling is not a novel one. Cavalli (1978) successfully employed a probability transition matrix scheme for state variable

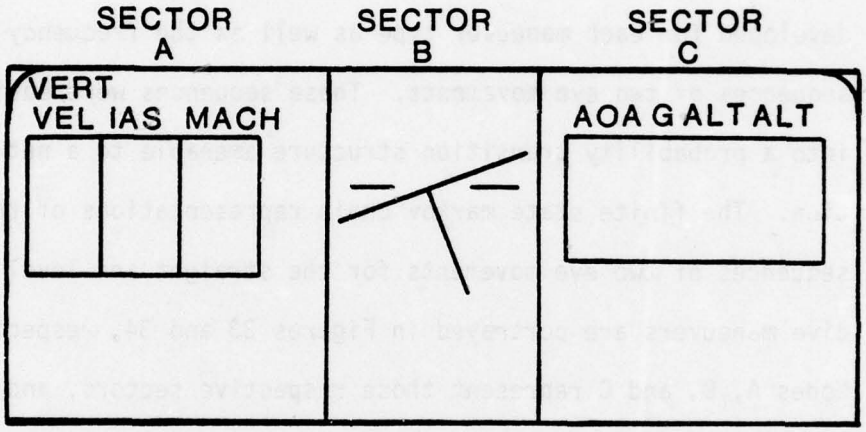

FIGURE 32. CRT SECTORS USED TO CLASSIFY EYE MOVEMENTS

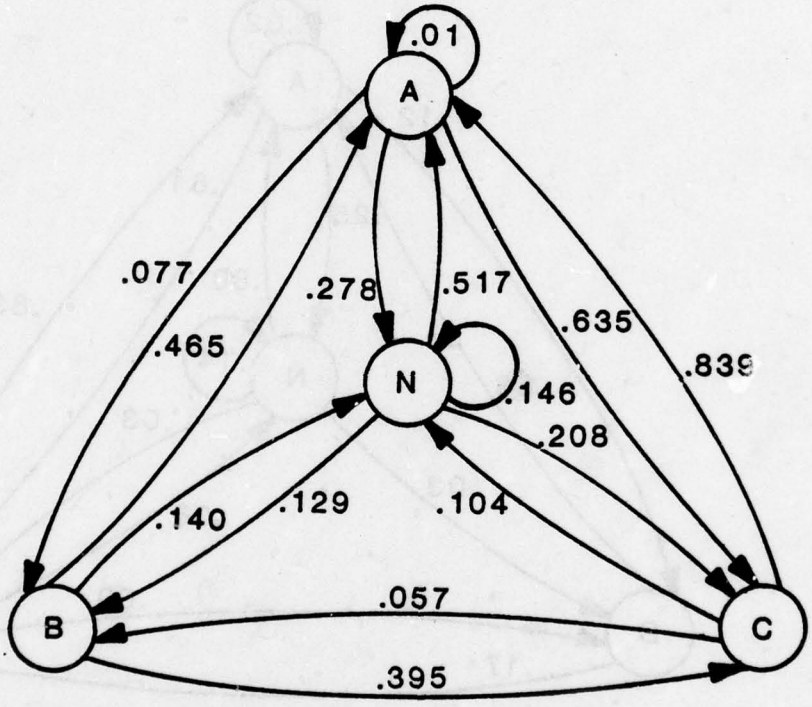

FIGURE 33. FINITE STATE MARKOV CHAIN FOR STRAIGHT AND LEVEL EYE MOVEMENTS

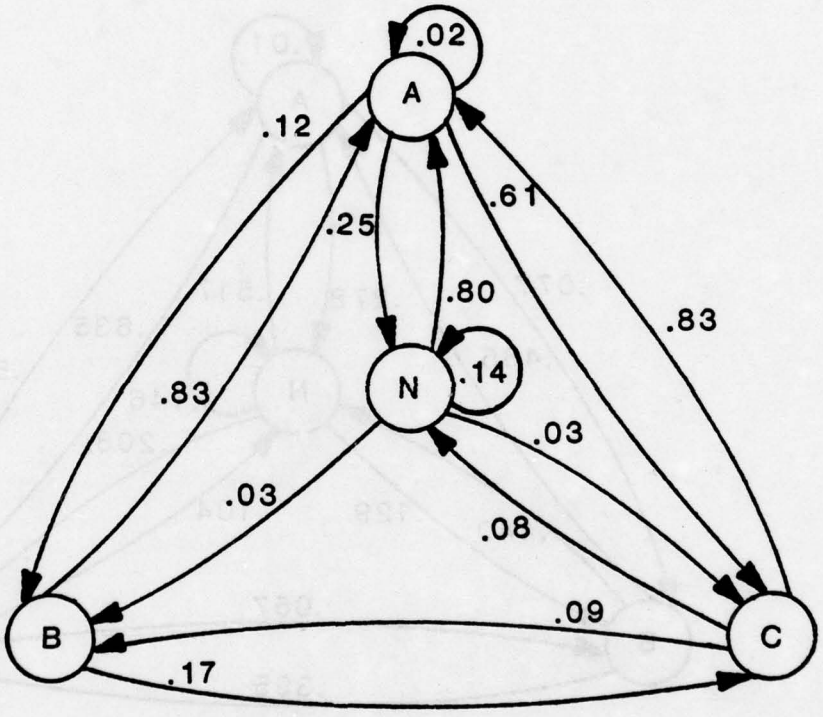

FIGURE 34. FINITE STATE MARKOV CHAIN FOR TURNING DIVE EYE MOVEMENTS

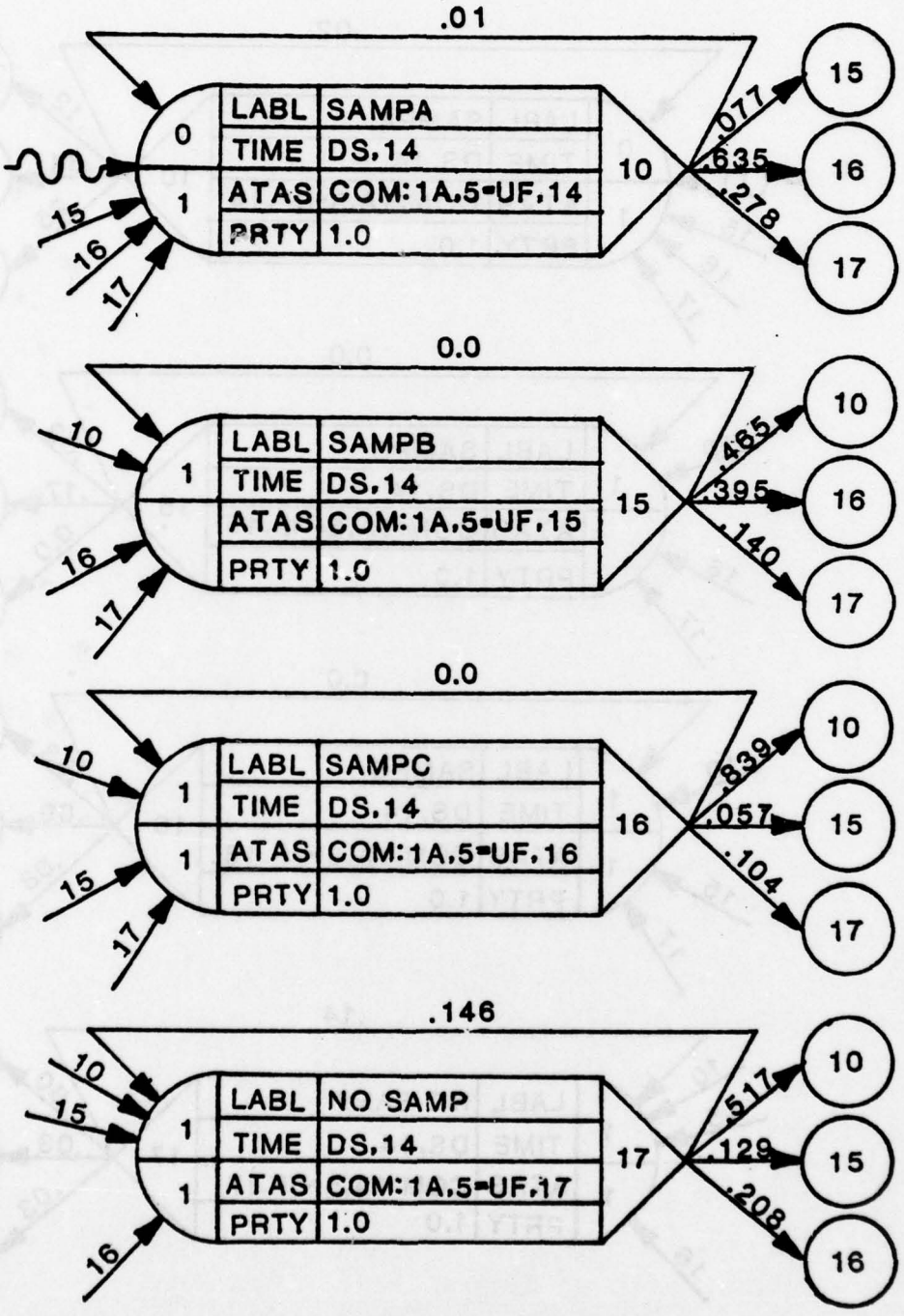

FIGURE 35. SAINT NETWORK FOR SAMPLING BASED ON EYE MOVEMENT DATA (STRAIGHT AND LEVEL)

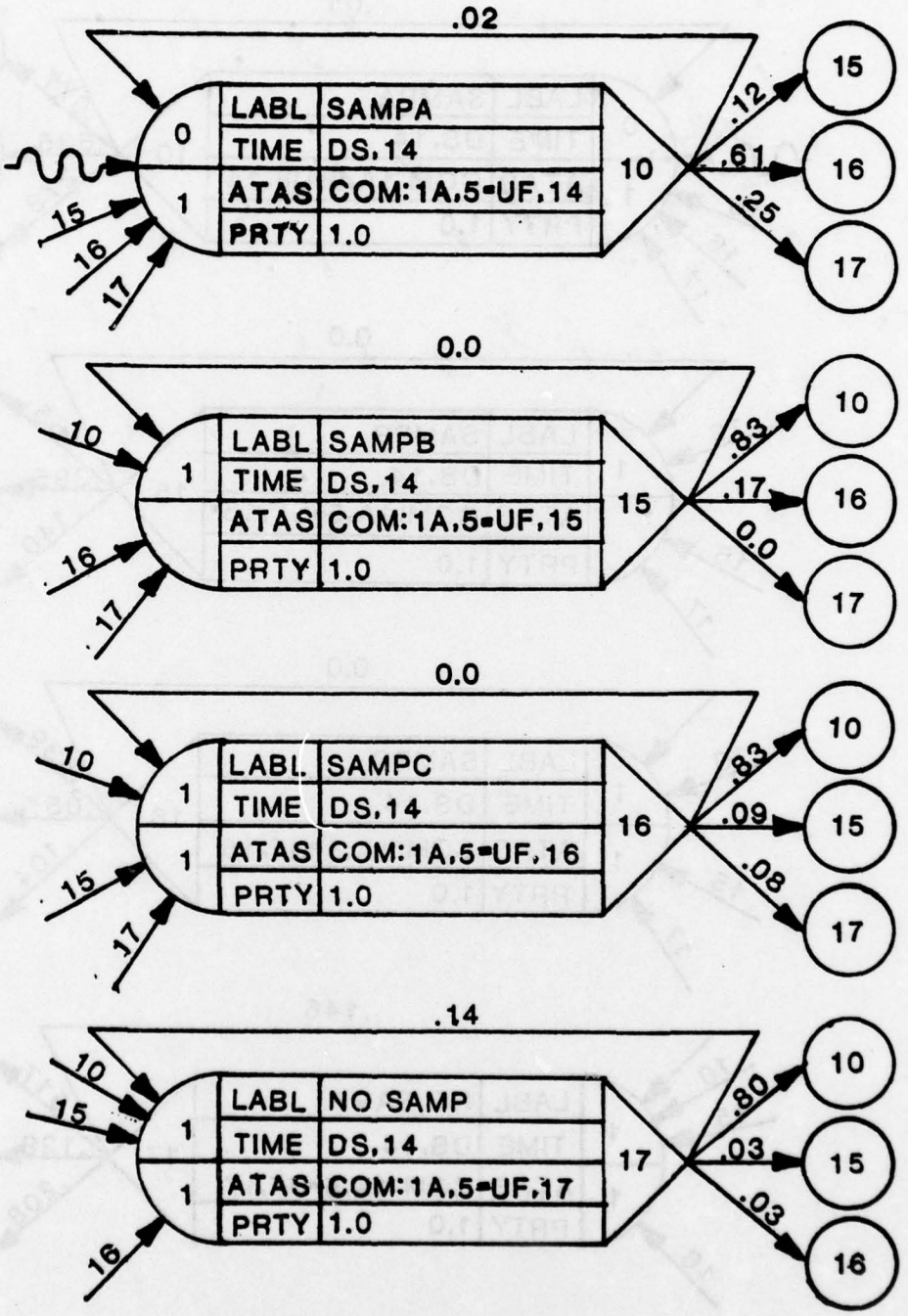

FIGURE 36. SAINT NETWORK FOR SAMPLING BASED ON EYE MOVEMENT DATA (TURNING DIVE)

sampling in his model of the ILS approach phase of an Airbus A-300B. He deviates from this structure slightly in that when a given variable exceeds its acceptable limits, that variable is sampled rather than the one indicated by the matrix. His model's outputs compare very favorably with actual pilot performance data, and he advocates the collection of eye movement data on other systems for use in similar analysis.

Higher order transition models have been shown to be more representative of eye movements than the simple first-order model contained here. That is, the probability transition to the next state (sector) is dependent not only on the current state, but also on what sector the subject was previously viewing. However, since this exercise is meant to be a demonstration of feasibility, the simple transition probabilities were deemed to be adequate.

The following discussion presents the results of employing alternate sampling schemes utilizing the eye movement data in the DAIS model. The original full control and display error distributions were employed in order to use the DAIS empirical data as a baseline for comparison. In sector B, the "steering T" presents the pilot with some limited information about the state variables. Discussions with pilots familiar with the DAIS flight control task indicated that the "steering T" provided feedback on roll and vertical velocity, with considerably less information on altitude, and none on g-load and velocity. Based on these discussions, a 25% higher display error distribution was placed on roll and vertical velocity, and a 50%

higher distribution was placed on altitude. It is assumed that velocity and g-load are not sampled in sector B. Table 20 indicates the state variable information available in each sector.

TABLE 20
STATE VARIABLE INFORMATION IN SECTORS A, B, & C

SECTOR	STATE VARIABLES
A	Vertical Velocity, Velocity
B	Steering T Altitude (50% more error) Roll (25% more error) Vertical Velocity (25% more error)
C	Altitude, G-load

Several different sampling algorithms based on the eye movement transition probabilities and the sector definition in the above table were tested. The resulting scores from applying this algorithm to the straight and level maneuver are summarized in Table 21. The first run assumed that the pilot sampled all the variables available to him in whatever sector he was viewing at the time. The scores for both Case 1 and Case 3 are extremely low. In algorithm 2, one variable in sectors A and C is randomly selected to be sampled with equal probability. Again the score is very low. This is also the case with sampling variations 3 through 5.

Two important things are apparent from these results. In this case the pilot obviously does not "process" display information just because he is visually fixated on the display. There have been a

TABLE 21

STRAIGHT AND LEVEL EYE MOVEMENT SAMPLING ALGORITHMS AND RESULTS

SAMPLING ALGORITHM	SCORE
1. Sample all variables in each sector	
Case 1	.134
Case 3	.152
2. A { vertical velocity 50%, velocity 50%	.156
B all variables	
C { altitude 50%, g-load 50%	
3. A vertical velocity	.226
B all variables	
C altitude	
4. A velocity	.165
B all variables	
C altitude	
5. A { vertical velocity 50%, velocity 50%	.185
B all variables	
C altitude	
6. Sector B only (steering T)	.963

number of empirical studies performed which back up this notion. Secondly, while additional replications would be required to formally substantiate this, it appears that little sensitivity exists among the first five sampling algorithms. For example, in sampling rule 4, only velocity and altitude are sampled in sectors A and C. Yet its score compares very favorably to the first algorithm in which all variables are sampled. This suggests that the pilot seldom needs to sample state variables other than velocity and altitude. Knowing this can free up the pilot to perform other secondary tasks.

Algorithm 6 resulted in a significantly higher score. This was most probably due to the fact that no velocity information was available and that the altitude feedback was extremely noisy.

A similar analysis was performed for the turning dive maneuver, with the sampling algorithms and associated scores displayed in Table 22. These results are quite different from the straight and level ones. Most of these sampling rules yield scores which very closely resemble the actual DAIS scores. Even in the first rule where all the variables in each sector are sampled every time, the score is only slightly lower than the 5.495 average of DAIS. This provides a lot of insight into the information processing rate required to "fly" the turning dive maneuver. It indicates that very close attention must be paid to the flight control task, whereas in straight and level there was considerably more leeway.

Other insights specific to turning dive can be gained from this analysis. It appears that g-load, velocity, and vertical velocity are all important and necessary variables, while altitude is not. This

TABLE 22

TURNING DIVE EYE MOVEMENT SAMPLING ALGORITHMS AND RESULTS

SAMPLING ALGORITHM	SCORE
1. Sample all variables in each sector	4.081
2. A vertical velocity	11.99
B all variables	
C altitude	
3. A vertical velocity	7.852
B all variables	
C g-load	
4. A velocity	4.171
B all variables	
C g-load	
5. A { vertical velocity 50% velocity 50%	5.211
B all variables	
C g-load	
6. A { vertical velocity 50% velocity 50%	5.497
B all variables	
C { g-load 50% altitude 50%	
7. Sector B only (steering T)	12.600

corresponds directly to the scoring formula, which employes these three variables. Once again, employing the steering T by itself does not produce good results. The high display errors coupled with no velocity information probably account for this poor behavior.

In summary, it is not advocated that eye movement data be collected for every system under study. This type of sampling severely restricts the analysis of alternative system configurations and new secondary tasks. However, the study demonstrates how this modeling technique can accommodate and assist in analyses based on past performance data. Eye movement data from other systems could be modeled in the combined simulation formulation in an attempt to gain insights into the information processing activity for given eye fixations. It might also be utilized in preliminary system modeling efforts to produce information on the sensitivity of the system to specific flight control parameters. It is anticipated that many other similar types of modeling analyses could be performed using this combined simulation approach.

VARIANCE SAMPLING

The operator control model includes estimates of the variance of each of the six vehicle state varaibles. The variance is one measure of the pilot's uncertainty about true system status. One approach to sampling is to sample whenever variance estimates exceed allowable limits; that is, whenever the pilot's uncertainty becomes too high. The assumption was initially made that the pilot would sample only the individual state variable whose variance had gone out of tolerance.

He would concentrate on "controlling" that particular variable, sampling it continuously until it was back within an acceptable range. Upon taking a sample, the variance of the sampled variable was reset to the variance of the observation error. If no variances exceeded thresholds, no sampling was performed. A discussion of the results in applying this sampling rule to both the straight and level and turning dive maneuvers follows.

Straight and Level

The initial variance limits were established from an earlier Case 1, sample everything every 5 sec., baseline run, which provided state variable variances ranging over zero to five second intervals. First estimates of variance thresholds were staggered between 4 and 5 seconds. Estimates on the bounds of the actual values of the state variables were selected to be in line with DAIS man-in-the-loop performance data.

The first application of this sampling algorithm in straight and level was less than successful. Shortly into the mission, altitude variance went out of limits. The model sampled altitude continuously but could not get it back into control without sampling any of the other state variables. Both vertical velocity and velocity were also out of control.

Since rate information is very often perceived coincident to the actual variable, the next trial involved sampling vertical velocity and altitude together whenever either of them exceeded limits. While performance was somewhat better, essentially the same problem occurred. After 3 seconds into the maneuver, only altitude and vertical velocity

were sampled, with acceptable control still not being achieved. Without being sampled, velocity was far out of bounds. Reductions on the altitude and vertical velocity constraints only delayed the problem.

A variation to the sampling rule was next examined in which everything was sampled if four or more of the variances were out of limits. First efforts at applying this algorithm were plagued by similar problems; one variable would be sampled most of the time, with the others consequently going out of control. By adjusting the variance limits, a good sampling mix was eventually achieved. However, while the scores were acceptable (.6), the behavior of individual variables was very erratic. Of even more concern was the sensitivity of the limits. For example, changing the g-load variance threshold from .00573 to .00572 brought the score from 2.79 down to .61.

A slight variation of this approach was then employed. The variable with the largest discrepancy between its variance and its limit, relatively speaking, would be sampled. That is, the difference between the actual variance and its threshold is divided by the threshold to produce a "relative error." The variable with the highest variance "relative error" was sampled. Again, if four or more variances were over their limits, all variables were sampled. With some variations in the limits, reasonable results were obtained. A good sampling mix was achieved; mostly altitude and velocity were sampled, with g-load and vertical velocity sampled on occasion. This is not surprising since altitude and velocity are the two variables in

the scoring formula for straight and level. In Case 3 runs, all variables were sampled for a period of time following the MFK task sequence in order to "recover." This too is very reasonable. While this approach behaved better than the preceding one, it was still very sensitive to the variance limits, and some of the individual variables were unstable.

Turning Dive

Because of the problems encountered in straight and level, great successes were not expected from turning dive. This did not prove to be wrong. Turning dive performance followed the same patterns as straight and level, only with much more severe and dramatic results. The limits were a lot more sensitive; slight variations often caused the plane to crash. Both the state variables and the control variables (u's) performed very erratically. Eventually, proper limits were selected in order to make the plane "fly." However, the stability of the aircraft was questionable, and time histories of the state variables certainly did not correspond to the DAIS empirical data.

"PROBABILITY OUT OF LIMITS" SAMPLING

Introduction

The preceding section described an algorithm for sampling based on the pilot's estimates of state variable error variances exceeding threshold limits. The variance is only a portion of the system status information available to the pilot; it is also assumed that he has estimates of the mean statistics for each of the six state variables. The previous results indicated that utilizing variance information

alone is inadequate. A low variance indicates high confidence in the knowledge of true system status, but does nothing to compensate for large state variable errors. On the other hand, it is suspected that knowledge of mean statistics by themselves is equally insufficient. Mean estimates of system state variables without their corresponding variances would most probably evoke inappropriate actions by either under or over-controlling selected system states. For example, the mean data estimate may indicate that a variable has exceeded its tolerance threshold; however, if this variable exhibits a great deal of variability, one may somewhat temper his decisior to sample the variable. Without the variance information, sampling for this variable may occur too frequently.

The obvious next approach to be investigated is to utilize a sampling algorithm which incorporates both the mean and variance estimates of system status. As mentioned in the introduction to this chapter, Senders (1965) implemented such an algorithm with some success. He proposed a sampling rule based on the "probability" that a given variable had exceeded its threshold limits. This probability estimate utilizes both the mean and variance statistics, and assuming a normal distribution, is derived as follows:

$$
\begin{aligned}
&P\ (x \text{ is out of limits}) \\
&\quad = 1. - P\ (LL < x < UL) \\
&\quad = P\ (x < LL) + P\ (x > UL) \\
&\quad = P\ \left(Z < \frac{LL - \bar{x}}{\sigma_x}\right) + P\ \left(Z > \frac{UL - \bar{x}}{\sigma_x}\right) \\
&\quad = F\ \left(\frac{LL - \bar{x}}{\sigma_x}\right) + 1. - F\ \left(\frac{UL - \bar{x}}{\sigma_x}\right)
\end{aligned}
$$

where,

LL = Lower limit (error)

UL = Upper limit (error)

$\bar{x}$ = Current estimate of mean error

σ_x = Current estimate of the standard deviation of x

F = Cumulative normal function.

The probability of exceeding its threshold limit is computed for each of the six state variables. Then the variable which has the highest probability of being out of limits is sampled, the mean error estimate is reset to the current display reading, and the variance is initialized to the display error variance. The results of applying this algorithm in the DAIS model for both maneuvers are discussed below.

Model Results

The state variable limits used by the sampling algorithm are contained in Table 23. These limits are simply estimates based on previous model runs. Symmetrical intervals were chosen, although this is not a prerequisite of the model. Limits with values of 99999. indicate variables where sampling based on limits is not desired. The 99999. assures that the probability of being out of limits will always be zero. In turning dives, for example, the altitude is continuously decreasing, and thus would always be out of limits. However, not sampling these variables at all is also inappropriate. The sampling algorithm was modified to permit all of the state variables to be sampled together periodically. In straight and level, all six state

TABLE 23

STATE VARIABLE LIMITS EMPLOYED IN SAMPLING ALGORITHM

STATE VARIABLE	STRAIGHT AND LEVEL	TURNING DIVE
Altitude	±15.0	±99999.
Roll	±99999.	±99999.
Heading	±99999.	±99999.
Vertical Velocity	±5.0	±8.0
G-load	±0.5	±0.5
Velocity	±4.0	±4.0

variables are sampled every 10 seconds, whether or not they are within limits. The period for the turning dive maneuver is 5 seconds.

These runs were made with the reduced display and control error distributions described in the previous chapter. The resulting scores for straight and level and turning dive, across all three cases, three replications each, are displayed in Tables 24 and 25, respectively.

In straight and level, altitude and velocity were the two primary variables that were sampled. Vertical velocity and g-load were seldom sampled between the 10 second, "sample everything," intervals. The mean scores for all three cases fall approximately between the 3 and 4 second time intervals of the reduced error case results found in Table 17. Sensitivity tests were not performed to determine the effects of varying the state variable limits.

In the turning dive maneuver, vertical velocity, g-load, and velocity were all sampled, with vertical velocity being sampled most frequently. The other three state variables were sampled together every 5 seconds. In comparing these results to the reduced error, equal-interval sampling scores in Table 18, it is apparent that these results fall just slightly above the 0.8 second interval scores. This suggests that similar scores can be obtained by sampling everything 0.8 seconds or by sampling one of three variables every 0.2 seconds.

Closer examination of the individual runs yields additional insights. In the equal-interval sampling runs, the standard deviation of the score is approximately equal to the mean overall score. Thus there is a great deal of variability in flight control performance, as evidenced by the peaks immediately following the MFK task sequence.

TABLE 24

STRAIGHT AND LEVEL SCORES FOR
"PROBABILITY OUT OF LIMITS" SAMPLING RULE

CASE	RANDOM NUMBER SEED			AVERAGE
	1	2	3	
1	.2166	.2106	.2135	.2136
2	.2044	.1935	.1977	.1985
3	.2730	.2628	.3100	.2819

TABLE 25

TURNING DIVE SCORES FOR
"PROBABILITY OUT OF LIMITS" SAMPLING RULE

CASE	RANDOM NUMBER SEED			AVERAGE
	1	2	3	
1	2.440	2.425	2.888	2.584
2	2.460	2.407	4.068	2.978
3	2.994	2.412	4.499	3.302

This is not true in the "probability out of limits" sampling case. There are no sharp peaks and the variances of the scores are much lower. These trends may be important in analyzing workload issues. In peak workload or stress situations, it may be critical that the score (as an estimate of the level of flight control) not go above a certain level at any given time, even though the average performance score is well within limits. If this type of behavior is required, one may opt for the "probability out of limits" type sampling approach. This type of sampling also appears to be more representative of actual pilot flight performance in that the variable which deviates the most from the allowable range is the one attended to. Thus, in a sense, a built-in priority scheme is exercised.

Ascribing a cost structure on taking samples might also prove interesting in comparing sampling schemes. Sampling more often, even though just a single variable, may prove to be more costly than sampling everything periodically, depending on the cost structure employed. Other variations to the model, such as not sampling until the probability that a variable is out of limits exceeds a given probability, would also make interesting studies. Such sampling schemes could readily be explored via the combined modeling technique described herein.

SUMMARY AND CONCLUSIONS

The role of the human operator in control systems is evolving towards that of a supervisor who plans, sequences, and monitors and away from strictly tracking. New modeling approaches and techniques are required to realistically represent and examine these new system configurations and resulting performance issues. This dissertation study proposed an alternate modeling approach comprised of discrete network models in combination with elements of an open-loop optimal control model formulation. The objective of this effort was to explore the feasibility of employing this combined approach for modeling complex man-machine systems in which both discrete task and continuous tracking behaviors are exhibited. Included in this objective is the identification of strengths, weaknesses, and issues which surfaced during the application of the approach.

These objectives have been achieved. The feasibility of employing this combined modeling approach has been demonstrated through its successful application to the DAIS system. This modeling approach greatly reduces the weaknesses of employing either network or continuous optimal control techniques independently in modeling monitoring and supervisory control systems. The discrete task activities and decision-making processes of the human operator can now be explicitly represented along with his continuous tracking behaviors.

This modeling technique also facilitates the examination of alternate state variable sampling algorithms. The effects on flight control performance of employing different sampling strategies can readily be determined. Flight control interruptions for the performance of monitoring activities or discrete tasks can now be modeled. Real-time man-in-the-loop system performance can be compared with that exhibited by various sampling strategies in an attempt to determine "how" the operator actually processes information. Issues such as whether the pilot multiplexes back and forth between his flight control and discrete task activities, or whether he performs both activities in parallel, can be addressed using this combined modeling technique.

The approach's utility as an analysis tool in the design of man-in-the-loop experiments has also been demonstrated. It can be used to evaluate and establish operator procedures and the experimental protocol or scenario prior to actually running the experiment. For example, results of the DAIS analysis indicated that the aircraft required a relatively long stabilization period and, hence, provided direction for the appropriate collection of data and the sequencing of maneuvers. This effort also demonstrated how the technique can be employed in determining optimal hardware configurations and accuracy requirements. The DAIS simulator stick and throttle devices were known to have defects. The simulation outputs indicated the severity of these defects and could be used to assess accuracy requirements in order to achieve predetermined levels of system performance.

While it is doubtful that models can predict performance as accurately as real-time man-in-the-loop simulations, they can be used

to determine the sensitivity of the system to various man-machine parameters. Those parameters which are deemed to be of importance can then be examined in more detail in a man-in-the-loop study. The elimination of insignificant variables could potentially be very cost effective in terms of time, personnel, and money.

A number of issues and problems surfaced during the course of this study. One problem is the non-availability of generic performance data for quantifying such parameters as task time and display reading error distributions. This has important implications for future man-in-the-loop experimentation. Most of the empirical work cited in the literature is recorded in very system and situation specific terms. Even in cases where the results may be generalized, the data are seldom presented in a format that is compatible with simulation model requirements. For example, often only summary ANOVA tables are displayed, while the mean and variance statistics necessary for defining performance distributions have been omitted. Experimenters must become more aware of and sensitive to the needs of modelers.

A similar problem is the quantification of the optimal control model parameters. The assignment of the cost functional weights Q and R are of particular concern. This still appears to be very much more an "art" than a science. More research is required in this area to develop better guidelines for the quantification of these and other optimal control model parameters, such as display and control error distributions.

A third area of concern, which was addressed in some detail in the model analysis chapter, is the measurement problem. The "mean-squared error" across an entire mission may no longer be an acceptable or realistic measure of man-machine performance in monitoring and supervisory systems. New scoring and measurement formulations which capture the effects of short-term behaviors and extreme or worst case performance histories will have to be considered. There is also a need for metrics which represent monitoring and discrete task activity performance. While these metrics would have to be tailored to the specific system under study, it is likely that many of them could be classified into general categories. Future systems analyses and modeling will undoubtedly require multi-attribute performance functions.

The combined discrete network and optimal control model employed here is but one approach to modeling complex, man-machine systems. It is anticipated that a wide range of models and approaches are required to represent monitoring and supervisory tasks. Other models which might be considered include those based on queueing theory, information theory, traditional control theory, decision analysis, and psychological theories. Because of the diversity of the origins of these theories (engineering, psychology, etc.), communication difficulties are inevitable. Miller (1975) suggests the need for new symbolic systems as a means to increase understanding and promote communications among disciplines. Miller (1978) proposes that the use of formal systems theory may encourage this interchange and facilitate the explicit definitions of objects, concepts, and their relationships within and among the modeling approaches.

There is also a requirement to develop a taxonomy of monitoring and supervisory tasks. Different types of tasks require different models. A taxonomy of pertinent tasks and available models should be assembled. For too long the modeling technology has been driving the analyses performed. We must begin employing models that are both pertinent to the tasks under consideration and at the level appropriate for addressing the issues of concern.

In conclusion, this effort in combined simulation modeling does not allow one to accept or reject the technique as it stands. Rather, it offers insight as to its utility and effectiveness in modeling and examining man-machine systems and issues. It is recommended that this approach be repeated in other man-machine systems, such as DAIS, which exhibit complex discrete and continuous task structures. It is anticipated that both additional insights and new areas for research will emerge from this exercise.

APPENDIX A

GLOSSARY OF TERMS

DAIS -- Digital Avionics Information System.

MFK -- Multi-Function Keyboard.

monitoring -- Observing displays or an information field in a purposive fashion to ensure that system operation is normal or as desired. If available information suggests abnormality, additional information is sought and a diagnosis of the difficulty is attempted.

open loop, closed loop control -- Between samples, the pilot operates in an "open-loop" fashion in that control inputs and adjustments are based on conditional estimates of system state variables status as opposed to actual display readings. On occasion, the operator "closes the loop" and obtains system status feedback by sampling the flight control displays.

real-time man-in-the-loop simulation -- The machine and environmental (e.g., exogenous events) components of the object system are simulated, with operator(s) working on-line to the simulation. The simulation (e.g., the events occurring therein) is executed according to the actual time dimension assumed for the object system.

sampling strategy -- Procedure by which to select what information to observe and with what frequency or under what contingency.

secondary task -- A task which the operator is asked to do in addition to his primary task. Two types are: "non-loading" (the operator attends to the secondary task when he has time) used to measure "reserve capacity"; and "loading" (the operator must always attend to the secondary task) so as to potentially cause performance degradation on the primary task.

supervisory control -- Controlling a semi-autonomous system through the intermediary of a computer. The human supervisor performs upper level goal-oriented functions such as planning system activities, programming the computer, monitoring the system behavior when computer-controlled, adjusting parameters on-line when appropriate, and intervening to take over control in an emergency or for normal reprogramming or repair.

GLOSSARY OF AIRCRAFT MODEL TERMS AND SYMBOLS

AREA	Area of aircraft in square feet (set to 202 $(ft)^2$)
CD	Coefficient of drag
CL	Coefficient of lift
D	Drag in lbs.
DENS	Air density
DT	Step size in seconds (set to 0.2 sec.)
K	Scaling factor in α equation used to specify the aircraft pitching rates with respect to the lift to weight ratio (set to .9)
L	Lift
M	Mach of aircraft
MASS	Weight of aircraft divided by G-load (slugs)
MAXG	Largest allowable positive acceleration (set to +15)
MING	Largest allowable negative acceleration (set to -5)
MT	Maximum thrust
PRES	Air pressure
Q	Dynamic pressure
SS	Speed of sound in ft/sec
TEMP	Air temperature in degrees
u_1	Input in radians/sec., controls the rate of change of attack angle (proportional to fore and aft movements of the stick)
u_2	Input in radians/sec., controls the rate of change of roll angle (proportional to lateral or side-to-side movements of the stick.

u_3	Input as normalized percentage of throttle (proportional to throttle position)
V	Velocity of aircraft in ft/sec
$\dot{V}$	Rate of change of velocity in ft/sec
W	Weight of aircraft in lbs. (set to 17,000 lbs.)
X	X position of aircraft in feet
$\dot{X}$	Rate of change in X coordinate in ft/sec
Y	Y position of aircraft in feet
$\dot{Y}$	Rate of change in Y coordinate in ft/sec
Z	Altitude in feet
$\dot{Z}$	Rate of change in Z coordinate in ft/sec
α	Attack angle in radians
$\dot{\alpha}$	Rate of change of attack angle in radians/sec
γ	Flight path angle in radians
$\dot{\gamma}$	Rate of change of flight path angle in radians/sec
ψ	Heading angle in radians
$\dot{\psi}$	Rate of change of heading angle in radians/sec
ϕ	Roll angle in radians
$\dot{\phi}$	Rate of change of roll angle in radians/sec

AD-A071 574 AEROSPACE MEDICAL RESEARCH LAB WRIGHT-PATTERSON AFB OH F/G 5/8
COMBINED DISCRETE NETWORK--CONTINUOUS CONTROL MODELING OF MAN-M--ETC(U)
MAR 79 D J SEIFERT

UNCLASSIFIED AMRL-TR-79-34 NL

3 OF 3
AD
A071574

END
DATE
FILMED
8-79
DDC

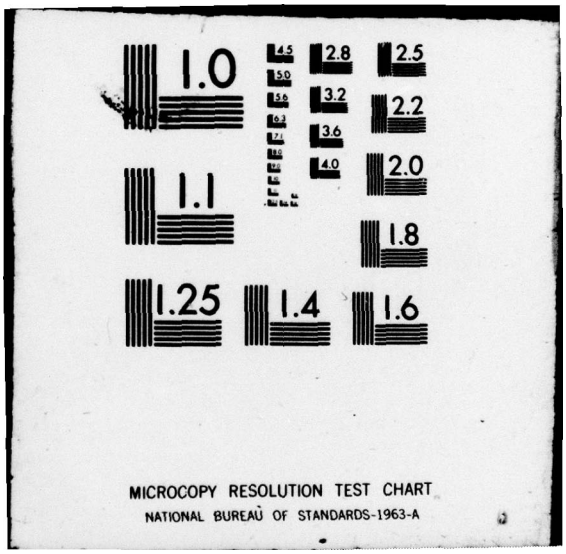
1.0
1.1
1.25
1.4
1.6
1.8
2.0
2.2
2.5
2.8
3.2
3.6
4.0
4.5
5.0
5.6
6.3
7.1
8.0
9.0
MICROCOPY RESOLUTION TEST CHART
NATIONAL BUREAU OF STANDARDS-1963-A

APPENDIX B
AERODYNAMIC EQUATIONS OF MOTION

1.0 ANGLE OF ATTACK, α

The angle of attack, alpha, is computed first. The following steps are executed in computing α.

1. Compute GLOAD $= \frac{L}{\text{Weight}}$

2. Compute the derivative of α based on GLOAD and u_1.

   When GLOAD ≥ 1, set

   $$\dot{\alpha} = u_1 - (\text{GLOAD} - 1) \frac{K}{\text{MAXG}}$$

   When GLOAD < 1 set

   $$\dot{\alpha} = u_1 + (\text{GLOAD} - 1) \frac{K}{(\text{MING})5}.$$

3. Compute present value of α from the previous value of α and the present value of $\dot{\alpha}$ as:

   $$\alpha = \alpha + \dot{\alpha}\, DT$$

   where DT is the time increment. This constitutes a numerical rectangular integration.

4. Test the value of α, and if $\alpha < -.2$, set $\alpha = -0.2$. This limits α at -.2 radians.

2.0 ROLL ANGLE, ϕ

Next, the program computes a new value for the roll angle, ϕ. The following steps are executed.

1. Set the negative derivative of roll angle to

   $$\dot{\beta} = u_2$$

   where u_2 is a control variable which is proportional to stick position.

2. Compute the present value of ϕ from the previous value of β and the present value of $\dot{\beta}$ using rectangular numerical integration. When the absolute value of the flight path angle, γ, is greater than or equal to $\frac{\pi}{2}$ radians, then

$\beta = \beta + \dot{\beta}\ DT + \pi.$

When the absolute value of γ is less than $\frac{\pi}{2}$ radians, set

$\beta = \beta + \dot{\beta}\ DT.$

Now convert the β values to positive roll angle:

$\phi = -\beta.$

3.0 COMPUTATION OF ENVIRONMENTAL PARAMETERS

Subroutine STATE next computes the environmental parameters for the aircraft model in the following steps:

1. The parameters associated with the atmosphere are calculated based on the altitutde of the aircraft, Z.

When $Z \geq 35{,}300$ ft., set

Temperature:

$$TEMP = -67.0$$

Pressure:

$$PRES = 489.456 \exp\left(\frac{-(Z - 35{,}300)}{20930}\right)$$

Density:

$$DENS = \frac{PRES}{673946}$$

When $Z < 35{,}300$ ft., set

$$TEMP = 59 - (.00357\ Z)$$

$$D_1 = 1 - \left(\frac{0.00357\ Z}{518.4}\right)$$

$$PRES = 2116\ D_1^{5.256}$$

$$DENS = .002378\ D_1^{4.256}.$$

2. The speed of sound is calculated as:

$$SS = \left(\frac{PRES\ 1.406}{DENS}\right)^{.5} \left(\frac{ft.}{sec.}\right)$$

and the MACH number as

$M_1 = \frac{V}{SS}$, where V is the velocity of the aircraft in ft/sec.

3. The dynamic pressure is calculated as:

$$Q = 0.5\ DENS\ (V)^2.$$

4.0 CALCULATION OF FORCES

The forces acting on the aircraft are calculated as follows:

1. The coefficient of LIFT is first calculated by:

$$CL = .1 + 2.5\ \alpha.$$

Then the coefficient of DRAG by:

$$CD = 0.03 + .27(CL)^2.$$

The DRAG is computed from

$$D = (Q)\ (CD)\ (AREA).$$

2. After the first computed value of CL is used to compute CD and D, CL and α are modified according to the value of α, as follows:

When $\alpha \geq .4$ and $\alpha < .6$, set

$$CL = 1 - 2.\ (\alpha - .4).$$

When $\alpha \geq .6$, set

CL = 0 and $\alpha = .6$; if $V < 100$, set $\alpha = 0$.

3. The thrust is computed as follows:

   If $V < 1$, set $V = 1.0$.

   Compute maximum thrust, MT, depending on whether the after-burner is on or off. When after-burner is on, set

   $$MT = 2[((2327. + .172Z - .0000031(Z)^2)M_1 + (11500. - .25Z)].$$

   When after-burner is off, set

   $$MT = \frac{(2327. + .172Z - .0000031(Z)^2)M_1}{2} + \frac{(11500. - .25Z)}{2}.$$

   Next, compute thrust from:

   $$T = u_3 \, MT.$$

   Where u_3 is a control input proportional to throttle.

4. The component of applied force normal to the flight path (Lift) is:

   $$L = ((Q)\ (CL)\ (AREA)) + T \sin(\alpha).$$

5.0 VELOCITY, V

The derivative of the aircraft velocity is computed according to:

$$\dot{V} = \frac{T \cos(\alpha) - D - W \sin(\gamma)}{MASS}$$

where MASS is in slugs. The present value of V is next computed from the previous value of V and the present value of $\dot{V}$ as:

$$V = V + \dot{V}\, DT.$$

6.0 HEADING ANGLE ψ AND FLIGHT PATH ANGLE γ

The present value of heading angle ψ and flight path angle γ are computed in the following steps:

1. The derivatives of ψ and γ are computed from the equations

$$\dot{\psi} = \frac{L \sin(\phi)}{MASS \cos(\gamma)\, V}$$

and

$$\dot{\gamma} = \frac{L \cos(\phi) - W \cos(\gamma)}{(MASS)\, V} .$$

2. The present value of ψ and γ are computed from the previous values of ψ and γ the present values of $\dot{\psi}$ and $\dot{\gamma}$, but with limits in the following way:

Set $\gamma_1 = \gamma + \dot{\gamma}\, DT$.

If the absolute value of γ_1 is less than $\frac{\pi}{2}$ radians, set the present values of ψ and γ equal to

$$\psi = \psi + \dot{\psi}\, DT$$

$$\gamma = \gamma_1 .$$

If the absolute value of γ_1 is greater than or equal to $\frac{\pi}{2}$ radians, set

$$\psi = \psi + \dot{\psi}\, DT + \pi$$

and set

$$\gamma = -\pi - \gamma, \text{ if } \gamma_1 < 0$$

or

$$\gamma = \pi - \gamma_1, \text{ if } \gamma_1 \geq 0.$$

7.0 POSITION OF THE AIRCRAFT

The position of the aircraft with respect to the earth is calculated next. In each step below, the derivative is calculated first, and then the present value is found from rectangular numerical integration. The steps are as follows:

1. X-position of aircraft

$$\dot{X} = V \cos(\gamma) \cos(\psi)$$

and $X = X + \dot{X}\,DT.$

2. Y-position of aircraft

$$\dot{Y} = V \cos(\gamma) \sin(\psi)$$

and $Y = Y + \dot{Y}\,DT.$

3. Z-position of aircraft (altitude)

$$\dot{Z} = V \sin(\gamma)$$

and $Z = Z + \dot{Z}\,DT.$

REFERENCES

Anderson, B. D. O. and Moore, J. B. Linear Optimal Control. Prentice Hall, 1971.

Askren, W. B., Campbell, W. B., Seifert, D. J., Hall, T. T., Johnson, R. C., and Sulzen, R. H. Feasibility of a Computer Simulation Method for Evaluating Human Effects on Nuclear Systems Safety. Air Force Human Resources Laboratory, Air Force Systems Command, Brooks Air Force Base, AFHRL-TR-76-18, 1976.

Athans, M., and Falb, P. L. Optimal Control: An Introduction to the Theory and Its Applications. New York: McGraw-Hill, 1966.

Baron, S. A Model for Human Control and Monitoring Based on Modern Control Theory. Journal of Cybernetics and Information Science, Vol. 1, No. 1, 3-18, January 1976.

Baron, S. and Kleinman, D. L. The Human as an Optimal Controller and Information Processor. IEEE Trans. Man-Machine Systems, MMS-10, No. 1, 9-17, 1969.

Baron, S. and Kleinman, D. L. Prediction and Analysis of Human Performance in a VTOL Hover Task. Proceedings of Seventh Annual NASA University Conference on Manual Control. USC, Los Angeles, California, 1971.

Baron, S. and Levison, W. H. A Display Evaluation Methodology with Application to Vertical Situation Displays for STOL Aircraft. Proceedings of Ninth Annual NASA-University Conference on Manual Control, M.I.T., May 1973.

Baron, S. and Levison, W. H. Analysis and Modeling Human Performance in AAA Tracking. BBN Report No. 2557, Bolt, Beranek and Newman, Inc., Cambridge, Mass., 1974.

Baron, S. and Levison, W. H. Display Analysis with the Optimal Control Model of the Human Operator. Human Factors, Vol. 19, No. 5, 437-458, 1977.

Bauerschmidt, D. and La Porte, R. Techniques for Display/Control System Integration in Supervisory and Monitoring Systems. In Sheridan, T. B. and Johannsen, G. (Eds.), Monitoring Behavior and Supervisory Control. New York: Plenum Press, 1976.

Bauershmidt, D. and La Porte, R. Techniques for Display/Control System Integration. Human Factors, Vol. 19, No. 5, 437-458, 1977.

Berisford, K. M. Statistical Analysis of DAIS Triple Task Data. Technical Memorandum, Systems Research Laboratories, Inc., Dayton, Ohio, December 1975.

Brandt, W. E., Jr. and Wartluft, D. L. Program Documentation for the DAIS Triple Task. Aerospace Medical Research Laboratory, AMRL-TR-75-24, Wright-Patterson AFB, Ohio, 1975. (AD A024101)

Carbonell, J. R. A Queueing Model of Many-Instrument Visual Sampling, IEEE Transactions on Human Factors in Electronics, Vol. HFE-7, No. 4, December 1966.

Cavalli, D. Discrete-Time Pilot Model. Proceedings of the 14th Annual Conference on Manual Control, Los Angeles, 25-27 April 1978.

Chubb, G. P. and Berisford, K. M. Manned System Modeling: SAINT Applied to Strategic Navigation. Record of Proceedings, Tenth Annual Simulation Symposium, pp. 321-352, 1977.

Crawford, B. M., Pearson, W. H. and Hoffman, M. S. Multipurpose Digital Switching and Flight Control Workload. Aerospace Medical Research Laboratory, Wright-Patterson AFB, Ohio, AMRL-TR-78-43, 1978.

Duket, S. D., Wortman, D. B., Seifert, D. J., Hann, R. L., and Chubb, G. P. Documentation for the SAINT Simulation Program. Aerospace Medical Research Laboratory, Wright-Patterson AFB, Ohio, AMRL-TR-77-63, July 1978 (a). (AD A059198)

Duket, S. D., Wortman, D. B., Seifert, D. J., Hann, R. L., and Chubb, G. P. Analyzing SAINT Outputs Using SPSS. Aerospace Medical Research Laboratory, Wright-Patterson AFB, Ohio, AMRL-TR-77-64, July 1978 (b). (AD A058723)

Edwards, E. Some Aspects of Automation in Civil Transport Aircrafts. In Sheridan, T. B. and Johannsen, G. (Eds.). Monitoring Behavior and Supervisory Control. New York: Plenum Press, 1976.

Elkind, J. I. Characteristics of Simple Manual Control Systems. Lincoln Laboratory Technical Report III, Massachusetts Institute of Technology, 1956.

Elkind, J. I., Falb, R., Kleinman, D. L., and Levison, W. H. An Optimal Control Method for Predicting Control Characteristics and Display Requirements of Manned Vehicle Systems. AFFDL-TR-67-187, Wright-Patterson AFB, Ohio, 1968.

Etkin, B. Dynamics of Atmospheric Flight. New York: John Wiley and Sons, Inc., 1972.

Fishman, G. S. Concepts and Methods in Discrete Event Simulation. New York: John Wiley and Sons, 1973.

Fogarty, L. E. and Howe, R. M. Computer Mechanization of Six-Degree of Freedom Flight Equations. NASA CR-1344, National Aeronautics and Space Administration, Washington, D.C., May 1969.

Hann, R. L. and Kuperman, G. G. SAINT Model of a Choice Reaction Time Paradigm. Proceedings of the Human Factors Society 19th Annual Meeting, Dallas, Texas, 1975.

Jacobs, D. M., Pritsker, A. A. B., and Chubb, G. P. Network Modeling and Simulation of Systems Involving Psychological and Human Factors. Unpublished technical report, 1973.

Johannsen, G. Preview of Man Vehicle Control Session. In Sheridan, T. B. and Johannsen, G. (Eds.). Monitoring Behavior and Supervisory Control. New York: Plenum Press, 1976.

Kantowitz, B. H. Human Information Processing: Tutorials in Performance and Cognition. Hillsdale, NJ, Erlbaum Associates, 1974.

Kleinman, D. L., and Baron, S. Analytic Evaluation of Display Requirements for Approach to Landing. NASA CR-1952, Bolt, Beranek and Newman, Inc., Cambridge, Mass., November 1971.

Kleinman, D. L., Baron, S., and Levison, W. H. An Optimal Control Model of Human Response, Part 1: Theory and Validation. Automatica, No. 6, 357-369, 1970.

Kleinman, D. L. and Curry, R. E. Some New Control Theoretic Models for Human Operator Display Monitoring. Proceedings IEEE Decision and Control Conference, 1976.

Kuperman, G. G., Hann, R. L., and Berisford, K. M. Refinement of a Computer Simulation Model for Evaluating DAIS Display Concepts. Proceedings of the Human Factors Society 21st Annual Meeting, San Francisco, CA, October 1977.

Kuperman, G. G. and Seifert, D. J. Development of a Computer Simulation Model for Evaluating DAIS Display Concepts. Proceedings of the Human Factors Society 19th Annual Meeting, Dallas, Texas, 1975.

Leonard, T. Optimizing Linear Dynamics for Human Operated Systems Minimizing the Mean Squared Tracking Error. WESCON, 4, Pt. 4: 57-62, 1960.

Levison, W. H., Elkind, J. I., and Ward, J. L. Studies of Multi-Variable Manual Control Systems: A Model for Task Interference. NASA-Ames Research Center, NASA CR-1746, 1971.

Maltas, K. L., and Buck, J. R. Simulation of Large Man/Machine Process Control System in the Steel Industry. Proceedings of the Human Factors Society 19th Annual Meeting, Dallas, Texas, pp. 193-205, 1975.

Miller, R. A. A Formal Model of the Adaptive and Discrete Control Behaviors of Human Operators. Ohio State University Research Foundation, Air Force Office of Scientific Research, Grant No. AFOSR-76-3003, May 1978.

Miller, R. B. A Break with the Bondage of Absolute Design Notations. IBM TR No. 2691, 1975.

Milton, J. L., Jones, R. E., and Fitts, P. M. Eye Fixations of Aircraft Pilots; II. Frequency Duration and Sequence of Fixations When Flying the Instrument Low Approach System (ILAS). Wright-Patterson AFB, Ohio, USAF TR-5839 (ATI-65996), 1949.

Moray, N. Attention, Control, and Sampling Behavior. In Sheridan, T. B. and Johannsen, G. (Eds.). Monitoring Behavior and Supervisory Control, New York: Plenum Press, 1976.

Parzen, I. Stochastic Processes. Holden Day, p. 83, 1962.

Pew, R. W., Baron, S., Feehrer, C. E., and Miller, D. C. Critical Review and Analysis of Performance Models Applicable to Man-Machine Systems Evaluation. Bolt, Beranek and Newman, Report No. 3446, Cambridge, Mass., 1977.

Randolph, P. H. and Ringeisen, R. D. A Network Learning Model with GERT Analysis. Journal of Mathematical Psychology, Vol. II, No. 1, 59-70, 1974.

Roig, R. M. A Comparison Between Human Operator and Optimum Linear Controller RMS-Error Performance. IEEE Trans. Human Factors in Electronics, HFE-3, No. 1: 18-21, 1962.

Senders, J. W. Tracking with Intermittently Illuminated Displays. Wright-Patterson AFB, Ohio, Rept. WADC TR-55-197 (AD 80941), 1955.

Senders, J. W. The Human Operator as a Monitor and Controller of Multidegree-of-Freedom Systems. IEEE Transactions on Human Factors In Electronics, Vol. HFE-5, pp. 2-5, September 1964.

Senders, J. W., Elkind, J. I., Grignetti, M. C., and Smallwood, R. An Investigation of the Visual Sampling Behavior of Human Observers. Bolt, Beranek and Newman, Inc., BBN Final Report, Contract NAS1-3860, May 1965.

Sheridan, T. B. On How Often the Supervisor Should Sample. IEEE Transactions on Systems Science and Cybernetics, Vol. SSC-6, No. 2, April 1970.

Sheridan, T. B. Toward a Model of Supervisory Control. In Sheridan, T. B. and Johannsen, G. (Eds.). Monitoring Behavior and Supervisory Control. New York: Plenum Press, 1976.

Sheridan, T. B. and Ferrell, W. R. Man-Machine Systems: Information, Control, and Decision Models of Human Performance. The MIT Press, Cambridge, Mass., 1974.

Siegel, A. I. and Wolf, J. J. Man-Machine Simulation Models. New York: Wiley and Sons, Inc., 1969.

Siegel, A. I., Wolf, J. J., and Allman, R. A Discontinuous Analytic Model for Simulating Apollo Vehicle Operator Actions and Information Exchange. Applied Psychological Services, Inc., 1962.

Simon, H. A. Models of Man. New York: John Wiley and Sons, Inc., 1957.

Singleton, W. T. The Model Supervisory Dilemma. In Sheridan, T. B. and Johannsen, G. (Eds.). Monitoring Behavior and Supervisory Control. New York: Plenum Press, 1976.

Spicuzza, R. J., Pinkus, A. R., and O'Donnell, R. D. Development of Performance Assessment Methodology for the Digital Avionics Information System. Systems Research Laboratories, Inc., 1974.

Teichner, W. H. Human Performance Simulation. Annual Report. AFOSR Contract No. F44620-76-C-0013, 1976.

Whitehouse, G. E. Systems Analysis and Decision Using Network Techniques. Englewood Cliffs, NJ: Prentice-Hall, Inc., 1973.

Wilke, T. L. and Miller, R. A. Information Requirements for Decision-Making in Large-Scale Systems. ORSA/TIMS Joint National Meeting, Boston, Mass., April 22-24, 1974.

Woodruff, K. R. Development of a Rate-of-Closure Display Using a CRT Symbol Generator. Systems Research Laboratory Technical Report, Dayton, Ohio, 1972.

Wortman, D. B., Duket, S. D., and Seifert, D. J. SAINT Simulation of a Remotely Piloted Vehicle/Drone Control Facility: Model Development and Analysis. Aerospace Medical Research Laboratory, Wright-Patterson AFB, Ohio, AMRL-TR-75-118, 1976. (AD A031085)

Wortman, D. B., Duket, S. D., Seifert, D. J., Hann, R. L., and Chubb, G. P. Simulation Using SAINT: A User-Oriented Instruction Manual. Aerospace Medical Research Laboratory, Wright-Patterson AFB, Ohio, AMRL-TR-77-61, July 1978. (AD A058671)

Wortman, D. B., Duket, S. D., Seifert, D. J., Hann, R. L., and Chubb, G. P. The SAINT User's Manual. Aerospace Medical Research Laboratory, Wright-Patterson AFB, Ohio. AMRL-TR-77-62, July 1978.*

Wortman, D. B., Hixson, A. L., III, and Jorgensen, C. C. A SAINT Model of the AN/TSQ-73 Guided Missile Air Defense System. Proceedings of the 1978 Winter Simulation Conference, Miami, Fla., December, 1978.

Wortman, D. B., Sigal, C. E., Pritsker, A. A. B., and Seifert, D. J. New SAINT Concepts and the SAINT II Simulation Program. Aerospace Medical Research Laboratory, Wright-Patterson AFB, Ohio, AMRL-TR-74-119, 1975. (AD A014814)

Zeigler, B. P. Theory of Modelling and Simulation. New York: John Wiley and Sons, Inc., 1976.

* AD A058724

*U.S.Government Printing Office: 1979 — 657-002/677